

**MEASURING THE EFFECT OF CONCENTRATE MINERALOGY ON  
FLASH FURNACE SMELTING USING DROP TOWER TESTING AND A  
NOVEL OPTICAL PROBE**

by

Arthur Stokreef

A thesis submitted to the Department of Mining

In conformity with the requirements for

the degree of Master of Applied Science

Queen's University

Kingston, Ontario, Canada

(December 2018)

Copyright © Arthur Stokreef, 2018

## Abstract

The selection of furnace operating parameters during the flash smelting of copper is based on the elemental composition of a blend and does not account for mineralogy, which may impact on the process. Thus, it is important to study the impact of blend mineralogy on flash combustion processes. This thesis investigates the impact of pure minerals, chalcopyrite and pyrite, on the flash combustion behaviour of three mineralogically distinct but chemically similar copper concentrates through experimental test work. In tandem, proof of concept testing of a novel fibre optic probe for monitoring flash combustion reactions was done.

A drop tower reactor was used to study the effect of  $O_2/S$  stoichiometry on flash combustion processes under 21 different test conditions. Tests were conducted at  $950^\circ\text{C}$  with  $O_2/S$  stoichiometries in the range of 0.8 to 4.0, and a solids feed rate of 3 grams per minute. The results suggest that concentrates with low pyrite mineralization require a higher  $O_2/S$  stoichiometry to be desulphurized to the target matte composition, and that the  $O_2/S$  stoichiometry impacts the fraction of dust in the products, the flame temperature as well as the flame brightness. In this work, the impact of mineralogy on flash combustion processes is studied using different monitoring techniques to gain real-time information about the process. Ultimately this information may then be used to optimize the blending process and to adjust the operation of a flash furnace in real time.

Monitoring of combustion reactions was done using emission spectroscopy, where the spectra were acquired through a custom-built fibre optic probe. The two-wavelength method was used to measure the temperature of combusting particles and the integrated intensity was used to measure the flame brightness. This information was found to be useful for identifying feed distribution problems, which are also experienced in commercial scale furnaces. There were no atomic or molecular Cu, Fe, S nor O emission lines or bands in the emission spectrum; however, alkali metal emissions from Na, K and Li were observed. The lack of Cu, Fe, S and O emissions is attributed to the low flame temperatures, which were between 900

and 1500°C. Testing of the sensor in a commercial scale furnace is recommended and is expected to expand the application range of the probe.

## Statement of Contributions

- Dr. Roberto Parra developed the fibre probe used in this thesis at the University of Concepcion, Chile. He guided us through the early design and operational stages of the drop tower and conducted the QEMSCAN® analysis.
- Kingston Process Metallurgy Inc provided their laboratory, equipment and expertise in support of this work.
- Dr. Jack Barnes helped with the design and construction of the fibre optic probe as well as the temperature calibrations. He was a great resource for all technical problems.
- Mark Woodrow did all the machining and fabrication work required to build the drop tower.

## **Acknowledgements**

Thank you to Dr. Boyd Davis, Dr. Hans-Peter Loock and Dr. Roberto Parra for your mentorship and guidance throughout this degree. I have gained important technical and life skills from you and I will use these throughout my career. I will always listen, value and look forwards to mentorship from you.

To Kingston Process Metallurgy and all your employees, thank you for allowing me to conduct research at your facility. It is truly a one of kind lab and I have enjoyed learning and growing at your facility. A special shout out to Alain Roy, Trevor Lebel and Mark Woodrow, all of whom were instrumental in helping me move this research forwards.

Thank you NSERC, MITACS and the Ontario Center for Excellence for your generous financial support to this research as well as our industrial partner who supplied the concentrate for experimental test work.

Thank you also to: Jack Barnes, Pablo Ruarte, Carlos Toro, The Robert M. Buchan Department of Mining and the Loock Laser Lab.

To my friends and family, thank you for the personal support you provided me with through degree. I really could not have done it without you and appreciate that I could rely on you when times were tough. I dedicate this work to my mum, Dr. Nicola Jones-Stokreef.

## Table of Contents

Abstract .....	ii
Statement of Contributions .....	iv
Acknowledgements .....	v
List of Figures .....	viii
List of Tables .....	x
Chapter 1 Introduction .....	1
Flash Smelting of Copper .....	2
Furnace Operation .....	3
Advantages and Disadvantages of Flash Furnace Smelting .....	5
Concentrate Blending .....	6
Pyrometallurgy of Copper Smelting .....	7
Project Goals .....	10
Chapter 2 Literature Review .....	12
Research into Flash Reactions .....	12
Laboratory Reactors .....	12
Particle Ignition .....	13
Desulphurization in Flash Smelting .....	15
Combustion Temperatures .....	16
Emission Spectroscopy of Flash Combustion Processes .....	19
Process control in metal production – Using sensors .....	20
Tenova Goodfellow – EFSOP® .....	21
Scandinavian Emissions Technology – Optical Production Control .....	23
Emission Spectroscopy of Flames .....	25
Blackbody Radiation .....	25
Line Spectra .....	26
Banded Spectra .....	27
Optical Characterization of Flames .....	27
Diagnostic Techniques .....	28
Measurement Variables .....	28
Temperature .....	29
Brightness .....	30
Flicker .....	30
Stability .....	31
Emitting Species .....	32
Chapter 3 Experimental Methodology and Material Characterization .....	33
Experimental Setup .....	33
Optical Instrumentation .....	39
Material Characterization .....	40
Measurement Principles .....	40
Elemental Sulphur .....	40
QEMSCAN® .....	40
Laser Particle Size Analysis .....	41
Pure Mineral Characterization .....	41
Concentrate Characterization .....	43
Test Conditions .....	47
Desulphurization Model Development .....	48
Chapter 4 Analysis & Results .....	50
Analysis of Drop Tower Reaction Products .....	51

Desulphurization .....	51
Pure Mineral XRD Analysis .....	53
QEMSCAN® Analysis .....	54
Product Particle Size Analysis .....	65
Analysis of the Emission Spectrum .....	71
Characteristic Emission Spectrum & Emitting Species .....	71
Flame Flicker .....	73
Combustion Temperatures .....	76
Flame Brightness .....	78
Chapter 5 Discussion .....	81
Drop Tower Reaction Products .....	81
Desulphurization in Flash Smelting – Impact of Mineralogy .....	81
Pure Chalcopyrite.....	83
Concentrates.....	84
Product Mineralogy .....	89
Pure Minerals .....	89
Concentrates.....	90
Particle Size Analysis .....	94
Emission Spectroscopy in Flash Furnace Smelting .....	99
Emitting Species .....	99
Flame Temperature .....	100
Flame Brightness .....	101
Flame Flicker .....	101
Opportunities for Process Monitoring & Control in a Plant .....	102
Flame Temperature Monitoring.....	103
Monitoring Feed Distribution .....	103
Dusting.....	106
Chapter 6 Conclusions .....	107
Chapter 7 References .....	113
Chapter 8 Appendices .....	118
Appendix 1: Temperature Calibration .....	118
Appendix 2: Experimental Heat Model .....	121
Appendix 3: Raw Experimental Data (Temperature and Brightness).....	123
Chalcopyrite.....	123
Pyrite.....	126
Concentrate A .....	128
Concentrate B.....	130
Concentrate AB.....	133

## List of Figures

Figure 1: Pure mineral, single particle combustion temperatures. Values were estimated from figures presented in [9] [12].....	17
Figure 2: Effect of concentrate composition and oxygen content in the process gas on flame temperature. Taken from ref [14].....	18
Figure 3: Drop tower reactor, furnaces and sampling spoon .....	33
Figure 4: Drop tower experimental setup; (1) Computer DAQ, (2) Spectrometer, (3) Fibre optic probe, (4) Powder screw feeder, (5) Solids feed lance cooling gas, (6) Reaction gas, (7) Resistance heated furnaces, (8) Mass flow controllers for O <sub>2</sub> and N <sub>2</sub> gas, (9) Flash reaction zone, (10) N <sub>2</sub> compressed gas cylinder, (11) O <sub>2</sub> compressed gas cylinder, (12) Scrubbed off-gas, (13) SO <sub>2</sub> containing off-gas, (14) caustic scrubbing solution. Adapted from [39].....	34
Figure 5: Solids feed lance – front and bottom views.....	35
Figure 6: Schematic showing the position of the fibre inside the solids feed lance .....	37
Figure 7: Pure mineral cumulative % passing particle size distributions .....	43
Figure 8: Concentrate cumulative % passing particle size distributions.....	46
Figure 9: Chalcopyrite and pyrite desulphurization curves .....	51
Figure 10: Concentrate desulphurization curves.....	52
Figure 11: QEMSCAN® mineralogical map for Concentrate A with O <sub>2</sub> /S = 1.9 .....	58
Figure 12: SEM-EDS QEMSCAN® mineralogical map for Concentrate AB with O <sub>2</sub> /S = 1.9 .....	59
Figure 13: SEM-EDS QEMSCAN® mineralogical map for Concentrate B with O <sub>2</sub> /S = 1.9 .....	60
Figure 14: SEM-EDS QEMSCAN® mineralogical map for Concentrate AB with O <sub>2</sub> /S = 2.5 .....	61
Figure 15: Chalcopyrite product particle size distributions (cumulative).....	66
Figure 16: Pyrite product particle size distributions (cumulative).....	67
Figure 17: Concentrate A product particle size distributions (cumulative) .....	68
Figure 18: Concentrate AB product particle size distributions and associated P80 particle sizes .....	69
Figure 19: Concentrate B product particle size distributions.....	70
Figure 20: A typical emission spectrum from flash combustion reactions in the drop tower.....	71
Figure 21: Emitting species from flash combustion reactions in the lab .....	72
Figure 22: Flame temperature profile used in the Fourier flicker analysis .....	73
Figure 23: Fourier transform of the temperature profile (Figure 22).....	74
Figure 24: Allan Variance Analysis.....	75
Figure 25: A comparison of the pure mineral combustion temperature profiles as a function of O <sub>2</sub> /S stoichiometry.....	76
Figure 26: A comparison of concentrate combustion temperature profiles as a function of O <sub>2</sub> /S stoichiometry.....	77
Figure 27: A comparison of pure mineral combustion brightness profiles as a function of O <sub>2</sub> /S stoichiometry.....	79
Figure 28: A comparison of concentrate combustion brightness profiles as a function of O <sub>2</sub> /S stoichiometry.....	80
Figure 29: Chalcopyrite desulphurization to a 62% grade matte .....	83
Figure 30: Pure mineral mapping to the desulphurization of Concentrate A.....	85
Figure 31: Pure mineral mapping to the desulphurization of Concentrate B.....	86
Figure 32: Consumption (production) of major sulphide minerals in concentrate flash combustion.....	92
Figure 33: Evolution of products – Dust fraction in the products (bars on primary y-axis) and P80 particle size (line on secondary y-axis).....	95
Figure 34: Evolution of products – Dust fraction in the products (bars on primary y-axis) and P80 particle size (line on secondary y-axis).....	97
Figure 35: SEM-EDX image of a pseudochalcopyrite particle with fused particles on the exterior .....	98

Figure 36: Relationship between flame temperature and brightness .....	104
Figure 37: Flame temperature and brightness profiles for the test with Concentrate AB ( $O_2/S = 2.49$ , % $O_2 = 60\%$ ) .....	105
Figure 38: Two-wavelength temperature calibration experimental setup.....	118
Figure 39: Wavelength and temperature dependence of correction factors ( $^{\circ}C$ ) .....	119
Figure 40: Least of squares fit of the Planck Distribution to the corrected blackbody spectrum .....	120
Figure 41: Chalcopyrite, $O_2/S = 0.8$ , % $O_2 = 20$ .....	123
Figure 42: Chalcopyrite, $O_2/S = 1.5$ , % $O_2 = 40$ .....	124
Figure 43: Chalcopyrite, $O_2/S = 2.2$ , % $O_2 = 60$ .....	124
Figure 44: Chalcopyrite, $O_2/S = 3.0$ , % $O_2 = 80$ .....	125
Figure 45: Pyrite, $O_2/S = 2.0$ , % $O_2 = 50$ .....	126
Figure 46: Pyrite, $O_2/S = 3.0$ , % $O_2 = 74$ .....	126
Figure 47: Pyrite, $O_2/S = 4.0$ , % $O_2 = 98$ .....	127
Figure 48: Concentrate A, $O_2/S = 1.0$ , % $O_2 = 25$ .....	128
Figure 49: Concentrate A, $O_2/S = 1.9$ , % $O_2 = 45$ .....	129
Figure 50: Concentrate A, $O_2/S = 2.5$ , % $O_2 = 60$ .....	129
Figure 51: Concentrate B, $O_2/S = 0.9$ , % $O_2 = 20$ .....	130
Figure 52: Concentrate B, $O_2/S = 1.0$ , % $O_2 = 25$ .....	131
Figure 53: Concentrate B, $O_2/S = 1.9$ , % $O_2 = 45$ .....	131
Figure 54: Concentrate B, $O_2/S = 1.9$ , % $O_2 = 45$ .....	132
Figure 55: Concentrate B, $O_2/S = 2.5$ , % $O_2 = 60$ .....	132
Figure 56: Concentrate AB, $O_2/S = 1.0$ , % $O_2 = 25$ .....	133
Figure 57: Concentrate AB, $O_2/S = 1.9$ , % $O_2 = 45$ .....	134
Figure 58: Concentrate AB, $O_2/S = 2.5$ , % $O_2 = 60$ .....	134

## List of Tables

Table 1: A summary of expected flash smelting reactions [1] [2] [3] .....	7
Table 2: ICP-OES chemical analysis of the chalcopyrite feed .....	42
Table 3: Calculated feed mineralogy of the chalcopyrite .....	42
Table 4: QEMSCAN® mineral analysis of the concentrates.....	44
Table 5: Chemical composition of the concentrates (mass %) .....	45
Table 6: Summary of experimental tests and conditions .....	47
Table 7: Pure mineral fitting parameters for the sulphur removal curves.....	51
Table 8: Fitting parameters of the concentrate desulphurization curves.....	52
Table 9: XRD analysis of the pyrite product .....	53
Table 10: XRD analysis of the chalcopyrite reaction products.....	54
Table 11: Concentrate QEMSCAN® analysis; mineralogy of the combustion products .....	55
Table 12: Compositional limits of QEMSCAN® pseudo species .....	56
Table 13: QEMSCAN® chemical analysis of the products of drop tower combustion (concentrates).....	56
Table 14: Phase legend for the QEMSCAN® particle maps .....	57
Table 15: Mass yield to the products for the concentrate QEMSCAN® samples .....	90
Table 16: Impurity composition of pseudo species from the QEMSCAN® Analysis .....	94
Table 17: Heat model output with a water-cooled solids feed lance .....	121
Table 18: Heat model output with an air-cooled solids feed lance .....	121

# Chapter 1

## Introduction

Flash furnace smelting is used around the world to process copper sulfide concentrates; however, the impact of blend mineralogy is generally not considered when choosing the  $O_2/S$  stoichiometry required for matte production. Before smelting, the operation blends concentrate(s) to a target chemical composition, typically given by the Cu/S ratio. It is possible to have many concentrates with equivalent elemental compositions but different mineralogies. This impact of mineralogy on the flash combustion behaviour of blends is important, poorly understood and not monitored.

The uncertainty around the feedstock composition on matte production is aggravated by the fundamental lack of monitoring and control technologies available for non-ferrous pyrometallurgical processes. Operators rely on experience, chemical analyses of products, and empirical models to operate the smelter. In flash furnace smelting, poor combustion conditions inside the furnace, that stem from changes in feed distribution, feed composition or other operational upsets, may not be identified until the next, off-line chemical analysis of the products, which may be on the order of hours. The implementation of monitoring technology, specifically into flash furnace smelters and generally in non-ferrous pyrometallurgical processes, has the potential to improve furnace operation and reduce operating costs. These improvements would stem from improved knowledge of the process and faster response times to operational upsets.

This thesis evaluates the impact of mineralogy on the flash combustion behaviour of pure minerals and concentrates through experimental research in a drop tower reactor. In tandem, the feasibility of emission spectroscopy for real time burner monitoring will be evaluated. The hypothesis of this work is that concentrate mineralogy is more important than conventionally thought and that emission spectroscopy may be useful for monitoring the burner in flash furnace

smelting. An explanation of the flash smelting process including its chemistry and operational strategy is given next to provide context to the details of this thesis.

## **Flash Smelting of Copper**

Flash furnace smelting is a continuous feed, batch tap, pyrometallurgical process. The process was commercialized by Outokumpu (now Outotec) in 1949 and as of 2016, was used to smelt >50% of the world's copper concentrate. [1] Flash smelting is used to process copper sulfide concentrates and small amounts of secondary materials such as dust generated by the process. The goal of the process is to pre-oxidize the iron sulfide and some impurities, provide the heat to smelt the concentrate and provide the infrastructure to capture the SO<sub>2</sub>. This is accomplished with a high utilization of O<sub>2</sub>. The products of flash smelting are a copper rich matte, a fayalite slag and an off-gas concentrated in SO<sub>2</sub>. The matte contains >98 wt. % of the feed copper and the fayalite slag is a molten Fe-Si-O system that typically has <2% copper metal in it (much of this as suspended matte). [1] The five main components of a flash smelting furnace are: the concentrate burner, reaction shaft, settler, tap holes and gas off take, each of which are explained in detail below.

The concentrate burner introduces fine, dried Cu-Fe-S concentrate and enriched air into the reaction shaft of the furnace. When operating the burner, the goal is to disperse the solids uniformly throughout the reaction shaft so that iron sulfides can be converted to iron oxides – it is also expected that some copper sulphides along with impurities are also oxidized. When operational issues with burner operation occur (ex: feed clogs, distribution problems) or the feed composition changes, interruptions to production can happen. For this reason, a sensor that monitors the burner and alerts operators to abnormal operating conditions would be of use.

The reaction shaft is where most of the oxidizing reactions occur. Particles introduced through the burner heat up rapidly and ignite. Post-ignition, exothermic reactions between the Cu-Fe-S concentrate and O<sub>2</sub> proceed, removing sulphur from the feed and supplying heat to the furnace. Excluding the dust, particles pass through the reaction shaft and settle out as molten phases in the

settler of the reactor. Usually, the chemical energy in the feed allows the furnace to be operated autogenously, however, in some cases, concentrates don't have enough chemical energy (ex: low sulphur concentrates) and extra heat is required to maintain the process heat balance. Additional heat may be supplied in the reaction shaft by burning natural gas ( $\text{CH}_4$ ) or by adding sulphur to the feed. A sensor that is installed within the reaction shaft of the furnace would allow the burner flame to be monitored and may be able to provide information that pertains to the furnace heat balance.

The tap holes in the settler of the furnace are used to remove molten material once enough has built up. Molten matte and slag are tapped (removed) from the settler and are transported to the next stages of processing (converting and slag cleaning). During tap cycles, samples of the product are taken and analyzed so that operators can make adjustments to operational parameters

The gas off-take is used to handle the  $\text{SO}_2$ -rich gas that forms from the flash reactions. One of the main problems of flash smelting is dust formation, which becomes entrained in the off-gas stream. Heat and dust are recovered from the off-gas before it is treated in a sulphuric acid plant to fix the  $\text{SO}_2$  into solution.

## **Furnace Operation**

Operators can tune the smelting process by adjusting a very limited number of control variables. The main control variables in a flash furnace are the concentrate feed composition, blast feed rate, blast oxygen enrichment, silica ( $\text{SiO}_2$ ) flux feed, rate and  $\text{CH}_4$  combustion rate. These parameters are typically measured relative to a set concentrate feed rate. [2] [3] Operational parameters that are used to control the process are summarized [2]:

- Concentrate feed rate: The concentrate feed rate is usually fixed. The other process control variables are adjusted relative to it.

- Feed Composition: The mineralogy and chemical composition of the concentrate can be controlled by blending. Operations teams may know the blend composition entering the furnace, however the blend is typically set by a separate team.
- O<sub>2</sub> feed rate & Enrichment Oxygen input to the furnace is controlled by the feed rates of pure oxygen and air. The furnace is typically operated with a highly enriched blast. The O<sub>2</sub> feed rate controls the oxidation of the feed.
- Flux feed rate SiO<sub>2</sub> flux is added to the furnace to control the behaviour of the slag. SiO<sub>2</sub> is added to lower the slag liquidus point and viscosity so that handling and separation from the matte is easy.
- Furnace temperature The furnace temperature is maintained at ~1300°C by adjusting the CH<sub>4</sub> combustion rate or the enrichment of the blast. Heat release increases with blast enrichment.

Furnace operators only have six operational variables available to them to control the process and the control variables impact each other which makes furnace operation difficult. Because technology does not exist for flash furnace smelting, many operational decisions are made after tap cycles from chemical analyses and temperature measurements of the matte and slag. Flash furnace smelting is a batch tap process which means that there is always a time delay associated with measures of operational performance. Real-time information from sensors could allow

operators to identify abnormal conditions between tap cycles which could improve furnace operation and economics.

## **Advantages and Disadvantages of Flash Furnace Smelting**

Advantages of the flash furnace smelting include:

- High throughput: Flash furnaces are productive with the largest furnaces using feed rates in the range of 165 – 210 MTPH. [4] Because of the high throughput, the unit cost of production is low. [1]
- Saleable byproducts The SO<sub>2</sub> content of the off-gas stream is typically in the range of 15 - 35% which allows for production of high quality sulphuric acid. The acid can be recycled in the process or sold as a byproduct.  
  
The fayalitic slag, if not contaminated with harmful compounds, can be sold as construction material.
- Energy efficiency: Flash smelting is usually operated close to autogenously. CH<sub>4</sub> fuel requirements are minimal and heat from the off-gas can be recovered & recycled.
- Flexibility: Flash furnaces can handle feeds of different compositions and produce mattes of varying grades. [5]
- Long campaign life: The campaign life of flash smelters is on the order of 10-years. [6]
- Environmentally friendly: A sealed reactor and SO<sub>2</sub> fixation mean that SO<sub>2</sub> emissions into the atmosphere are minimal. As well, a stable, saleable slag can be produced. This means large amounts of waste material are not generated.

Disadvantages of flash furnace smelting include:

- Dust production: 5 – 10% of the feed to a flash furnace is recovered as dust. The dust has value as it is rich in copper and can contain precious metals. [3] Dusting reduces throughput and can create operational issues by accumulating in the waste heat boiler. [5]
- Accretions Dust production can lead to accretions in the off-gas handling system of the furnace. If accretions are not managed, they can damage infrastructure when they get too big. [7]
- Inability to smelt scrap Flash furnaces are only able to smelt material with a fine size distribution. The economics of size reduction for scrap does not justify their processing in a flash furnace. [3]
- High Cu losses to slag Flash smelting has copper losses to the slag which necessitates slag cleaning to recover the copper. [1]

Flash furnace smelting is a complex process. Even though feed flexibility is considered an advantage, it can lead to tough operational situations. A sensor for burner monitoring would be useful for real-time identification of changes in feed composition. This may be useful for identifying poor combustion situations that lead to increased dusting and accretion formation. Through burner monitoring, it may be possible to minimize the disadvantages of flash furnace smelting, such as dusting and accretions.

### **Concentrate Blending**

Concentrate blending is done to maintain a target Cu/S ratio by mixing concentrate(s), SiO<sub>2</sub> flux and other materials. [3] The chemical composition of copper concentrate from the mine is

typically 20-30 wt. % Cu, 25 – 35 wt. % Fe and 25 – 35 wt. % S. [8] When comparing two blends to a flash furnace, they may have the same chemical composition but different mineralogies. The mineralogy impacts furnace operation since minerals have distinct reaction mechanisms and conditions required for smelting (see Chapter 2 - Literature Review). This challenge of processing different concentrate blends is especially true for custom smelters, which may process over 50 different concentrate blends in a year. It would be useful to have a quantitative understanding of the impact that typical minerals in a concentrate have on the flash smelting process, as this information could be used to improve operation and help with the sourcing of new feeds and modifying blend compositions.

Changing blends during the continuous operation of a flash furnace is an operational challenge because feed composition entering the furnace is not measured in real time and the effect of mineral constituents on the flash combustion reactions is not well understood. When the blend changes, the heat balance of the process is affected, and operational variables need to be adjusted to maintain product quality and furnace throughput. Changes in furnace temperature can be measured; however, the product composition is not known until the next tapping cycle. A sensor that can identify changing conditions associated with the feed composition may be useful for identifying poor combustion situations between tap cycles and improving furnace operation.

## **Pyrometallurgy of Copper Smelting**

Flash combustion reactions are mostly completed in the reaction shaft of the furnace, where the reaction kinetics and residence time are fast. The reaction mechanisms for typical concentrate minerals are summarized in Table 1, and mainly involve the oxidation of iron sulphide feed.

**Table 1: A summary of expected flash smelting reactions [1] [2] [3]**

Reaction	Equation No.
----------	--------------

<i>Primary</i>	
$2CuFeS_2 + 2.5 O_2 \rightarrow Cu_2S + FeS + FeO + 2SO_2$	1-1
$2Cu_5FeS_4 + 2.5O_2 \rightarrow 5Cu_2S + FeS + FeO + 2SO_2$	1-2
$FeS_2 + O_2 \rightarrow FeS + SO_2$	1-3
$FeS + 1.5O_2 \rightarrow FeO + SO_2$	1-4
<i>Secondary</i>	
$2CuS + O_2 \rightarrow Cu_2S + SO_2$	1-5
$2FeO + SiO_2 \rightarrow Fe_2SiO_4$	1-6
<i>Over Oxidized</i>	
$Cu_2S + 1.5O_2 \rightarrow Cu_2O + SO_2$	1-7
$Cu_2S + O_2 \rightarrow 2Cu^o + SO_2$	1-8
$FeS + Cu_2O \rightarrow FeO + Cu_2S$	1-9
$6FeO + O_2 \rightarrow 2Fe_3O_4$	1-10

The reactions in Table 1 show that the products of reaction in the furnace shaft are a mix of oxides and sulphides. The reactions that happen in the shaft of the furnace (Equations 1-1, 1-2, 1-3, 1-5) pre-oxidize the feed before the particles settle out as molten phases. These reactions and the associated kinetics produce a flame underneath the concentrate burner. Monitoring of the reactions that happen in the shaft of the furnace may be useful for quantifying the performance of the burner and identifying poor combustion situations.

The target (Cu + Fe) : S ratio in the matte is one which is represented by the compounds  $Cu_2S$  and  $FeS$ , and the weight percent of copper is called the matte grade. As the matte grade is increased, iron and sulphur are removed from the matte by Equation 1-4 in Table 1. If copper

becomes over oxidized to  $\text{Cu}_2\text{O}$  in the reaction shaft, it will react with  $\text{FeS}$  in the settler according to Equation 1-9 as Fe has a greater affinity for oxygen than Cu. [1] The matte-slag interface is important as liquid phase reactions limit the transport of Cu into the slag.

The heat balance of the flash furnace is an important variable to control. The process is usually operated autogenously, with much of the heat supplied by the exothermic reactions in Table 1. In cases where the feed does not have enough energy,  $\text{CH}_4$  burners can be employed. The reaction shaft  $\text{CH}_4$  burners are used in cases where the concentrate is low in energy (low sulphur content) or when the temperature is dropping. In the settler of the reactor,  $\text{CH}_4$  burners are used to maintain the molten phases at a desired temperature. The heat balance of the furnace can be changed through the following variables:

- Feed Composition: Feed composition to the furnace affects the heat balance through the mineralogical and chemical composition. Heats of reaction for different minerals will affect the thermal balance of the furnace. Sulfides act as fuel, adding heat to the furnace while oxides act as heat sinks.
- $\text{O}_2$  Enrichment (%): The amount of air that is introduced to the furnace affects the heat balance because of the nitrogen content. The nitrogen is an inert gas and will act as a heat sink for the process. Air may be enriched by  $\text{O}_2$  to a maximum of 100%  $\text{O}_2$ .
- $\text{O}_2$  Feed Rate The heat balance of the furnace is affected by the  $\text{O}_2/\text{S}$  stoichiometry through the pre-oxidation of the feed in the furnace shaft. If desulphurization of the feed does not happen in the furnace shaft, additional heat will be required to maintain the thermal balance of the furnace.

- Furnace heat loss                      Furnaces lose heat through water cooling elements in the furnace walls as well as by heat that is conducted through the walls and eventually away from the furnace by convection. [2]
- CH<sub>4</sub> combustion rate:              CH<sub>4</sub> can be burned to add more heat to the furnace in the reaction shaft or settling zone.
- Blast preheat                              Many operations pre-heat the blast so that particles reach ignition temperature faster.

Exothermic reactions in the reaction shaft of the furnace supply the heat required for smelting. If the pre-oxidation of the feed does not occur in the shaft of the furnace, the heat balance will be impacted, and additional heat will be required to maintain the furnace temperature. Burner monitoring has the potential to identify poor combustion situations in the furnace shaft. Identification of such situations has the potential for better thermal management, reduced CH<sub>4</sub> usage and the ability to produce a matte with consistent Cu grade. .

## **Project Goals**

There is a fundamental lack of process control technology available for flash furnace smelting, because the hot and corrosive environment inside the furnace is hostile to conventional optical and electrical as well as electrochemical sensors. Because of this challenging environment, instrumentation typically does not hold up well inside the furnace – in fact, it is not even generally attempted. An optical sensor for burner monitoring in copper flash smelting was developed by the

University of Concepcion. Kingston Process Metallurgy is working on the commercialization of the sensor which uses fibre-optics and optical emission spectroscopy to analyze the light emitted from the combusting particles in the flash furnace reaction shaft. It is hypothesized that there may be correlations between the emission spectrum, process control variables and the outcome of flash combustion reactions. Through lab scale, experimental research of the reaction shaft of a flash furnace, a deeper understanding of the chemistry of the burner reactions will be gained, while completing proof of concept testing of this novel optical sensor for burner monitoring. It is the goal of this research to quantify the impact of pure minerals, chalcopyrite and pyrite, on the flash combustion of concentrates, while evaluating the commercial viability of emission spectroscopy for burner monitoring in flash furnace smelting. By knowing the impact that minerals in a blend have on the combustion process, O<sub>2</sub> inputs to the furnace could be optimized so that a consistent matte grade is produced. Such knowledge would be especially useful for custom smelters where feed composition changes. The results of this research will indicate whether development of this sensor should progress to a plant trial.

## Chapter 2

### Literature Review

#### Research into Flash Reactions

The literature on flash smelting has focused on the reaction & ignition mechanisms, desulphurization behaviour as well as particle combustion temperatures of pure minerals ( $\text{FeS}_2$ ,  $\text{CuFeS}_2$ ,  $\text{ZnS}$ ,  $\text{PbS}$ ) as a function of experimental variables; namely oxygen enrichment, experimental temperature and particle size. Experimental work has been done using laminar flow or stagnant gas furnaces at very low feed rates ( $< 250 \text{ mg/min}$ ) to approximate single particle feeding. In these tests, the  $\text{O}_2/\text{S}$  stoichiometry was maintained far in excess of 1.0 such that mass transport of  $\text{O}_2$  to the particle did not limit the progress of the reaction. The literature on flash furnace smelting has captured differences in mineral behaviour; however, the feed rates were very low and the  $\text{O}_2/\text{S}$  ratios were not representative of the industrial process, which operates close to  $\text{O}_2/\text{S} = 0.8$ . This thesis used increased feed rates (3-5 g/min) with  $\text{O}_2/\text{S}$  stoichiometries that better capture the commercial reactor. Further, the behaviour of pure minerals and concentrates will be studied in an attempt to quantify the effect of pure minerals on the flash behaviour of concentrates. Previously reported research as well as findings about ignition, reaction mechanisms, desulphurization behaviour, combustion temperatures and emission spectroscopy of flash processes have been summarized to provide the context for this thesis.

#### Laboratory Reactors

Lab scale research into flash combustion reactions has been done in laminar flow and stagnant gas furnaces. [9] [10] [11] [12] [13] Both furnaces consist of a heated reaction tube through which gas and particles are dropped. Experimental variables that can be controlled are the reactor temperature, feed composition, feed PSD, %  $\text{O}_2$ ,  $\text{O}_2/\text{S}$  stoichiometry and gas residence time. The main difference between these reactors is related to gas flow: a laminar flow furnace has a

continuous, non-turbulent flow of gas through the reactor, whereas a stagnant gas furnace has almost no gas flowing through it. These techniques have been very useful for advancing flash smelting research, however the feed rates are very low and the O<sub>2</sub>/S reaction stoichiometries are much higher than practical in commercial operations. Research into flash combustion reactions using higher feed rates in continuously fed reactors is much less prevalent. Dr. Roberto Parra's research group has studied flash smelting using a continuously fed, drop tower reactor, with feed rates in the range of 3-5 grams per minute. [14] There are no other continuously fed, experimental studies of copper flash smelting in the literature that use feed rates in this range. Thus, the scope of the current research will evaluate, in part, how the results from single particle tests scale up to continuously fed experiments, while completing proof of concept testing of a novel optical probe for burner monitoring. All of this is important in the context of being able to test the sensor on both single minerals and on blends to be able to understand the capabilities of the probe in a commercial setting.

### **Particle Ignition**

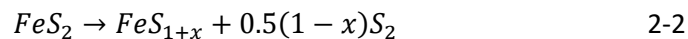
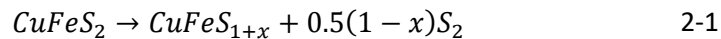
Particle ignition in flash furnace smelting is important to consider as oxidizing flash reactions cannot proceed without it. Once ignited, the oxidizing flash reactions proceed quickly. Particles first heat to reach their ignition temperature, which is a rapid, endothermic reaction. Jorgensen, Moyle and Wadsley found that "the ignition temperature of a particular combination of solid substance and gaseous oxidant is not a fixed property of that combination. It is determined by the interplay of heat and mass transfer prevailing in each combustion situation". [11] This observation is significant for an industrial furnace because operators must process blends with different mineralogies. Within a single blend, there is temporal and spatial variability in feed composition entering the furnace. Further, there may be operational issues such as feed distribution that create poor or variable combustion/ignition conditions in the shaft of the furnace, which can lead to variable product quality that can only be identified once tapped from the furnace. Because

there is no fixed condition for ignition, monitoring of the burner may be useful for identifying situations that aren't promoting the ignition of the feed.

Jorgensen has grouped minerals into three categories based on their ignition mechanism [10]:

1. Ignition is achieved when the particle melts. (ex:  $\text{Cu}_2\text{S}$ ,  $\text{FeS}$ ,  $(\text{Fe,Ni})_9\text{S}_8$ ,  $\text{NiS}$ ,  $\text{FeNiS}_4$ )
2. Vaporization of the mineral produces a fume around the particle. The ignition of the fume drives the increase in the particle temperature and its ignition. (ex:  $\text{ZnS}$ ,  $\text{PbS}$ )
3. Thermal decomposition and structural changes on the mineral surface drive particle ignition. (ex:  $\text{CuFeS}_2$ ,  $\text{FeS}_2$ )

It is clear from these three types of ignition mechanisms that minerals require distinct conditions to achieve ignition and the mechanism is dependent on the mineral as well.  $\text{CuFeS}_2$  and  $\text{FeS}_2$  are key minerals in the feed for flash smelters and the behaviour of these minerals is being studied as part of this thesis. Their ignition mechanisms are presented (2-1 & 2-2) and are discussed in detail.



For both  $\text{CuFeS}_2$  and  $\text{FeS}_2$ , thermal decomposition and structural changes are the key steps that drive ignition. A porous structure is created on the particle surface after decomposition, which increases the surface area to volume ratio and allows oxygen to penetrate the reaction surface. Sulphur that is evolved from the decomposition reaction is thought to “kick start” ignition when it becomes oxidized near to the particle surface providing the heat required for smelting. [11]

The effect of experimental variables on ignition was studied by Jorgensen. He made the following findings about the effect of oxygen, reactor temperature and particle size on the ignition behaviour of  $\text{CuFeS}_2$  and  $\text{FeS}_2$  particles [9]:

- Oxygen enrichment in the range 5 – 100% does not seem to impact the time to reach ignition but rather influences the reactions that take place post ignition.
- Reactor temperature affects the time particles take to ignite, however the effect seems to plateau after a certain temperature. It is likely that this is a case of improved heat transport to the particle.
- The particle size distribution affects the time it takes a particle to ignite, where larger particles require more time to reach their ignition temperature. This is likely related to heat transport and heat capacity where larger particles require more time to reach their ignition temperature.

Promoting the optimum ignition conditions in the shaft of the furnace is important for operation. In a pilot plant study by Kemori, it was found that a higher concentrate combustability (referred to as desulphurization in this study) and furnace oxygen efficiency could be achieved with the early ignition of concentrates. As well, the concentration of inerts in a blend affects the desulphurization as inerts have high ignition temperatures and act as heat sinks to the process. [15] It is hypothesized that the optical probe being tested in this thesis will be able to identify poor ignition conditions in realtime. Such a monitoring capability could improve furnace operation by allowing operators to proactively adjust furnace parameters in between tap cycles with the goal of producing a consistent grade matte.

### **Desulphurization in Flash Smelting**

Many of the single particle combustion tests in the literature use sulphur removal curves to show the effect of experimental variables on the conversion of the flash combustion reactions. Typical sulphur removal curves show the % sulphur remaining as a function of oxygen enrichment. The effect of %O<sub>2</sub>, reactor temperature and PSD have been researched with the results summarized:

- Desulphurization of the feed increases with % O<sub>2</sub> in the range of 0 – 60% for chalcopyrite. [9]
- At low temperatures, ignition, reaction kinetics and desulphurization are impacted. [9]
- If particles are too coarse and ignition is not achieved, less desulphurization of the feed occurs.

To date, research has focused on sulphur removal of single particles for pure minerals. [9] [11] [12] [13] [16] [17] [18] [19] The existing literature has already identified that minerals behave differently in flash combustion reactions, however this data has never been used to quantify the behaviour of multicomponent concentrates. It is hypothesized that pure mineral desulphurization behaviour can be mapped onto a concentrate when its mineralogical composition is known.

### **Combustion Temperatures**

Optical pyrometry has been used to characterize particle combustion temperatures for flash smelting in the lab. There seems to be no experimental work at the industrial scale to evaluate the scale up of these combustion temperature results. Figure 1 summarizes the maximum temperature of single CuFeS<sub>2</sub> [9], FeS<sub>2</sub> [9] and PbS [12] particles combusting in laminar flow or stagnant gas furnaces. The values used to generate Figure 1 were estimated from the cited articles and thus, the values are approximated.

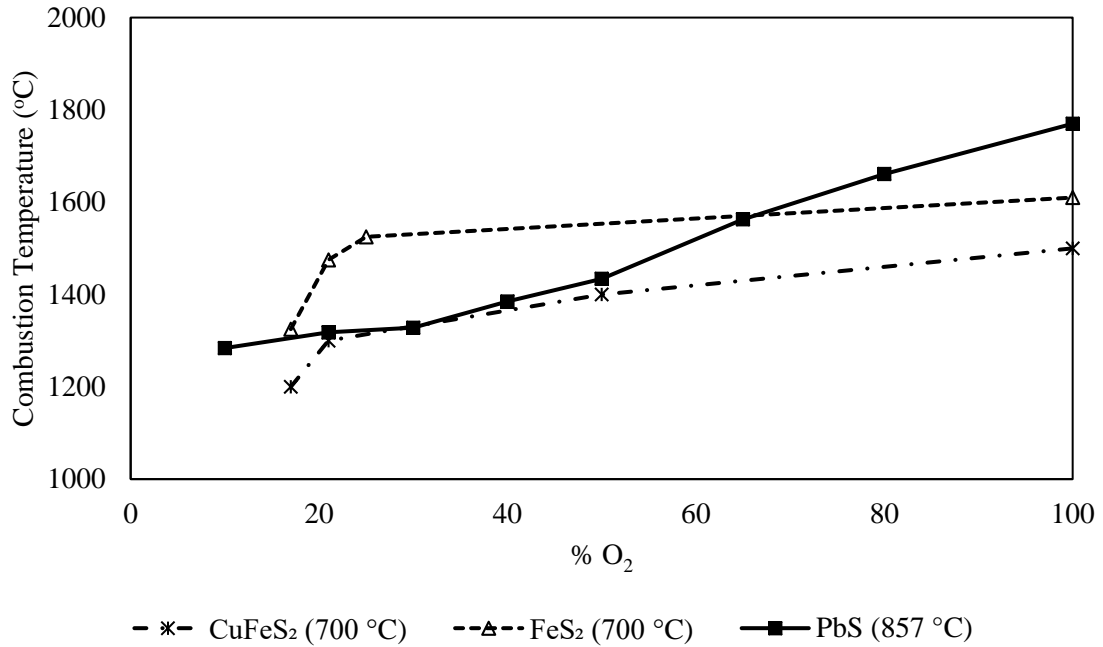


**Figure 1: Pure mineral, single particle combustion temperatures. Values were estimated from figures presented in [9] [12]**

Tuffrey et al. characterized the temperature of single FeS<sub>2</sub> particles combusting in an 857°C stagnant gas furnace. [17] Their temperature measurements showed that pyrite was burning at temperatures in the range of 2000 – 3500°C under conditions of 10 – 100% O<sub>2</sub>. [12] [17] These combustion temperatures are very high compared to those reported by Jorgensen. [9]

Figure 2, which was taken from one of Dr. Parra's papers, shows the combustion temperatures of three chemically and mineralogically distinct concentrates. [14]

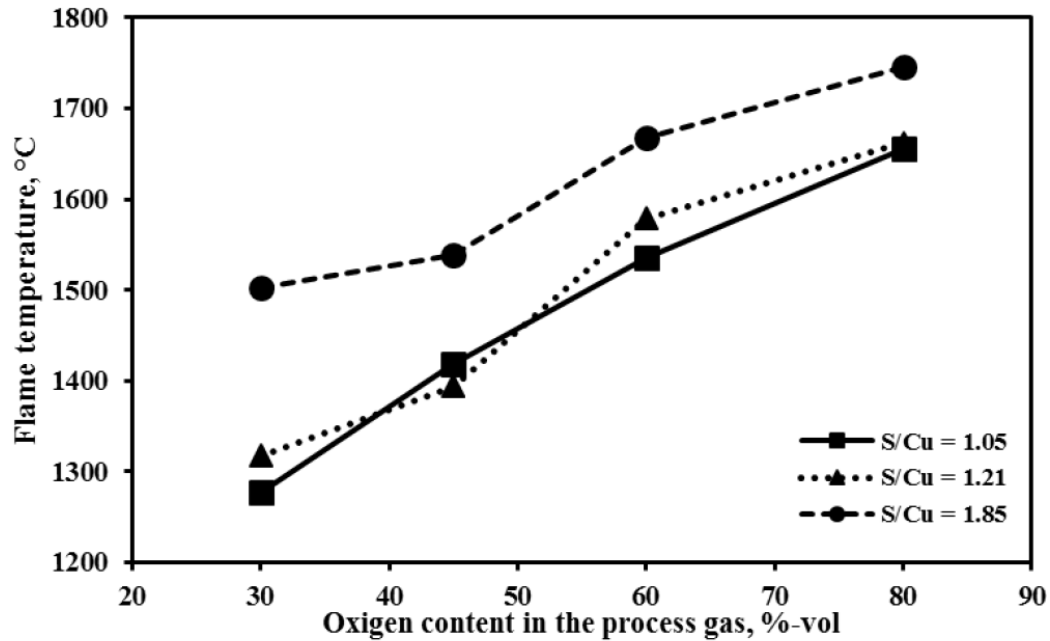


**Figure 2: Effect of concentrate composition and oxygen content in the process gas on flame temperature. Taken from ref [14]**

The flame temperatures in Figure 2 were calculated from the emission spectrum using the two-wavelength method, the same technique used in this thesis. [14] The trend in Figure 2 is that the concentrate flame temperature increases with O<sub>2</sub> enrichment when O<sub>2</sub> mass transport is not limiting the reactions (the O<sub>2</sub> flow rate was ~100× the stoichiometric requirement). [14] This is consistent with pure mineral studies. It is interesting that the concentrates with S/Cu ratios of 1.05 and 1.21 cannot be differentiated based on their temperature. [14] With greater S content, there should be more fuel available for combustion, which would increase the flame temperature. The mineralogy of the concentrates in Figure 2 may be affecting the combustion temperatures of these three concentrates. In this thesis, the Cu, Fe and S assays of the three concentrates that are tested are the same, which allows for their mineralogy to be isolated.

The key variables, aside from oxygen, that were found to affect the combustion temperature are:

- Particle size: Larger particles typically burn at cooler temperatures than fine particles except for  $\text{FeS}_2$  in which combustion temperature was found to be independent of particle size. [9]
- Furnace/reactor temperature: The combustion temperature of minerals increases with the furnace temperature which is likely related to heat transfer. [9]

Minerals burn at different temperatures and combustion temperature is driven by oxygen enrichment. In previous studies, mass transport as a limiting factor has been removed from the experiments by maintaining  $\text{O}_2$  stoichiometries far in excess of S. For example, in the tests by Tuffrey et al, a 250 mg/minute feed rate was used with a 12 LPM gas flow rate through the reactor. [17] With  $\text{CuFeS}_2$  this represents a range of  $\text{O}_2/\text{S}$  stoichiometries of 15 – 181, which is much greater than the commercial operating point (typically  $< 1$ ). In the current research, testing where mass transport was not a limiting factor was done first to verify that the experimental technique works in the drop tower. Once a flame was produced, tests with lower  $\text{O}_2/\text{S}$  ratios were then executed to capture combustion temperatures in situations where mass transport may be a limiting factor and more representative of the commercial operating condition. Similar to previous studies in the literature, the two-wavelength method will be used to calculate the flame temperature from its emission spectrum. Because flame temperature is tied so closely to oxygen enrichment and because oxygen is one of the key control variables for commercial furnaces, flame temperature may be a useful diagnostic measure for burner performance in flash smelting.

### **Emission Spectroscopy of Flash Combustion Processes**

The research of this thesis was guided by Dr. Roberto Parra, who has also worked on burner monitoring with an optical probe, at the University of Concepcion, Chile. Dr. Parra's group

provided a license to KPM to develop and commercialize the sensor in this thesis, which uses emission spectroscopy and fibre optics to study the radiation of a flame formed in flash furnace smelting. Dr. Parra has studied the impact of O<sub>2</sub> enrichment and concentrate composition on the emission spectrum of the flame as well as the flames emissivity. [14] [20] For the emission spectrum of the flame, Dr. Parra's group found that as the O<sub>2</sub> enrichment is increased, the intensity (referred to as brightness in this thesis) of the emission spectrum increases [14]. In laboratory tests, Dr. Parra identified emission lines at 588.9 nm and 767 nm (as a doublet). [20] The 767 nm emission was assigned to K. [20] Emissivity calculations showed that copper concentrates exhibit graybody behaviour in the visible region of the spectrum between 600 to 760 nm. [20] Dr. Parra was also able to complete a trial of the sensor in a commercial flash furnace, in which other emitting species appeared in the spectrum. [20]

### **Process control in metal production – Using sensors**

R&D is difficult in the metallurgical industry because of the capital-intensive nature of metal production. Operations do not want to be the first to try something, but if successful, they certainly want to be the second. As well, smelting operations are hesitant to provide plant data due to the competitive advantage that one's optimized process provides. Process control technology would ideally be developed in-house, but this assumes that the expertise was present and there is a perceived need for such technologies. The secrecy surrounding the process and the reluctance to accept outside support are part of the reason why there are almost no third-party technologies available to non-ferrous, base metal producers. The Expert Furnace System Optimization Process (EFSOP) and Optical Production Control (OPC) are two process control technologies that have been commercialized for pyrometallurgical applications. Case studies of the two technologies as well as how they were commercialized are summarized with implications for the commercialization of the optic sensor being developed in the current research.

### **Tenova Goodfellow – EFSOP®**

Tenova Goodfellow Inc. commercialized the Expert Furnace System Optimization Process (EFSOP), which is a process control technology for electric arc furnace (EAF) steelmaking. EAF steelmaking is a batch, pyrometallurgical process for scrap and by-product recycling. The process involves melting charged scrap and bubbling oxygen through the melt to oxidize impurities into the slag or off-gas. Process heat is supplied chemically by decarburization reactions in the melt, by methane burners as well as electrically using an arc between graphite anodes and the charge. EFSOP is used to optimize EAF steelmaking by continuously analyzing CO, CO<sub>2</sub>, H<sub>2</sub> and O<sub>2</sub> concentrations in the off-gas in real time. EFSOP measures CO and CO<sub>2</sub> concentrations using infrared spectroscopy, H<sub>2</sub> concentration using a thermal conductivity sensor and O<sub>2</sub> concentration with an electrochemical cell. [21] These measures are used to quantify combustion, chemical and electrical energy efficiency and dynamically control oxygen injection to the process.

EFSOP was commercialized between 1996-98 by Tenova Goodfellow in partnership with Canadian government funding agencies (SDTC, OCETA), academia (University of Toronto) and industry (Hamilton Steel Group, St. Mary's Cement). [22] The first unit was installed in the UK in 1998 and presently, there are more than 95 EFSOP units installed around the world. The commercial success of the EFSOP can be attributed to the following factors:

- The first installation succeeded in adding value to the operation. This early success became an excellent marketing strategy to further its development.
- The benefits of the technology are quantifiable and has led the company to guarantee performance savings as part of the purchase agreement. [23] Quantifiable impacts on the operation are key for marketing the sensor.
- The payback period of the technology is fast as the optimisation process can be completed in 3-4 months.

- Installation is quick and uncomplicated. EFSOP can be installed without causing EAF downtime and once installed, EFSOP operates with < 10% downtime. This is essential as operations cannot afford downtime.
- Little maintenance time is required - approximately 15 minutes per week is needed and calibrations are only required every two weeks both of which do not affect furnace availability

The design of the EFSOP technology is extremely robust as demonstrated by the functionality of the first sensor, which lasted more than 10-years. The technology consists of a custom-made gas analyzer, a water-cooled gas sampling probe as well as a control and data acquisition system that is connect to the plant programmable logic control system. Gas samples, taken at the outlet of the EAF, are filtered and dried using a high-pressure filter before passing through the analyzer. Entrained dust in the gas builds up over time in the sample line and in the filter, however EFSOP has gas purge systems built into it that can remove buildup during operation. [21] To have success with a sensor, it needs to have a high operational availability. A key design consideration for the sensor in this research will be robustness of design when commercial testing begins. The successes of EFSOP in this regard can be drawn on for the flash furnace burner monitoring sensor.

### **Scandinavian Emissions Technology – Optical Production Control**

The Optical Production Control (OPC) technology was developed and commercialized by Scandinavian Emissions Technology (SEMTECH) for Pierce Smith (PS) copper converting. PS converting is a batch, pyrometallurgical process that is used to convert copper matte to blister copper (99 wt% Cu) by injecting oxygen through submerged tuyeres into a molten bath. Converting is accomplished in two stages: the slag forming stage, during which the Fe in the matte is oxidized into the slag, and the copper making stage, where sulphur is oxidized to SO<sub>2</sub>. The OPC uses fibre optics and emission spectroscopy to monitor emitting, vaporized species above the bath to identify the end point of the slag making stage. The OPC is one of the only real-time, continuous sensors that has been commercialized for non-ferrous, pyrometallurgical, base metal production.

The OPC sensor consists of a fibre optic probe and a spectrometer. Light emitted from the vapour phase above the bath is sampled. The signal consists of a continuum of blackbody radiation which is overlaid with discrete atomic and molecular emission lines, like the signal that is acquired in the current research. Molecular emission lines from lead species PbS, PbO and CuOH were found to be good indicators of the oxidation state of the process. The lead emission lines are present throughout the converting cycle and the CuOH emission line appears and persists during the copper making stage of the converting cycle. [24] Calibration factors are applied to the emission lines and the optical data is presented to operators in the form of an optical production parameter which can support operator decision making. [25]

Based on literature about OPC, the development of the technology began in 1987. SEMTECH identified the opportunity for spectroscopic monitoring of the PS converting process and for improvement in end-point determination of the process. Before OPC, operators used the colour of the flame as a process indicator. The first OPC test involved plant data collection of the absorption and emission spectra of the vapor phase. Differences in the emission spectra and emitting species during the slag and copper making stages were identified and supported with thermodynamic modelling of the process which justified further development of the technology.

The first technology was installed in 1994 and by 1999, the OPC had been installed on 19 PS converters. The benefits of the OPC are that they reduce converter cycle time and increase unit productivity of PS converters. As well as the PS converter, the OPC has been tested in Ausmelt, anode and flash furnaces as well as kaldo, anode, CLU and LD converters. [26]

The use of OPC in PS converting has persisted; in 2017, 25-30% of the world blister copper production from PS converting was monitored by OPC. From the literature, it seems that the OPC was commercialized by first collecting industrial data, building a technical case for the technology, validating the initial results through further testing and using the results for marketing. While OPC has had a lot of success testing their technology in different applications, it appears they have not built upon the original measuring principle. Unlike the EFSOP, there are no documented improvements to the OPC technology.

The measurement principle of the OPC is the same as the optical sensor which is under commercialization in this study. Based on the commercialization path of SEMTECH, the key to gaining access to operations is being able to support your technical case with actual plant data. SEMTECH was very successful in testing their technology in many different types of furnaces. This is likely because of the passive nature of fibre optic sensors which do not interact with the process and have a low likelihood of impacting production. As well, fibre optic sensors can 'see' the emitting body without having to interact or touch the hot, corrosive environment. Such stand-off sensors are a much more robust option for monitoring pyrometallurgical processes. SEMTECH's OPC was tested on a flash smelting furnace however they didn't garner any success with it. This may be because they limited their control applications to lead and copper emission lines. There is a lot of other information that can be extracted from a flame emission spectrum. This study aims to demonstrate that emission spectroscopy is a viable technique for monitoring the burner in flash furnace smelting.

## **Emission Spectroscopy of Flames**

Emission spectroscopy is the study of the energy that is emitted by atoms or molecules due to electronic or vibrational transitions. This technique is useful for studying flash combustion processes because at high temperatures, electromagnetic radiation is emitted in the visible region of the spectrum and one might expect atomic and/or molecular emissions from Cu and Fe species as well as molecular S, O or N species on top of a continuous blackbody emission background. [27]

Within a flame, there are thus three different types of spectra that can be observed: [28]

- i. Continuous (blackbody) emission
- ii. Line Spectra from free atoms
- iii. Band Spectra from molecules

### **Blackbody Radiation**

Continuous, or blackbody radiation, is emitted from heated solid or liquid bodies, predominately in the infrared and visible regions of the spectrum. [29] In the drop tower, blackbody radiation is emitted from the glowing reactor walls and the heated and combusting solid concentrate particles. The energy distribution of a blackbody, i.e. its emission spectrum, is a function of the emitting body's temperature. As the temperature of the emitting body is raised, the brightness of the radiation, i.e. the integral of the emission spectrum, increases with the fourth power of the absolute temperature according to the Stefan-Boltzmann law. [29] An increase in the temperature also causes the maximum of the emission spectrum to shift to shorter wavelengths – red emission turns to white and eventually blue emission as the temperature increases. [29] When monitoring the emission spectrum, the position of the emission maximum therefore reflects changes in the flame temperature. Mathematically, blackbody radiation is described by the Planck distribution law [29]:

$$I(\lambda, T) = \varepsilon \frac{8\pi hc}{\lambda^5} \frac{1}{\exp\left(\frac{hc}{\lambda K_b T}\right)} \quad 2-3$$

where,

$I(\lambda, T)$  is the emission intensity  
 $\varepsilon$  is the emissivity (unitless)  
 $h$  is Planck's constant (6.626E-34 J s)  
 $K_b$  is the Boltzmann constant (1.381E-23 J K<sup>-1</sup>)  
 $T$  is the absolute temperature in Kelvin  
 $c$  is the speed of light (3E8 m s<sup>-1</sup>)  
 $\lambda$  is the wavelength in meters

The emissivity value of a radiating body is a measure of the body's ability to emit radiation relative to a blackbody. Mathematically,

$$\varepsilon = \frac{I(\lambda, T)}{I_{BB}(\lambda, T)} \quad 2-4$$

where,

$I_{BB}(\lambda, T)$  is the blackbody emission intensity  
 $I(\lambda, T)$  is the actual emission intensity

In blackbody radiation, the emissivity value is equal to 1.0, which means that all wavelengths of radiation are emitted and absorbed uniformly. In graybody radiation ( $0 < \varepsilon < 1$ ), the emissivity is independent of wavelength and less than 1.0 due to some of the radiation being reflected, absorbed or transmitted. [28] For the purposes of this research, it is assumed that the flame and the calibration source (tungsten halogen lightbulb) are similar graybody emitters and thus, the emissivity of the emitting body is compensated for in the calibration.

### **Line Spectra**

Line spectra, or emission lines, come from free atoms when electronic transitions occur between excited and lower energy orbitals. Spectral lines in the UV-VIS region of the spectrum come from valence shell electron transitions. [28] When such a transition occurs, the excess energy

is emitted in the form of a photon, which is a discrete packet of energy. [29] Emission lines are species specific and correspond to defined electronic transitions for the atom. The intensity of each atomic emission line depends on the combination of the two orbitals involved, on the population of molecules in their excited state (a function of the flame conditions including its temperature), and, of course, on the concentration of the atoms in the sample. The atomic emission lines are useful not only in identifying the elemental composition of the sample, but at a given temperature they can also give an estimate of the concentration of the emitting species. [28]

Thus, any emission lines that are observed in the spectral signal can be used to identify and quantify the emitting species in the flame. Information such as this may be useful for understanding the combustion stoichiometry in real time for flash reactions.

### **Banded Spectra**

Banded spectra in the UV-VIS region are produced from electronic transitions (the same as for line spectra) that occur simultaneously with changes in internal vibrational and rotational energies of the molecule. [28] Gaseous molecules such as O<sub>2</sub>, N<sub>2</sub>, CO and H<sub>2</sub>O produce molecular emission bands in the deep UV region of the spectra, however flames are typically not hot enough to produce such emission bands. [28] The experiments being conducted as part of this research involve heating and feeding of an O<sub>2</sub> – N<sub>2</sub> mixture as the reaction gas. While it is unlikely that O<sub>2</sub> or N<sub>2</sub> emission bands will be observed, gaseous S-O combustion products may produce emission bands that can be monitored. If such emission bands (or others) can be identified in the emission spectrum, they may represent an opportunity for diagnosing and quantifying the combustion reactions occurring in the flame.

### **Optical Characterization of Flames**

The flame is the central reaction zone of a combustion process. [30] This is certainly true in the flash furnace reaction shaft, where all major chemical reactions occur in the flame. The most

common method of monitoring industrial flames is through off-gas monitoring. Flame performance can be characterized by measuring off-gas compositions of undesirable reaction products such as CO, NO<sub>x</sub> and particulates. With knowledge of undesirable reaction products, the process can be adjusted to improve operation. [31] Using off-gas concentrations for control strategy is captured by the EFSOP technology (see Section 2 - Tenova Goodfellow – EFSOP®). The use of advanced control systems for flame monitoring is difficult because of lack of reliability and complexity in models which creates a risk of bringing the process into an unstable regime that may result in downtime. [31] The optical sensor under development uses fibre optics and emission spectroscopy to characterize the flame formed in flash furnace smelting. A review of optical techniques for diagnosing flames as well as opportunities for measurement variables from the emission spectrum are summarized, next.

### **Diagnostic Techniques**

There are many different optical techniques that can be used to study a flame, however the selection of the method must consider the characteristics and type of flame that will be studied. Spatially resolved techniques, such as laser-based systems, are useful for gas flames however they cannot typically be used for particulate laden flames. Line of sight techniques, such as optical pyrometry and flame emission spectroscopy, are suitable for particulate laden flames, however it is not possible to spatially resolve measurements using these techniques. [28] [32] In flash furnace smelting, the burner flame forms from the combustion of solid concentrate particles. Flame optical emission spectroscopy between 200 – 1100nm has been selected as a line of sight technique to study and characterize the flash smelting burner flame.

### **Measurement Variables**

From the burner emission spectrum, information about the flame can be collected including: flame temperature, brightness, stability, flicker (e.g. frequency of oscillation) as well as

combustion stoichiometry from emitting species. Previous studies on flash furnace smelting have used optical pyrometry to study the effect of experimental variables on the particle combustion temperatures, however these other measures of flame characteristics have not been documented. This study aims to cover this gap in the literature as well as demonstrate that flame optical emission spectroscopy is a useful tool for burner monitoring in flash furnace smelting.

### ***Temperature***

Optical pyrometry is a common, line of sight technique used to measure the combustion temperature of particles in a flame. Particle combustion temperature is an important variable to measure because it “characterizes the enthalpy of reaction and controls many of the important chemical and physical process, which also influence composition” of the reaction products. [32] While temperature measured along the line of sight represents an average, this average is skewed towards hotter particles because radiative intensity scales with the fourth power of temperature ( $I \propto T^4$ ) according to the Stefan-Boltzmann Law. [31] Research presented in Chapter 2 - Combustion Temperatures summarizes temperature measurements of pure minerals and concentrates undergoing flash reactions in the lab. In the current study, optical pyrometry using the two-wavelength method was used to extract the combustion temperatures of combusting particles from the continuous part of the emission spectrum. This technique is useful because it is reasonably accurate and provides a fast response time. The two-wavelength method for temperature calculation is based on the Planck distribution law (Equation 2-3 above) and uses the ratio of radiative intensities at two wavelengths to calculate temperature. [31] Mathematically, the two-wavelength temperature approximation is expressed as:

$$T = \frac{hc}{K_b} \left( \frac{1}{\lambda_2} - \frac{1}{\lambda_1} \right) \left[ \ln \left( \frac{CF_1 I_1 \lambda_1^5}{CF_2 I_2 \lambda_2^5} \right) \right]^{-1} - 273 \quad 2-5$$

where,

T is the temperature in °C

$\lambda_i$  is the emission wavelength

$I_i$  is the blackbody emission intensity at  $\lambda_i$

$CF_i$  is the calibration factor at  $\lambda_i$

An explanation of the calibration procedure and the correction factors, CF, for the optical signal is included in Appendix 1.

### ***Brightness***

Flame brightness is a luminous parameter that is related to the flame size and temperature. [33] It may be related to the amount of material combusting or the reaction conversion. In this study, the flame brightness is calculated as the total integrated intensity of the emission spectrum. It is thought that the flame brightness may be useful for characterizing the solids feed rate.

### ***Flicker***

Flame flicker measures the oscillation frequency of the flame. It is calculated using the Fourier transform of the time-dependent integrated intensity and is used to identify underlying frequency components in the signal which fluctuate around the baseline. [33] Flicker is useful for identifying different flame conditions such as structure, stability, energy conversion and emission forming processes. [34] In a pulverized fuel coal flame, Lu, et al found that low frequency components in the flame stem from geometric fluctuations in the flame due to flow or convection effects, while the high frequency components reflect variations in reaction kinetics. [34] Further, they also found that the flame flicker frequency was impacted by the oxygen concentration.

Because of the similarity of the PF and flash furnace flames, it is hypothesized that there may be a frequency component to either the flame temperature or brightness. A goal of the current research will be to identify any such frequency components.

### ***Stability***

Stability represents the statistical estimate of a parameter and doesn't imply correctness in the signal, but rather whether it stays the same. [35] One potential measure of the flame stability is the standard deviation. [30] The standard deviation of the flame temperature and brightness were analyzed to understand the impact of O<sub>2</sub>/S stoichiometry on flame stability.

An analysis of frequency stability can also be done with an Allan Variance analysis, which is corollary to the two-sample variance. [36] The Allan Variance analysis is a useful way to analyze frequency stability and for selecting a sampling time that minimizes the frequency instability of an oscillator. [36] For this research, the oscillator being studied is the flame, which is the source of the emission spectrum. Allan Variance analysis works by calculating the Allan Deviation of the signal over different sampling periods using discrete, evenly spaced measurements. This type of analysis is useful for characterizing noise types that give rise to changes in oscillation frequency identified with the Fourier analysis.

Oscillation instability can occur over long and short time periods. Long-term frequency instability is characterized by drifts in the oscillation frequency, which is often attributed to the aging of the "resonator" material. [37] In the case of the flash smelting flame, the resonator does not age, however there may be conditions that cause long-term instability such as drifts in calibrations (feeder, MFC, etc) and buildup of accretions in the process. Short-term instability can be caused by either random or periodic (driven and underdamped) fluctuations in temperature, pressure and/or vibrations. [37] In the drop tower, this type of instability may be caused from feed pulsation and reaction conversion. There are different types of short-term noise which includes:

white noise, random walk noise and flicker noise. White noise is independent of the frequency while random walk and flicker noise are dependent on the oscillation frequency. [36] [37] [38]

### *Emitting Species*

Emitting species provide information about the combustion reactions that occur as well as the temperature at which they occur. [39] Heat from the flame provides the thermal energy required to excite the electrons in atoms and molecules to excited states. If the temperature of the flame is not high enough, there may not be enough energy to induce emissions from atomic and/or molecular species. This study will present a characteristic emission spectrum for concentrate flash combustion and identify any such emissions.

## Chapter 3

### Experimental Methodology and Material Characterization

#### Experimental Setup

Experimental test work was done in a drop tower style reactor. The drop tower is a vertically oriented, sealed, continuously fed reactor that aims to emulate the reaction shaft of a flash furnace. The reactor is made from 304 stainless steel with length and diameter dimensions of 1660 mm and 114 mm (4" Sch. 40 pipe size) respectively. Solid products collected from the experiment do not settle out into a matte and slag as in the commercial furnace; rather, they are collected as a combined solid product at the bottom of the reactor. Figure 3 & Figure 4 show a labelled picture and a schematic of the drop tower respectively.

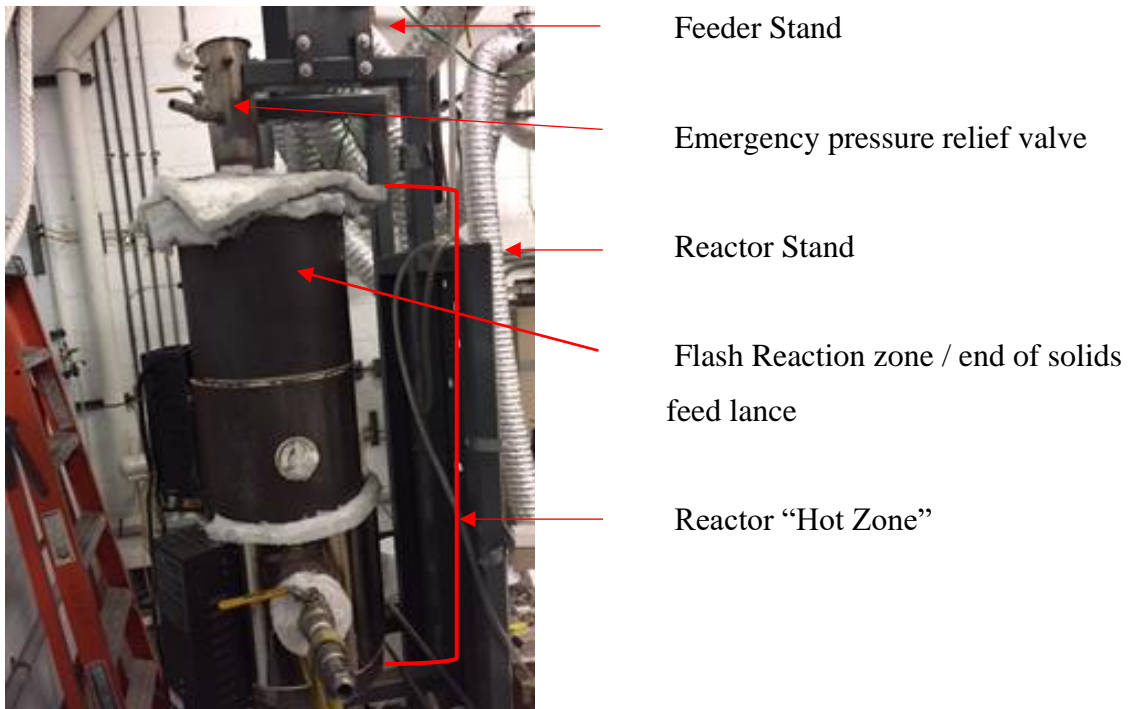


**Figure 3: Drop tower reactor, furnaces and sampling spoon**

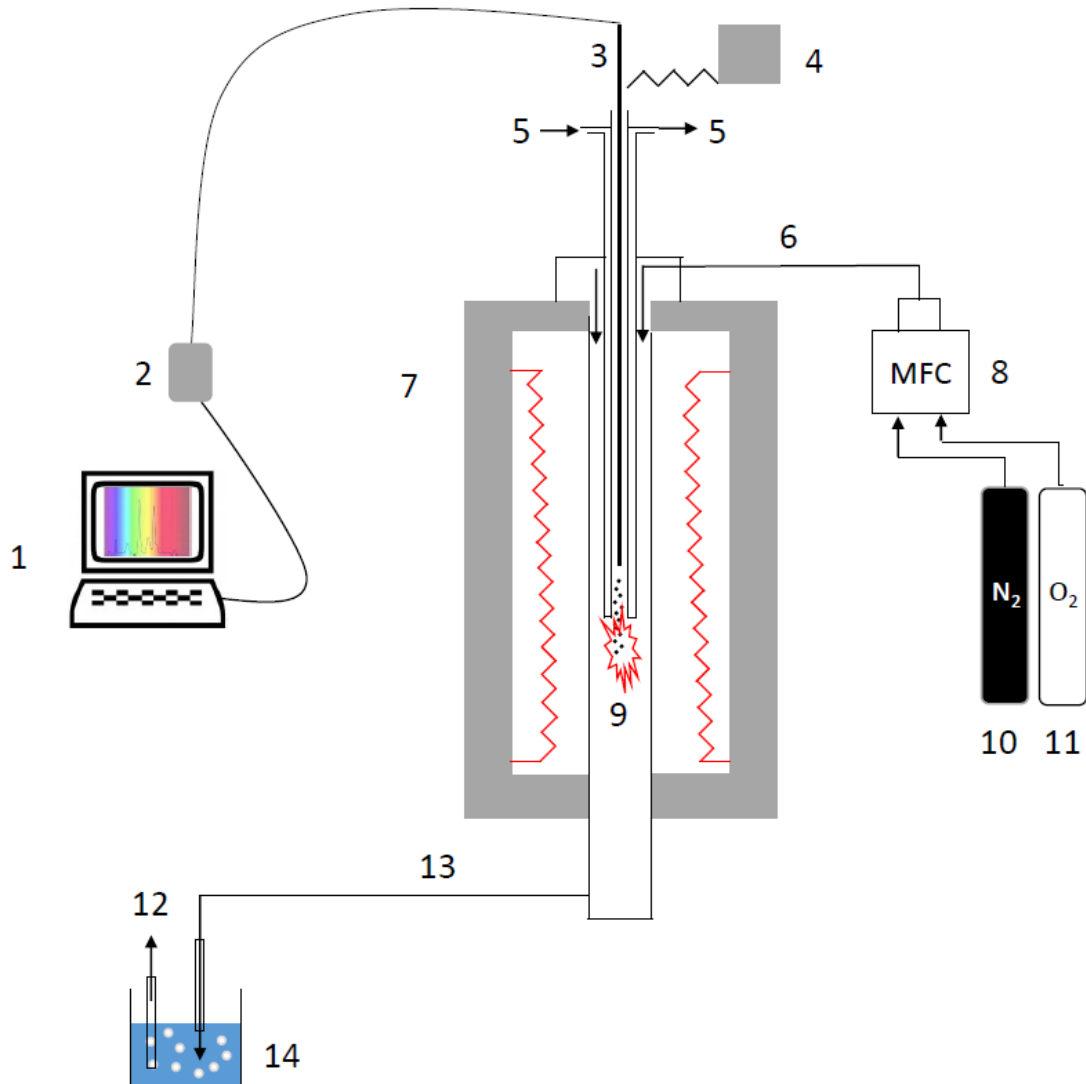


**Figure 4: Drop tower experimental setup; (1) Computer DAQ, (2) Spectrometer, (3) Fibre optic probe, (4) Powder screw feeder, (5) Solids feed lance cooling gas, (6) Reaction gas, (7) Resistance heated furnaces, (8) Mass flow controllers for O<sub>2</sub> and N<sub>2</sub> gas, (9) Flash reaction zone, (10) N<sub>2</sub> compressed gas cylinder, (11) O<sub>2</sub> compressed gas cylinder, (12) Scrubbed off-gas, (13) SO<sub>2</sub> containing off-gas, (14) caustic scrubbing solution. Adapted from [40]**

Solids feeding was done using an MT-1 MiniTwin Feeder from Brabender Technologie Inc. For each material, calibration curves of the feed rate versus screw speed (RPM) were made to achieve the target feed rate, which was 3 grams per minute. Once discharged from the screw feeder, particles were dropped into the reactor through an air-cooled solids feed lance, which is shown in Figure 5.



**Figure 5: Solids feed lance – front and bottom views**

The solids feed lance was used to drop solid particles into the hot zone of the reactor. A low flow of nitrogen gas was used to guide the solids through the feed lance, preventing clogs and oxidizing flash reactions from occurring inside the lance. The lance was designed with a counter-current cooling jacket through which different cooling media could be passed. For all the results in this report, air as the cooling medium was used. During commissioning stages of the reactor, water was used as the cooling medium, however it did not work well. This is because the water cooling removed too much heat from the reactor and caused water in the reaction gas to condense on the inside of the feed lance, which created feeding issues. A heat model of the process was developed to justify the change from water to air cooling and is discussed in Appendix 2.

The reaction zone is defined as the location at which the flame forms and where the flash reactions occur. This location was at the exit of the solids feed lance where the particles first meet O<sub>2</sub> enriched reaction gas and the experimental temperature (950°C). When the solids exit the feed lance, they heat rapidly and undergo flash combustion reactions forming a flame.

The stability and temperature of the flame was studied using a 600- $\mu\text{m}$  core, solarization resistant, multimode fibre and an Avantes ULS-3648 spectrometer sensitive to light in the UV/VIS/NIR region of the spectrum (200 – 1100 nm). The fibre optic probe was installed inside

the solids feed lance such that it looked down the center axis of the reactor at the flame. The tip of the fibre probe was set back 150 mm inside the feed lance to protect it from heat. Because the fibre was set back inside the solids feed lance, the field of view (FOV) was limited. The fraction of the FOV that was captured was calculated from the numerical aperture, NA, of the fibre as

$$NA = \sin(\theta_{fiber}) = 0.22$$

$$FOV = \theta_{fiber} = \sin^{-1}(0.22) = 12.71^\circ$$

where,

$\theta_{fiber}$  is the solid angle captured by the fibre

NA is the numerical aperture of the fibre as specified

by the supplier

Thus, the fibre with NA = 0.22, has a 12.7° field of view. Using trigonometry and the position of fibre inside the solids feed lance (Figure 6), the reduction in the fibres FOV was calculated:

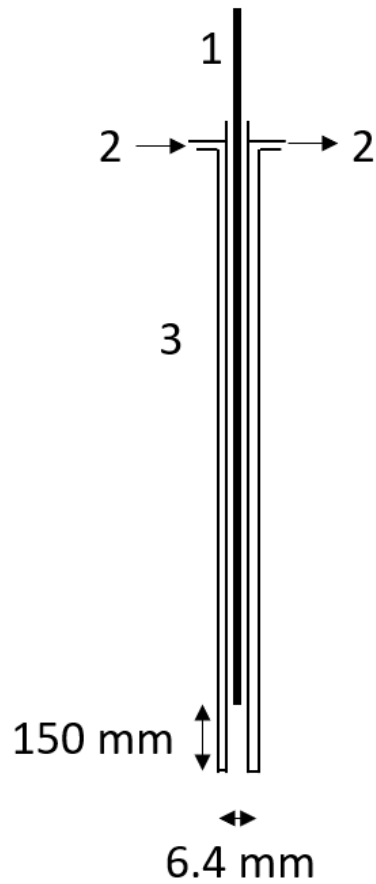


**Figure 6: Schematic showing the position of the fibre inside the solids feed lance**

$$\theta_{exp} = \tan^{-1} \left( \frac{6.4 \div 2}{150} \right) = 1.22^\circ$$

$$\%FOV \text{ Captured} = \frac{1.22}{12.71} = 0.096 = 9.6\%$$

The fibres position inside the solids feed lance means that its FOV is reduced to 2.4°. The effect of setting it back inside the feed lance was that only 9.6% of the fibres field of view was captured. This was not found to be a problem as there was more than enough light to acquire a signal from the flame. In cases where there is not enough light for a signal, the fibre tip could be moved closer to the reaction zone (this may require more cooling) or using a larger diameter fibre.

The reactor was heated using three furnaces that were stacked on top of each other creating a 1030 mm long hot zone. During commissioning stages, it was found that the temperature inside the reactor was the same as the furnace set point, and thus, thermocouple measurements along the length of the reactor were not needed. The position of the reactor hot zone was set such that the solids feed lance extended 130 mm into it. For the upper portion of the reactor there was a 315 mm section that was outside of the hot zone. This portion of the reactor was used as the gas preheating zone where radiation from the hot zone heated the gas.

The reaction gas was a mixture of oxygen and nitrogen. The gas was premixed outside of the reactor and injected through the lid. The gas was preheated such that when it reached the reaction zone, it was close to the experimental temperature of 950°C. The gas flow rates were regulated with Aalborg Mass Flow Controllers (Model GFC17).

Flash reactions produce an off-gas of SO<sub>2</sub>, O<sub>2</sub> and N<sub>2</sub>. Approximately 1 liter per minute of the off-gas stream was directed to an ABB Easy Line Continuous Gas Analyzer (Model EL3020), which was used to detect O<sub>2</sub> and SO<sub>2</sub> concentrations. The remainder of the off-gas was passed through a series of wet and dry traps to scrub the gas and fix SO<sub>2</sub> into solution. The off-gas analysis represented a major operational challenge for the drop tower experiments. For most of the tests, the O<sub>2</sub> and SO<sub>2</sub> concentrations in the off-gas were above the linear response range of the analyzer; thus, the gas stream to the analyzer had to be diluted. Dilution presented a problem because it was hard to keep the sample gas flow rate to the analyzer constant. Without an instantaneous history of the sample gas flow rate to the analyzer, an accurate off-gas profile for each experiment could not be obtained. Off-gas analysis represents an area for improvement in future testing.

Solid reaction products were collected for analysis at two different points: inside the reaction zone using a sampling spoon and outside of the reaction zone in a capsule. The sampling spoon was water cooled and was designed such that it spanned the entire diameter of the reactor. It was used to collect a representative sample of the falling stream with time, however it can only collect small masses of material (<10 grams). The solids collection capsule at the bottom of the

reactor was used to collect the remainder of the solid products. The products collected in the capsule represent an average composition for the run and were used for the results and analysis portion of this thesis as the spoon operation had not been optimized.

The drop tower coupled with the fibre optic probe proved to be a useful tool for studying flash combustion reactions. The drop tower allowed for the study of the flash combustion behaviour of different feeds, while the fibre optic probe was useful for identifying operational upsets to the process.

### **Optical Instrumentation**

A custom fibre optic probe was built for the hot, dusty environment inside the drop tower. It was built out of stainless steel and ceramic tubing, Swagelok fittings, an optical fibre (Thorlabs Part # UM22-600) as well as an armored fibre patch cable (Thorlabs Part # MHP550L02). The fibre probe was installed inside the solids feed lance which meant that dust accumulation on the fibre tip was a significant risk. To mitigate this risk, a low flow of gas was passed around the fibre tip, which allowed experiments to be run indefinitely without dust compromising the signal.

The Avantes AvaSpec ULS-3648-USB2 spectrometer was coupled to the fibre optics through the armored fibre patch cable. It had a CCD detector in the UV/VIS/NIR region of the spectra, 200 – 1100 nm. The raw signal was calibrated for temperature and validated using a Chino Corporation IR-CA Series High-speed compact radiation thermometer. The calibration procedure and results are summarized in Appendix 1. Spectral data collection was done using the software AvaSoft 8, which was sold with the spectrometer. This software was used to display the raw signal flame temperature and brightness during experimental tests as well as for data logging of the optical signal.

## **Material Characterization**

Tests in the drop tower were conducted with pure mineral feeds: pyrite and chalcopyrite, as well as three copper concentrates: Concentrate A, Concentrate B and a 1:1 blend by weight of the Concentrates A & B. The blended concentrate is referenced in this report as Concentrate AB.

### **Measurement Principles**

The analytical techniques used in this research includes elemental sulphur (LECO), XRD, QEMSCAN® and laser particle size analysis. XRD and LECO analyses were done in house, while laser particle size and QEMSCAN® were conducted by third parties. Representative sub-samples from the bulk product were obtained for these analyses through cone and quartering and riffing. Each of the measurement principles for these techniques are explained.

#### ***Elemental Sulphur***

Elemental sulphur analysis was done on all reaction products from drop tower testing using an ELTRA CS-2000 Carbon/Sulphur Analyzer. [41] The scope of this work did not require knowledge of carbon content in the reaction products and thus, only the sulphur analyses were retained. The measurement principle of this analyzer is infrared spectroscopy. Batch samples loaded into a crucible with iron and tungsten accelerators combust in an induction heated furnace (>2000°C) in the presence of pure oxygen. Complete conversion of S to SO<sub>2</sub> and C to CO<sub>2</sub> is achieved in the furnace. The concentration of SO<sub>2</sub> and CO<sub>2</sub> in the gas is used to determine both C and S-content of the sample using IR absorption spectroscopic cells. [41]

#### ***QEMSCAN®***

QEMSCAN® analysis is a spatially resolved analytical technique for evaluating the mineralogy of samples. The measurement principle is scanning electron microscopy (SEM) and energy dispersive X-ray spectroscopy (EDS) paired with digital image analysis. [42] Solid samples are mounted in resin and polished before being loaded into the QEMSCAN® analyzer. [43] The

machine divides the sample into a grid using a user defined pixel spacing. Each pixel is then scanned using EDS and the measured spectra is compared against a library to assign a mineral or phase to the pixel. The machine automatically scans every pixel, identifies the phase and then builds a digital image of the polished section. [42] QEMSCAN® is useful as it can analyze individual particles as well as the distribution of phases as a function of particle size. [42] This analytical technique was chosen for studying the concentrates because they have a complicated composition.

#### ***Laser Particle Size Analysis***

Laser particle size analysis was done on the drop tower products using the Malvern Mastersizer MS3000. This instrument uses Mie and Fraunhofer scattering to measure the volume-based size distribution in the range 0.1 – 3500 µm. [44] Particle size distributions can be represented using different bases such as particle count, area, volume or mass and it is possible to convert between the bases assuming a homogenous sample density. Regardless of the basis, a few large particles (in terms of mass, volume and area) can skew the particle size distribution to over represent the coarser size fraction.

#### **Pure Mineral Characterization**

Chalcopyrite and pyrite were chosen as the pure minerals for testing because they are common minerals in copper concentrates. As well, there is a significant body of literature on the single particle combustion behaviour of these minerals.

95% pure pyrite was sourced from STREM CHEMICALS (CAS# 12068-85-8) in a 5-kilogram batch. As purchased, the feed was coarse and was not suitable for the screw feeder. To reduce the particle size, the pyrite was pulverized in a shatter box and then screened to be 100% passing 150 µm. The oversize material was recycled back into the pulverizer and the undersize was kept for feeding. No analysis for chemical or mineralogical composition was done, as the purity was certified by the supplier.

Coarse pieces of chalcopyrite (> 25.4 mm) were sourced from a mineral trade show. Particle size reduction was done using a Boyd crusher to -2mm. Visually, the -2mm product showed contaminant particles in it, which were identified by XRD to be sphalerite (ZnS). These particles were picked over manually to upgrade the purity of the chalcopyrite before it was crushed in a rod mill. The final product was analyzed for Cu, Fe and Zn using ICP-OES with the results summarized in Table 2.

**Table 2: ICP-OES chemical analysis of the chalcopyrite feed**

[Cu] %	[Fe] %	[Zn] %
34.3	26.8	2.4

Using the chemical analysis, the calculated mineralogical composition of the chalcopyrite feed is summarized in Table 3.

**Table 3: Calculated feed mineralogy of the chalcopyrite**

[CuFeS <sub>2</sub> ] %	[ZnS] %	[Other] %
96	3.6	0.04

The results of laser particle size analysis for the pure mineral feeds are presented in Figure 7.

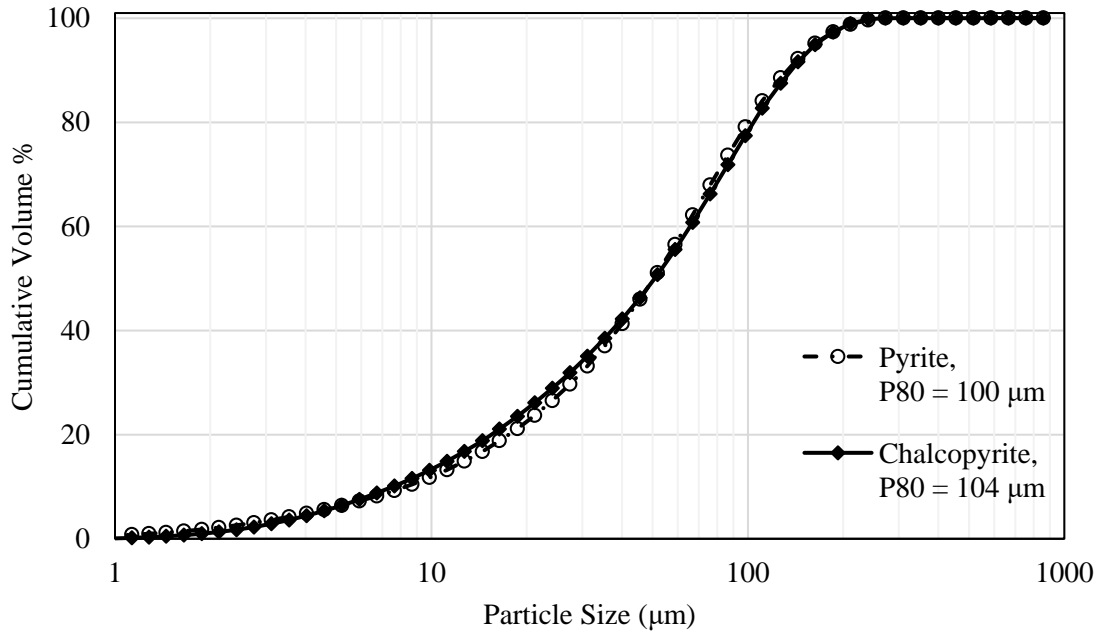


**Figure 7: Pure mineral cumulative % passing particle size distributions**

Figure 7 shows that pyrite and chalcopyrite have almost identical particle size distributions. The P80 of chalcopyrite is 4 µm larger than that of pyrite. The similar size distributions of these minerals will be useful when comparing the behaviour of these pure minerals in the drop tower and with the sensor.

### **Concentrate Characterization**

Concentrates A and B were chosen for drop tower testing to see how differences in mineralogy and particle size distribution affect combustion behaviour in flash smelting. A 1:1 blend by weight of the concentrates was prepared as a third concentrate (Concentrate AB).

QEMSCAN® analysis of Concentrates A and B was done to understand their mineralogies and chemical composition. The composition of the blended concentrate was calculated as an average of A and B. Table 4 summarizes the results of the feed material QEMSCAN® analysis:

**Table 4: QEMSCAN® mineral analysis of the concentrates**

<b>Mineral Species / Mass [%]</b>	<b>Concentrate A</b>	<b>Concentrate AB</b>	<b>Concentrate B</b>
Chalcopyrite	79.15	69.15	59.15
Pyrite	3.30	8.92	14.53
Sphalerite/Wurtzite	8.28	4.41	0.53
Bornite	0.94	4.31	7.68
Pyrrhotite	0.89	1.83	2.77
Piroxene	0.71	1.34	1.96
Enargite/Tennantite	0.21	1.21	2.21
Covellite	0.00	1.14	2.28
The rest	6.52	7.69	8.89
<b>Total</b>	<b>100</b>	<b>100</b>	<b>100</b>

The QEMSCAN® analysis shows that chalcopyrite is the main copper, iron and sulphur bearing mineral in both concentrates. It will be interesting to compare the behaviour of Concentrate A to that of pure chalcopyrite, as Concentrate A has a very high proportion of it. This will give an indication of the impact of other minerals on the flash combustion characteristics of a concentrate. Concentrate B has secondary copper, iron and sulphur mineralization to chalcopyrite in pyrite, bornite, covellite and pyrrhotite. Table 5 summarizes the chemical composition of the three concentrates, which was calculated from the QEMSCAN® analysis.

**Table 5: Chemical composition of the concentrates (mass %)**

<b>Element</b>	<b>Concentrate A</b>	<b>Concentrate AB</b>	<b>Concentrate B</b>
S	33.35	33.29	33.22
Fe	27.47	28.13	28.79
Cu	28.15	28.12	28.08
O	2.41	3.51	4.61
Zn	5.11	2.73	0.34
Si	0.96	1.61	2.26
Ca	1.07	0.86	0.64
Mg	0.11	0.55	0.99
Al	0.23	0.30	0.37
As	0.04	0.24	0.44
Pb	0.19	0.10	0.00
K	0.07	0.09	0.11
Sb	0.04	0.04	0.04
Na	0.01	0.02	0.03
Bi	0.01	0.01	0.00
The rest	0.78	0.40	0.80
<b>Total</b>	<b>100</b>	<b>100</b>	<b>100</b>

The chemical analysis of the concentrates makes it clear that they are very similar in terms of Cu, Fe and S content. The Fe content of Concentrate B is slightly higher than of Concentrates A and AB, which is likely due to the pyrite mineralization. Concentrate A has a much higher proportion of zinc in it than Concentrate B. One of the goals of this research is to identify emission lines in the spectra as opportunities for use in process control; the chemical analysis will aid in this endeavor. The similar chemistry and the mineralogical differences make these excellent concentrates to compare in the drop tower.

Laser particle size analysis of the concentrates was done with the results summarized in

Figure 8.

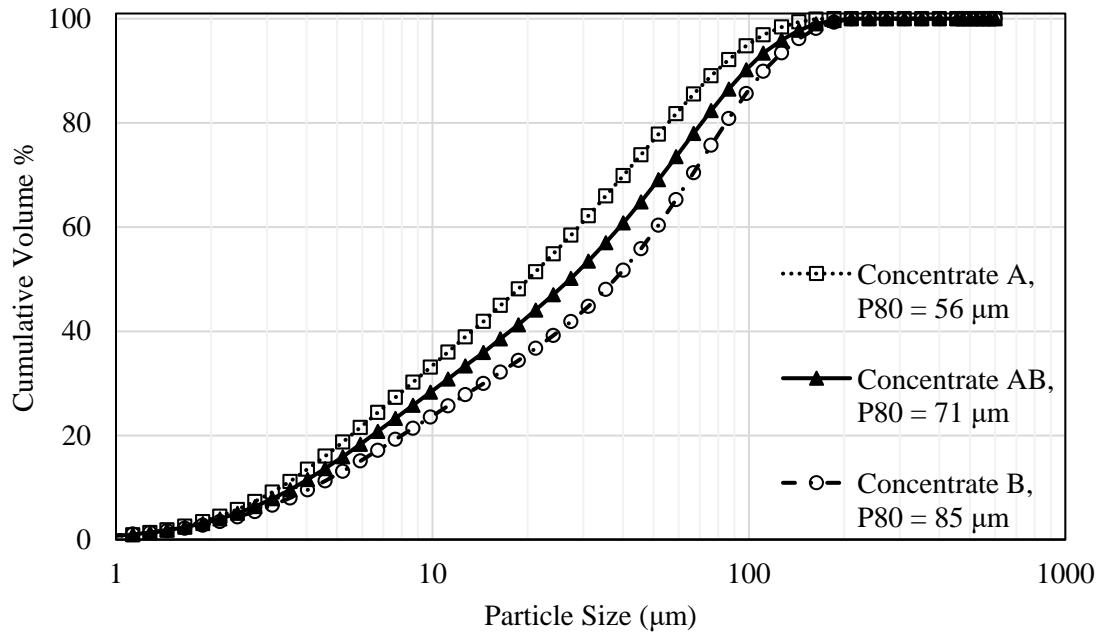


**Figure 8: Concentrate cumulative % passing particle size distributions**

Particle size analysis of the concentrates shows that the Concentrate A has the finest PSD. The difference in P80 particle sizes between Concentrates A and B is 29µm. It will be important to consider the differences in PSD on the analysis of the results, as this variable may impact the behaviour of the concentrates.

### Test Conditions

As part of this research, the impact of oxygen on the flash combustion behaviour of pure minerals and concentrates is being studied. The experimental test conditions according to feed material are summarized in Table 6.

**Table 6: Summary of experimental tests and conditions**

Feed Material	Test No.	Reactor Temperature (°C)	Solids Feed Rate (gpm)	Oxygen Enrichment (%)	O <sub>2</sub> /S Stoichiometry	Total Gas (LPM)
Pyrite	1	850	3	50	2.0	5.0
	2	850	3	98	4.0	5.0
	3	900	3	74	3.0	5.0
	4	950	3	50	2.0	5.0
	5	950	3	98	4.0	5.0
Chalcopyrite	1	950	5	20	0.8	5.0
	2	950	3	30	1.1	3.0
	3	950	5	40	1.5	5.0
	4	950	5	60	2.2	5.0
	5	950	3	80	3.0	3.0
Conc. A	1	950	3	25	1.0	3.2
	2	950	3	45	1.9	3.2
	3	950	3	60	2.5	3.2
Conc. B	1	950	3	20	0.9	3.2
	2	950	3	25	1.0	3.2
	3	950	3	45	1.9	3.2
	4	950	3	45	1.9	3.2
	5	950	3	60	2.5	3.2
Conc. AB	1	950	3	25	1.0	3.2
	2	950	3	45	1.9	3.2
	3	950	3	60	2.5	3.2

Most of the tests were done using a reactor temperature of 950°C, except for Tests 1-3 with pyrite. Tests 1-3 with Pyrite were done early in the test work and the results showed that the drop tower flash combustion processes were not significantly impacted by the reactor temperature in the range of 850 – 950°C. Thus, it was decided that for all other feeds, a reactor temperature of 950°C

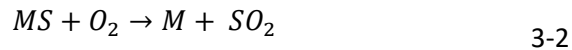
would be used. The pyrite data is presented as if all the data points were collected at a reactor temperature of 950°C.

### Desulphurization Model Development

Desulphurization curves were modelled for O<sub>2</sub>/S ratios between  $R = 0.8 - 4.0$  for each of the five feeds. To model the desulphurization curves, the elemental sulphur assays were first normalized against the feed sulphur assay. Mathematically, this was done according to Equation 3-1.

$$\% \text{ Sulphur Remaining} = \frac{\% \text{ Sulphur in Products}}{\% \text{ Sulphur in Feed}} \quad 3-1$$

Desulphurization curves for each of the feeds were modelled assuming the simplified and general reaction mechanism represented by Equation 3-2.



where,

MS = metal sulfide

M = metal

Assuming a second order reaction and representing [O<sub>2</sub>] as  $R \cdot [MS]$  the rate equation for the general reaction (3-2) is shown by 3-3:

$$-r_{MS} = \frac{d[MS]}{dt} = k[MS][O_2] = k \cdot R[MS]^2 \quad 3-3$$

Simplifying assumptions for the model are:  $[MS] \approx [S]$  and the residence time,  $t$  is constant.

The  $[MS] \approx [S]$  assumption was made to simplify the reaction mechanism for the concentrates. Rather

than examine the individual reaction mechanisms of each mineral component, the concentrate was treated as MS with the [S] given by the elemental sulphur analysis. For consistency, this assumption was applied to the pure minerals as well. Integration of Equation 3-3 with respect to dt and d[MS] yields Equation 3-4 which is a relationship between the concentration of MS and the O<sub>2</sub>/S ratio, R.

$$[MS]_R = \frac{[MS]_0}{1 + [MS]_0 \cdot R \cdot k \cdot t} \quad 3-4$$

where,

[MS]<sub>0</sub> is the concentration of MS at R = 0

[MS]<sub>R</sub> is the concentration of MS at R = O<sub>2</sub>/S

R is the stoichiometric ratio of O<sub>2</sub> gas / feed S

k is the equilibrium constant

t is the residence time

When modelling the desulphurization behaviour of the feeds, the variable [MS]<sub>R</sub> stems from the elemental sulphur analysis of products formed under O<sub>2</sub>/S conditions, R. The fitting parameters for the model then become [MS]<sub>0</sub> and kt. The model fit was optimized using the Microsoft Excel Solver function to minimize the sum of the squared error between the experimental and modelled values, which was the objective function. No constraints were placed on the variables.

It would also be possible to fit this data with a sigmoidal decay shaped curve, which would capture the onset of ignition. For the data in this thesis, a sigmoidal decay curve could fit the chalcopyrite data, however the second order kinetic model was used due to the limited data available. With more data at lower O<sub>2</sub>/S stoichiometries, the sigmoidal decay shape would become apparent for all feeds.

## Chapter 4

### Analysis & Results

Experiments in the drop tower were conducted to measure the impact of O<sub>2</sub>/S stoichiometry and feed composition on the flash combustion behaviour of pure minerals, chalcopyrite and pyrite, as well as three copper concentrates. The concentrates have similar chemical compositions but different mineralogies. The results from this investigation are organized into two sections:

1. Analysis of the drop tower reaction products: This section focuses on the study of the reaction products using elemental sulphur, XRD, QEMSCAN® and laser particle size analyses.
2. Analysis of the emission spectrum of the flame: This section focuses on the development of the optical sensor through analysis of the emission spectrum. The results in this section includes the identification of emitting species, an analysis of flame flicker as well as the calculation of flame temperature and brightness profiles.

Chapter 5, which is the discussion of the results, will draw these two results sections together and provide implications for the industrial furnace.

## Analysis of Drop Tower Reaction Products

### Desulphurization

Elemental sulphur analysis of reaction products was used to generate desulphurization curves for each of the feeds. Experimentally modelled desulphurization curves for pyrite and chalcopyrite are presented in Figure 9, with the oxygen enrichment for each experiment shown next to the data point.

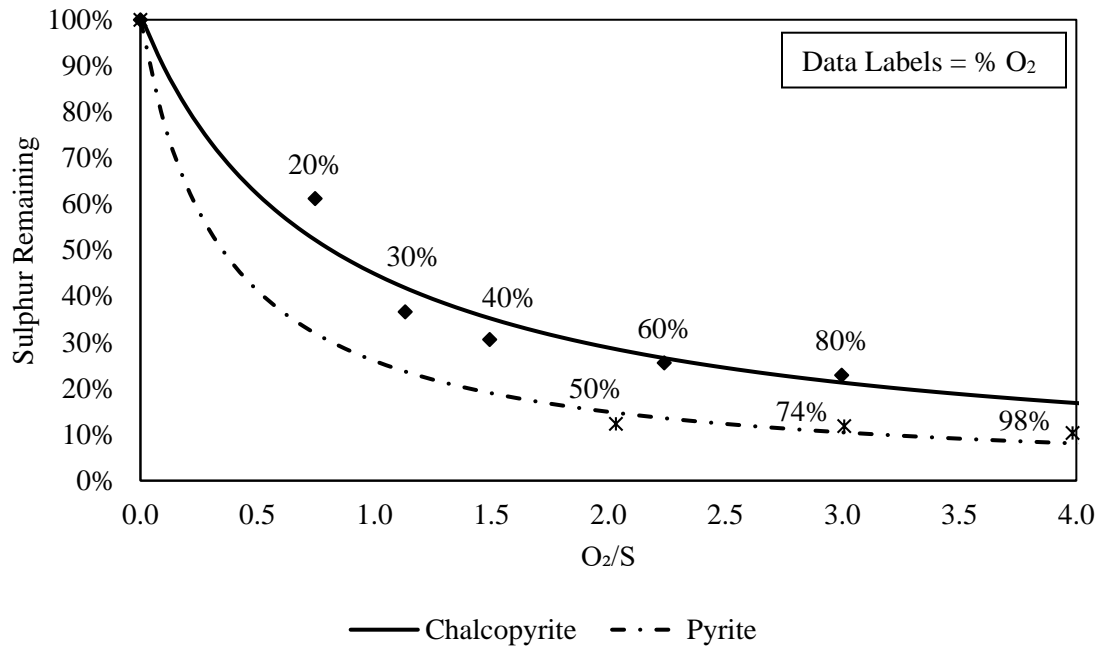


**Figure 9: Chalcopyrite and pyrite desulphurization curves**

The fitting parameters for the pyrite and chalcopyrite curves are summarized in Table 7.

**Table 7: Pure mineral fitting parameters for the sulphur removal curves**

Fitting Parameters	Pyrite	Chalcopyrite
$[MS]_0$	1.00	1.00
kt	2.85	1.24

The pure mineral desulphurization curves show different rates of sulphur removal and a different limiting residual sulphur content as the O<sub>2</sub>/S stoichiometry goes to infinity. Pyrite is

desulphurized more than chalcopyrite for a given  $O_2/S$  condition and the residual sulphur value for pyrite is lower than that of chalcopyrite. This result is reflected in the fitting parameter  $kt$ . Assuming that the residence time is constant for the two minerals, the rate constant,  $k$ , for pyrite is greater than that of chalcopyrite. Thus, the desulphurization of pyrite occurs more readily than for chalcopyrite.

Figure 10 compares the desulphurization curves for the three concentrates that were tested.

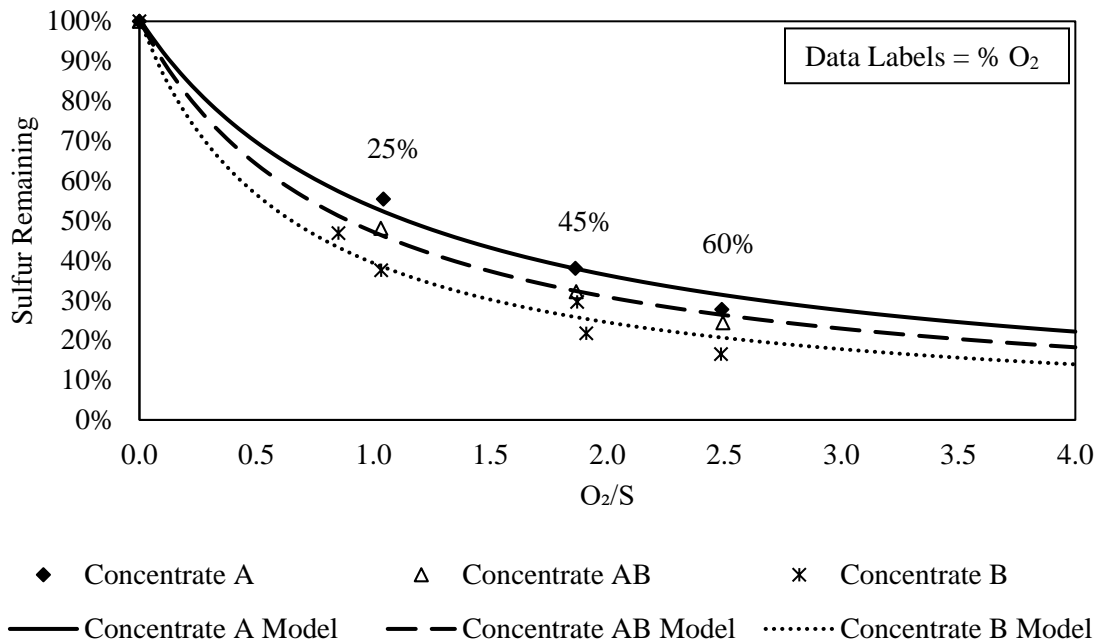


**Figure 10: Concentrate desulphurization curves**

The concentrate desulphurization curve fitting parameters are summarized in Table 8.

**Table 8: Fitting parameters of the concentrate desulphurization curves**

Fitting Parameters	Conc. A	Conc. AB	Conc. B
$[MS]_0$	1.00	1.00	1.00
$kt$	0.90	1.12	1.54

Like the pure minerals, the concentrates have different capacities for sulphur removal. For a given  $O_2/S$  stoichiometry, Concentrate B has the greatest sulphur removal and Concentrate A the

least. The Concentrate AB desulphurization curve lies in between the other two sulphur removal curves, which was expected as it is an average of Concentrates A and B. These differences in desulphurization are captured in the fitting parameter  $kt$ , where concentrates that are more “easily” desulphurized, have a higher rate constant. The rate constants of the concentrates are lower than those of the pure minerals.

### Pure Mineral XRD Analysis

The composition of the pure mineral products was studied using XRD analysis to understand the reaction pathway. The products of pyrite flash combustion are summarized in Table 9.

**Table 9: XRD analysis of the pyrite product**

	<b>Mineral Type (increasing oxidation →)</b>			
<b>Molar Ratio (O<sub>2</sub>/S)</b>	<b>FeS<sub>2</sub></b>	<b>Fe<sub>(1-x)</sub>S<sub>x</sub></b>	<b>Fe<sub>3</sub>O<sub>4</sub></b>	<b>Fe<sub>2</sub>O<sub>3</sub></b>
<b>2.0</b>			High	High
<b>3.0</b>			High	High
<b>4.0</b>			High	High

For the O<sub>2</sub>/S conditions tested, pyrite was oxidized into Fe<sub>3</sub>O<sub>4</sub> and Fe<sub>2</sub>O<sub>3</sub>. To better capture the reaction mechanism of pyrite, tests with lower O<sub>2</sub>/S stoichiometries are required. Table 10 summarizes the results of XRD analysis for the products of chalcopyrite flash combustion.

**Table 10: XRD analysis of the chalcopyrite reaction products**

<b>Molar Ratio (O<sub>2</sub>/S)</b>	<b>Mineral Type (increasing oxidation →)</b>						
	<b>CuFeS<sub>2</sub></b>	<b>CuS</b>	<b>Cu<sub>2</sub>S</b>	<b>CuFeO<sub>2</sub></b>	<b>CuO</b>	<b>Fe<sub>3</sub>O<sub>4</sub></b>	<b>Fe<sub>2</sub>O<sub>3</sub></b>
<b>0.8</b>	High	Low				High	
<b>1.1</b>	Medium					High	
<b>1.5</b>				Medium		High	
<b>2.2</b>				Medium	Medium	Medium	
<b>3.0</b>					Medium	High	Medium

The XRD analysis of chalcopyrite shows that it first forms intermediate phases CuS and CuFeO<sub>2</sub> before reaching its fully oxidized products, CuO, Fe<sub>3</sub>O<sub>4</sub> and Fe<sub>2</sub>O<sub>3</sub>. (refer to chemical equations in introduction) Regardless of the O<sub>2</sub>/S condition, Fe<sub>3</sub>O<sub>4</sub> was identified in the reaction products of chalcopyrite. At low O<sub>2</sub>/S stoichiometries, some of the feed CuFeS<sub>2</sub> does not react and only under the highest oxidizing conditions does Fe<sub>2</sub>O<sub>3</sub> form.

#### **QEMSCAN® Analysis**

QEMSCAN® analysis was done on 4/11 of the combustion products from concentrate testing in the drop tower: Concentrate A – O<sub>2</sub>/S = 1.9, Concentrate AB – O<sub>2</sub>/S = 1.9, Concentrate AB – O<sub>2</sub>/S = 2.5 and Concentrate B – O<sub>2</sub>/S = 1.9. The mineralogical composition of the combustion products from these tests are summarized in Table 11.

**Table 11: Concentrate QEMSCAN® analysis; mineralogy of the combustion products**

Phase	Concentrate	Concentrate	Concentrate	Concentrate
	A	AB	AB	B
	O <sub>2</sub> /S = 1.9	O <sub>2</sub> /S = 1.9	O <sub>2</sub> /S = 2.5	O <sub>2</sub> /S = 1.9
FeOx+Cu	11.48	20.61	41.72	26.51
Pseudochalcopyrite	37.61	19.52	13.47	15.65
FeOx Impure	10.87	21.05	10.17	18.82
Hematite/Magnetite	11.37	9.92	10.94	10.58
Pseudobornite	11.98	8.91	4.51	7.78
Delafossite	5.32	3.47	7.41	3.96
Cuprite	3.22	3.18	4.00	3.23
Pseudochalcocite	2.87	4.42	2.90	3.45
Bornite	1.39	1.92	1.14	2.61
Pseudochalcopyrite2	0.18	1.10	0.69	1.40
Pyrrhotite	0.02	0.70	0.34	1.75
Pyrite	0.06	0.65	0.51	0.76
Quartz	0.50	0.67	0.30	0.48
Diopside	0.32	0.34	0.40	0.81
Wurtzite	0.61	0.71	0.28	0.02
Chalcopyrite	0.13	0.53	0.24	0.36
Andradite	0.67	0.31	0.04	0.00
Actinolite	0.08	0.17	0.16	0.39
Muscovite	0.02	0.22	0.11	0.35
Microcline	0.35	0.18	0.11	0.04
Molybdenite	0.26	0.08	0.03	0.00
Chalcocite-Digenite	0.20	0.08	0.01	0.07
Calcite	0.03	0.25	0.03	0.01
Pigeonite	0.00	0.13	0.01	0.14
Enargite	0.00	0.12	0.00	0.03
The rest	0.46	0.74	0.46	0.81
<b>Total</b>	<b>100</b>	<b>100</b>	<b>100</b>	<b>100</b>

In Table 11, the phases FeOx + Cu, pseudochalcopyrite, FeOx impure, pseudobornite, pseudochalcocite and pseudochalcopyrite2, herein referred to as pseudo species, are compositionally defined based on detailed analysis (microanalysis) of individual particles. Using the microanalysis results, compositional limits for these pseudo species were identified. Table 12 summarizes the average Cu, Fe, S, O and Impurity assays and the standard deviation in composition for the pseudo species where composition is measured using atomic %.

**Table 12: Compositional limits of QEMSCAN® pseudo species**

Phase	Cu	S	Fe	O	Impurities
Pseudochalcocite	60.0 ± 1.7	27.1 ± 2.6	2.5 ± 1.4	10.4 ± 2.7	0.0 ± 0.0
Pseudobornite	38.9 ± 4.9	30.2 ± 5.8	16.5 ± 2.2	12.7 ± 6.1	1.3 ± 2.8
Pseudochalcopyrite	24.2 ± 3.1	37.2 ± 2.6	27.7 ± 2.2	9.5 ± 2.5	1.5 ± 2.4
FeOx + Cu	16.5 ± 2.5	0.1 ± 0.4	28.7 ± 2.8	44.7 ± 1.7	9.9 ± 3.0
FeOx Impure	0.5 ± 0.6	1.1 ± 0.7	22.1 ± 12.6	43.7 ± 24.4	12.6 ± 7.6

Table 12 has some very interesting trends occurring with respect to impurity behaviour in these pseudo species. It appears that the concentration of impurities tends to increase with the atomic % of oxygen in the phase. Thus, impurities tend to stick to the oxide phases.

The chemical composition of the 4 samples analyzed by QEMSCAN® was calculated from the mineralogical analysis and is presented in Table 13.

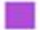

**Table 13: QEMSCAN® chemical analysis of the products of drop tower combustion (concentrates)**

Element	Concentrate A O <sub>2</sub> /S = 1.9	Concentrate AB O <sub>2</sub> /S = 1.9	Concentrate AB O <sub>2</sub> /S = 2.5	Concentrate B O <sub>2</sub> /S = 1.9
Fe	36.53	38.89	42.27	40.55
Cu	31.16	26.71	28.23	26.25
O	12.47	16.42	17.27	17.07
S	15.51	11.03	6.84	9.67
Si	1.80	2.96	2.61	3.03
Ca	0.94	1.55	1.15	1.45
Al	0.47	0.86	0.87	0.92
Mg	0.31	0.62	0.32	0.65
Zn	0.52	0.67	0.30	0.20
K	0.10	0.14	0.07	0.13
Mo	0.16	0.04	0.02	0.00
Ti	0.01	0.02	0.02	0.04
As	0.00	0.04	0.00	0.03
C	0.00	0.03	0.00	0.00
Na	0.00	0.01	0.01	0.01
The rest	0.01	0.01	0.01	0.01
<b>Total</b>	<b>100</b>	<b>100</b>	<b>100</b>	<b>100</b>

The combustion products of the concentrates consist mainly of the elements Fe, Cu, O and S. In terms of minor metals present in the combustion products, Group 2 elements Mg and Ca are present in significant amounts as well as Si, Al, Zn and K.

Digital image maps of all the particles analyzed in the QEMSCAN® were generated as part of the analysis output. The maps are a 5 X 5 grid where the rows separate the particles according to size and columns by major phase. The columns group particles together that have a significant amount of a common phase. Columns are labelled according to the main phase associated with particles in that column. Rows are labelled according to the size fraction of particles contained in the row. It is possible for particles to be captured in more than one column of the map when there is a significant portion of two phases in that particle. The phase legend for the maps is shown in Table 14.

**Table 14: Phase legend for the QEMSCAN® particle maps**

	Pseudobornite
	[Unclassified]
	Pseudochalcopyrite
	FeOx Impure
	Hematite/Magnetite
	FeOx+Cu
	Bornite
	Delafossite
	Quartz

The mineralogical maps of the 4 samples analyzed with QEMSCAN® are shown in Figure 11, Figure 12, Figure 13 & Figure 14.



Figure 11: QEMSCAN® mineralogical map for Concentrate A with O<sub>2</sub>/S = 1.9

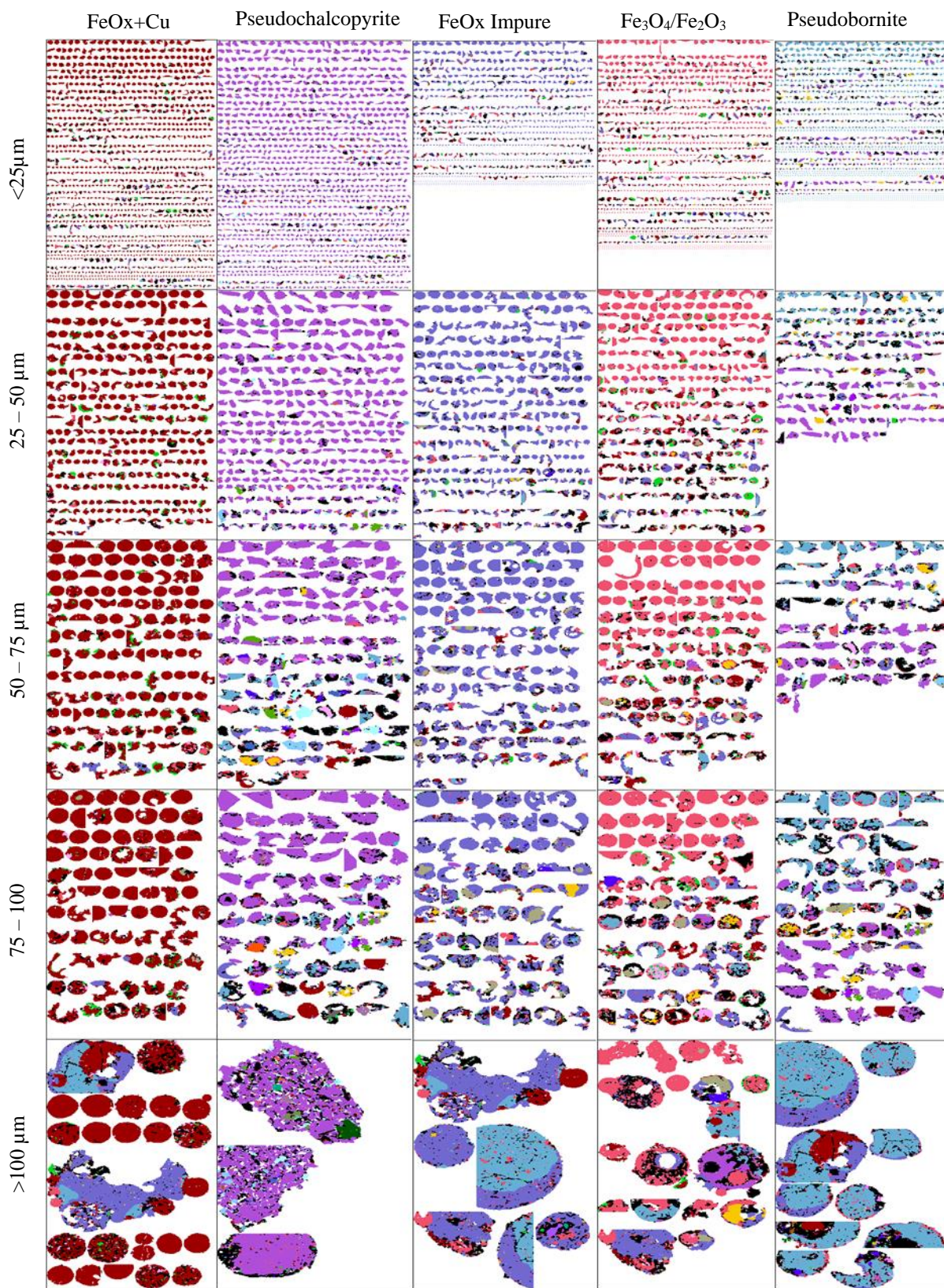


Figure 12: SEM-EDS QEMSCAN® mineralogical map for Concentrate AB with O<sub>2</sub>/S = 1.9



Figure 13: SEM-EDS QEMSCAN® mineralogical map for Concentrate B with O<sub>2</sub>/S = 1.9

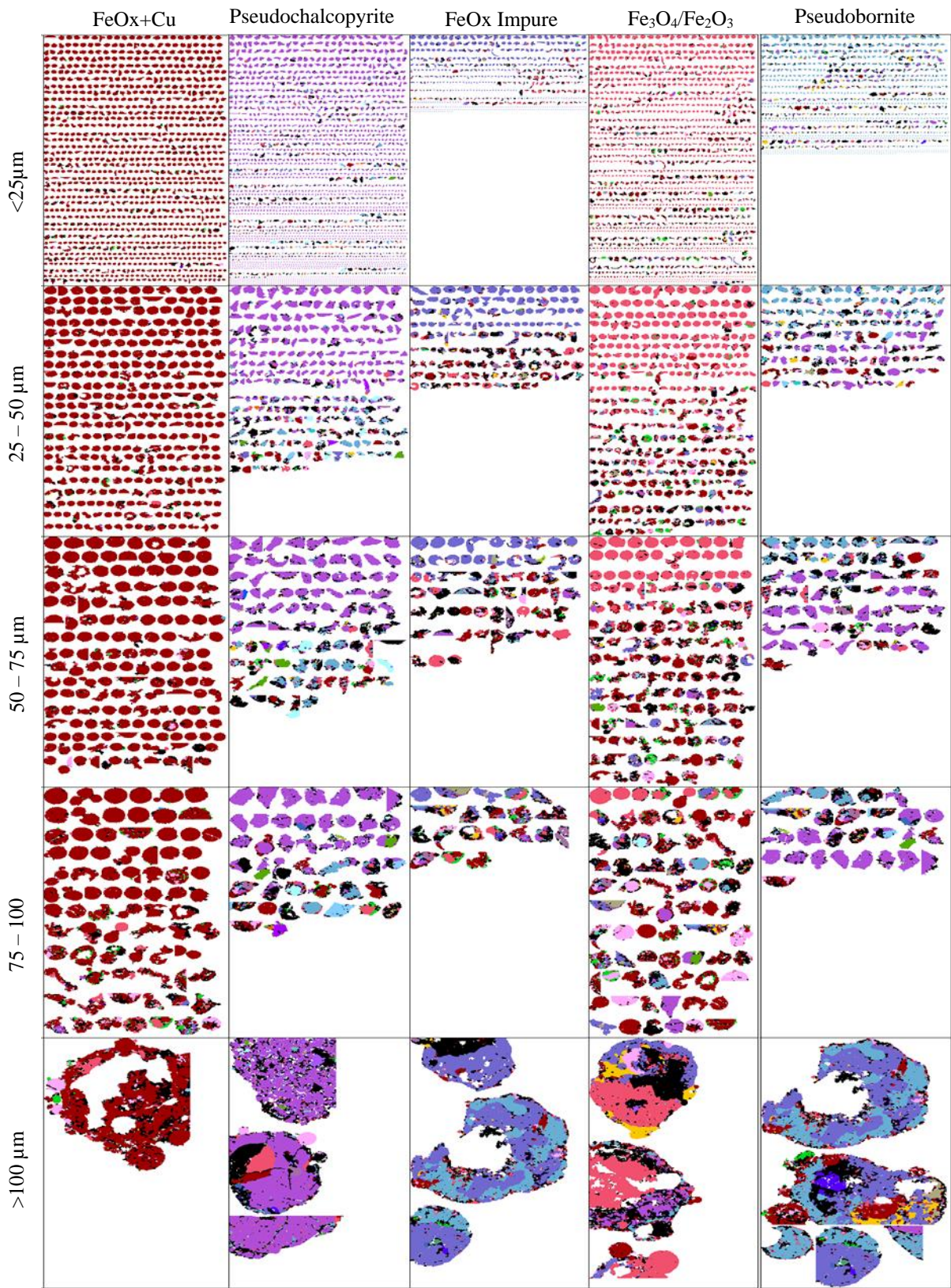


Figure 14: SEM-EDS QEMSCAN® mineralogical map for Concentrate AB with O<sub>2</sub>/S = 2.5

The QEMSCAN® mineralogical maps, Figure 11 - Figure 14, were analyzed qualitatively to gain insight into:

- Morphology is a useful indicator for particle melting. A spherical morphology suggests the particle melted whereas an angular morphology indicates that little to no melting occurred.
- Particle fragmentation is sometimes indicated by hollow spheres (cenospheres) which cause dust to be produced in flash furnace smelting. [45]
- Composition and phase associations that are identified in the QEMSCAN® maps can be used to gain insight into reaction mechanisms. Samples analyzed by QEMSCAN® are mounted and polished in resin. By polishing the particles, the composition of the particle exterior and interior can be identified. Such information is useful for evaluating the impact of mass transport on flash combustion processes through an analysis of particle encapsulation.

An overview of the qualitative analysis follows according to the phase:

- FeOx + Cu:
- Generally, particles that are  $> 25 \mu\text{m}$  are spherically shaped. Particles  $< 25 \mu\text{m}$  have irregular morphologies. The edges of the smaller particles tend to be more angular and jagged compared to the larger particles which are smooth.
  - All combustion products show evidence of particles fusing together in the  $> 100 \mu\text{m}$  size fraction.
  - There are a few hollow spheres in this phase, all within the size fraction 25 - 100  $\mu\text{m}$
  - The composition of particles in the FeOx + Cu maps is generally uniform throughout the particle.

- The most notable phase that associates with FeOx + Cu is cuprite. Cuprite appears to form on the surface of FeOx + Cu particles as some of the edges of particles are cuprite.

- Pseudochalcopyrite:
- Pseudochalcopyrite particles have non-spherical morphologies.
  - Pseudochalcopyrite particles do not appear to be fusing with other particles in any of the size fractions.
  - There is very little evidence for particle fragmentation or hollow spheres
  - Pseudochalcopyrite particles are either uniform in composition throughout the particle or occluded by unclassified material which may be gangue.
  - There is very little evidence of chalcopyrite phase associations with pseudochalcopyrite, except in the <25  $\mu\text{m}$  size fraction in which this association is observed in small amounts.

- FeOx Impure:
- FeOx Impure particles seem to be very fragmented. There is a mixture of spherical and non-spherical, irregularly shaped particles.
  - All FeOx particles in concentrates show evidence of particles fusing together in the >100  $\mu\text{m}$  size fraction. There are some instances of FeOx + Cu particles adhering to the surface of FeOx Impure particles.
  - FeOx Impure particles appear to be heavily fragmented. There is evidence of hollow spheres for particles > 25  $\mu\text{m}$ .

- There are fewer FeOx Impure particles in the Blended sample at  $O_2/S = 2.5$ , compared to the other 3 samples.
- The phases that seem to associate with FeOx Impure are: FeOx + Cu, bornite, Pseudobornite and magnetite-hematite.

Fe<sub>2</sub>O<sub>3</sub> – Fe<sub>3</sub>O<sub>4</sub>:

- Particles >25 μm tend to have spherical morphologies.
- Particles <25 μm appear to have jagged edges and irregular morphologies.
- Particles >75 μm are often fused with other particles. It seems that the phase FeOx + Cu is sometimes fusing to the outside of particles of the phase Fe<sub>2</sub>O<sub>3</sub> – Fe<sub>3</sub>O<sub>4</sub>.
- There are only a few hollow spheres in this phase.
- The Fe<sub>2</sub>O<sub>3</sub>-Fe<sub>3</sub>O<sub>4</sub> phase appears to form on the edges of particles that have occlusions or variable composition. This is especially true with pseudobornite particles.
- There is also a trend whereby cuprite seems to form around the edges of particles that have Fe<sub>2</sub>O<sub>3</sub>-Fe<sub>3</sub>O<sub>4</sub> interiors.

Pseudobornite:

- Pseudobornite particles appear to be heavily fragmented with non-spherical morphologies for particles > 25 μm.
- Particles <25 μm are less fragmented with irregular, non-spherical morphologies. The edges of these particles are angular.
- There is little evidence of particles fusing to Pseudobornite particles.
- There is evidence of hollow sphere formation in particles > 75 μm.

- Concentrate A @  $O_2/S = 1.9$  has the highest frequency of fragmented Pseudobornite particles.
- The  $Fe_2O_3$ - $Fe_3O_4$  phase appears to form on the edges of pseudobornite particles which suggests encapsulation.
- There are not a lot of pseudobornite and many are associated predominantly with unclassified and pseudochalcopyrite. The unclassified material may be gangue.

### **Product Particle Size Analysis**

Laser particle size analysis of all the combustion products was done to understand how particles evolve during flash combustion reactions. Semi-log graphs of the cumulative volume % vs the particle size were made. The P80 particle size, which represents the size at which 80% of the material is finer, was interpolated for each test condition. The F80 particle size is the same as the P80, except the F refers to the feed material.

Figure 15 compares the product particle size distributions for chalcopyrite over experimental  $O_2/S$  conditions of 0.8 - 3.0.

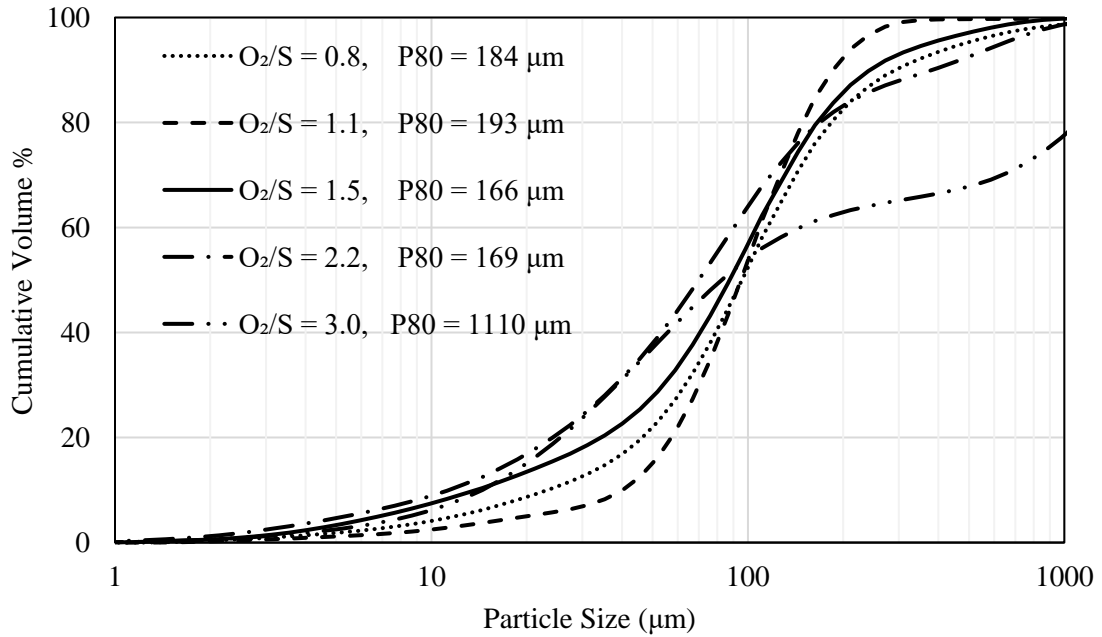


**Figure 15: Chalcopyrite product particle size distributions (cumulative)**

All frequency distributions of the chalcopyrite products were unimodal except for the products collected from the test at  $O_2/S = 3.0$ . For this condition, the shape of the frequency distribution was bimodal which explains the different shape of the cumulative PSD (for  $O_2/S = 3.0$ ). In terms of the P80 particle size, there was an increase relative to the F80 (104  $\mu m$ ) for chalcopyrite products collected at all  $O_2/S$  conditions. The P80 particle sizes are in the range of 166 – 193  $\mu m$  except for the  $O_2/S$  condition of 3.0 which had a P80 of 1110  $\mu m$ . The particle size distribution from testing with  $O_2/S = 3.0$  is rejected because the P80 is  $\sim 30\sigma$  higher than the average P80 (measured for  $O_2/S$  between 0.8 – 2.2). For this reason, this data point will not be included in the discussion.

Figure 16 compares the product particle size distributions for pyrite over experimental  $O_2/S$  conditions of 2.0 – 3.0.

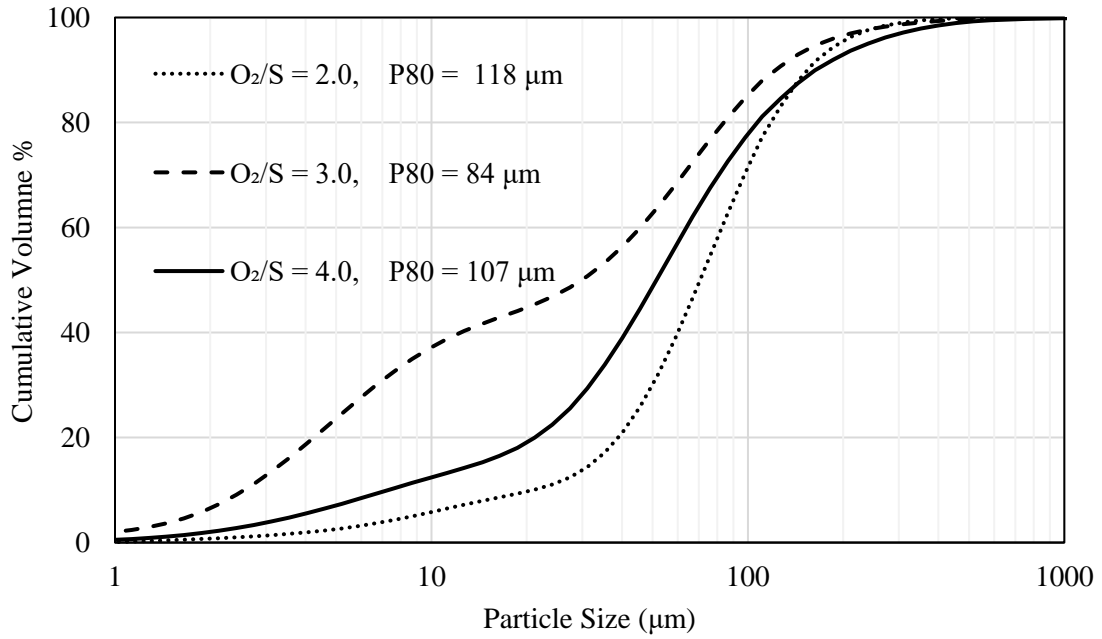


**Figure 16: Pyrite product particle size distributions (cumulative)**

$P80$  particle sizes for the products of pyrite flash combustion are in the range of 84 - 118  $\mu m$ . Relative to the  $F80$  (100  $\mu m$ ), the  $P80$  particle size increased at  $O_2/S$  stoichiometries of 2.0 and 4.0. For the  $O_2/S$  condition of 3.0, the  $P80$  particle size decreased relative to the feed.

Figure 17 compares the product particle size distributions for Concentrate A over experimental  $O_2/S$  conditions of 1.0 – 2.5.

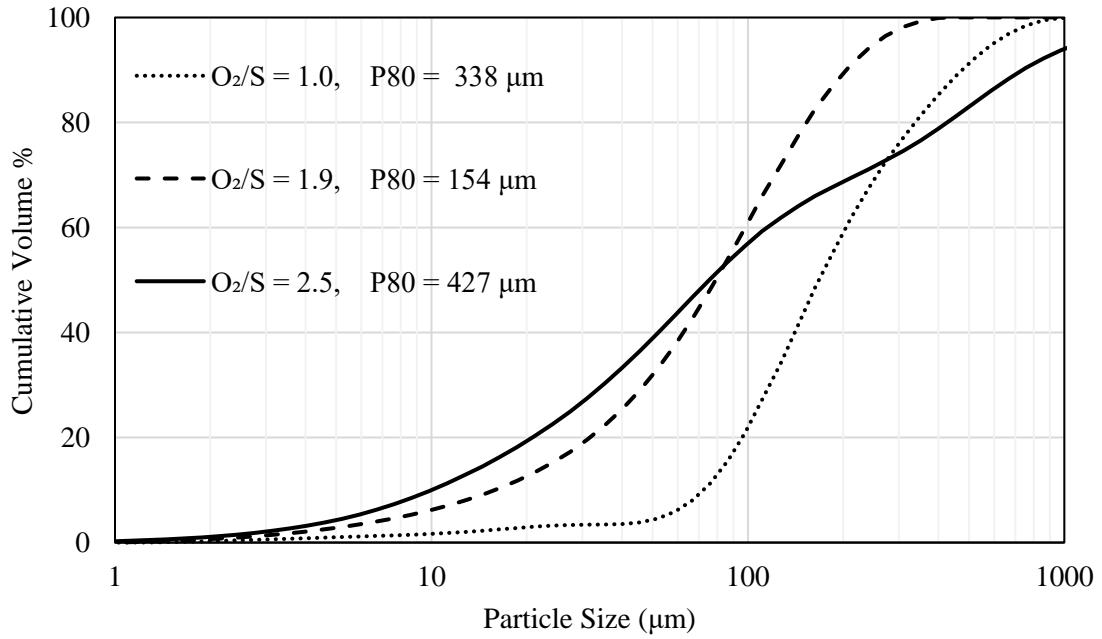


**Figure 17: Concentrate A product particle size distributions (cumulative)**

Concentrate A had the smallest F80 particle size of 56 μm. The P80 particle size increased relative to the feed at all experimental test conditions. The P80 measured at  $O_2/S$  of 1.0 and 2.5 is ~6-8X larger than the feed, while the P80 at  $O_2/S = 2.9$  is 2.75X the F80.

Figure 18 compares the product particle size distributions of Concentrate AB at  $O_2/S$  conditions of 1.0 – 2.5.

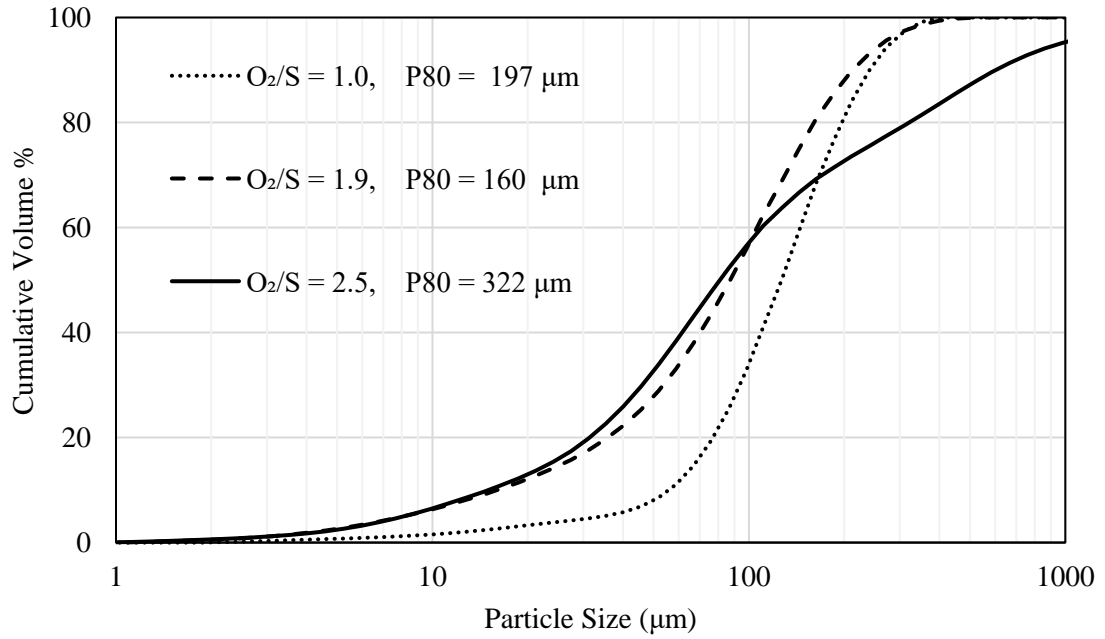


**Figure 18: Concentrate AB product particle size distributions and associated P80 particle sizes**

For Concentrate AB, there is a positive correlation between the P80 particle size and the  $O_2/S$  stoichiometry. The P80 increased relative to the feed at all  $O_2/S$  conditions.

Figure 19 compares the product particle size distributions of Concentrate B at  $O_2/S$  conditions of 0.8 – 2.5.

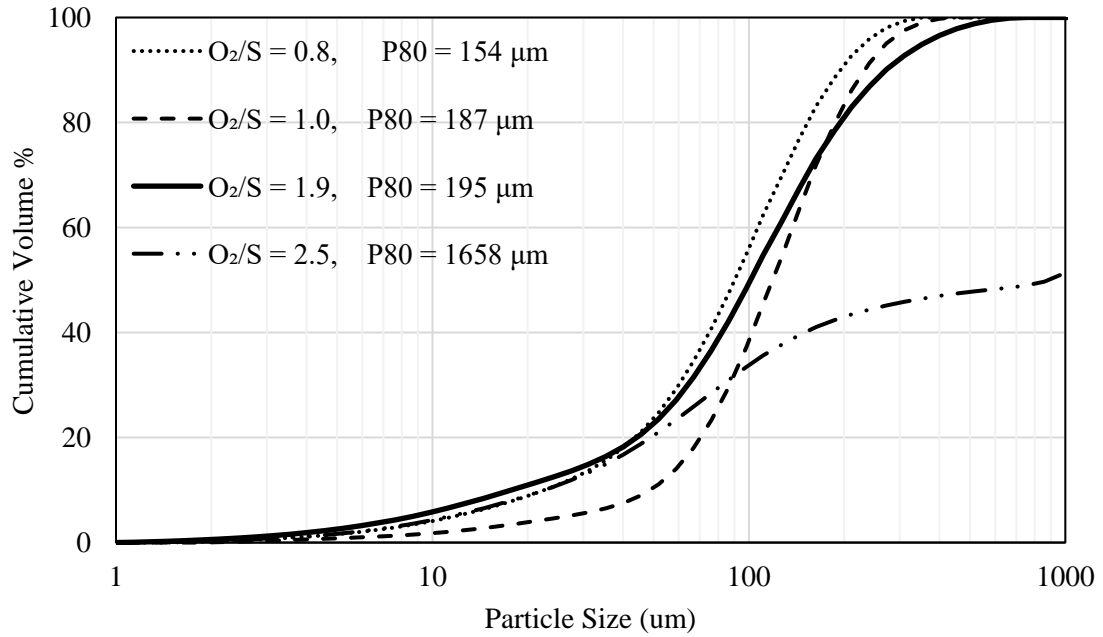


**Figure 19: Concentrate B product particle size distributions**

Like the other feed materials, the P80 particle size increased for Concentrate B relative to the feed. There is a positive correlation between the P80 particle size and the  $O_2/S$  experimental condition. At the  $O_2/S$  condition of 2.5, the P80 particle size is  $\sim 68\sigma$  larger than the mean (measured for  $O_2/S = 0.8 - 1.9$ ). This data point is rejected and will not be included in the discussion.

## Analysis of the Emission Spectrum

### Characteristic Emission Spectrum & Emitting Species

To provide context for the experiments using the fibre probe, a discussion of the characteristic emission spectrum measured during experimentation is necessary. During an experiment, the emission spectrum of the flame was displayed and logged in real time. A typical spectrum taken from Test #5 with Pyrite (Table 6,  $O_2/S = 4.0$ ,  $\%O_2 = 98$ ) is shown in Figure 20.

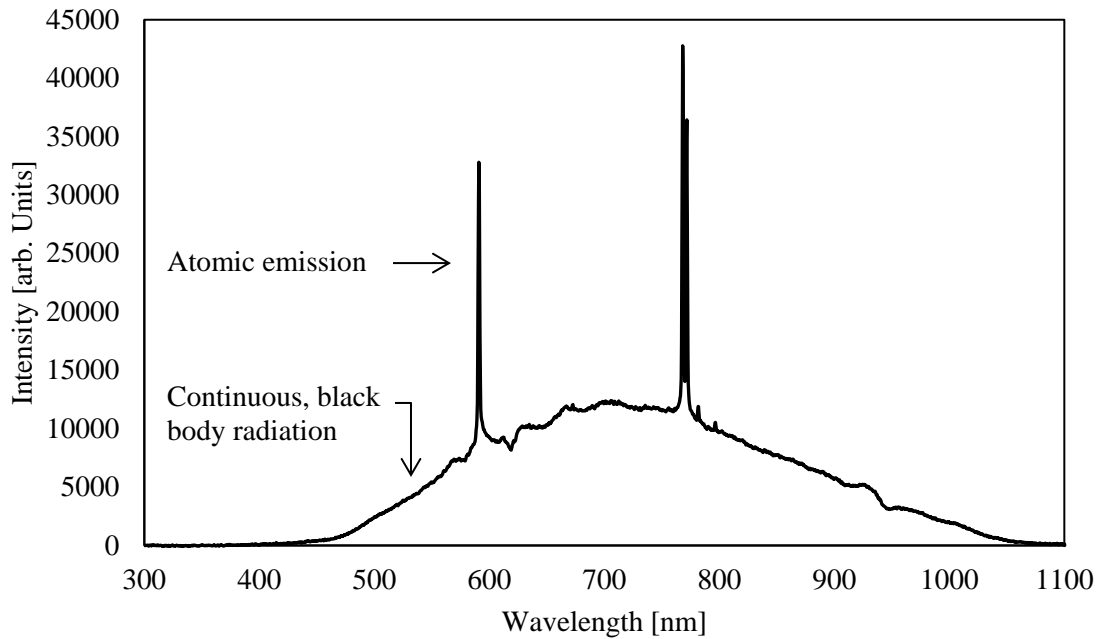


**Figure 20: A typical emission spectrum from flash combustion reactions in the drop tower**

The shape of the continuous part of the spectrum shown in Figure 20 is characteristic of the flash reactions that were observed in the lab and the instrument that was used.

Zooming in on the 550 – 850 nm region of the spectrum, Figure 21 shows the observed atomic emission lines with assigned species labelled. [27] [46]

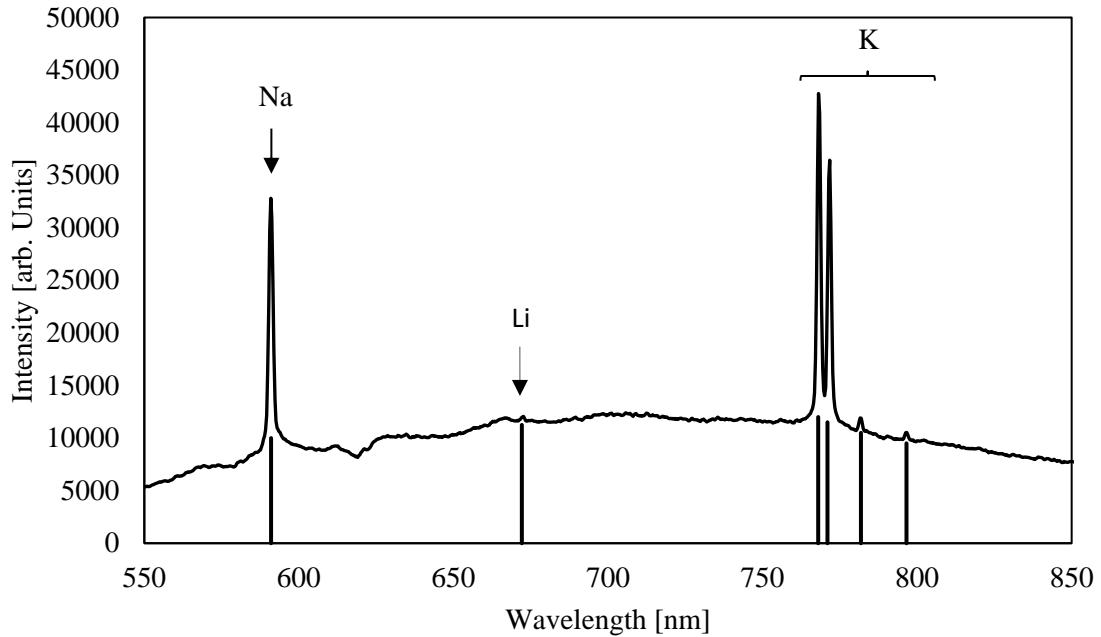


**Figure 21: Emitting species from flash combustion reactions in the lab**

As seen in Figure 21, a total of six emission lines were observed in the signal. These are assigned to alkali metals Na (589.4 nm), K (766.5, 769.9, 779.6 & 795.6 nm) and Li (670.8 nm). [27] [46] The Na and Li emission lines are doublets, however the resolution of the spectrometer used for this work is not fine enough to separate the peaks. [27]

Emission lines from Na, K and Li salts in the combustion reactions are attributed to their low ionization energies. The strongest emissions were from Na at 589.4 nm and the potassium doublet at 766.5 and 769.9 nm. These Na and K emissions were observed in the signal regardless of the feed material. Only in tests with pyrite were emissions from Li (760.8 nm) and K (779.6 and 795.6 nm) observed.

At the start of this research, it was thought that the reaction stoichiometry of flash combustion reactions could be monitored with Cu, Fe, S and/or O emission lines and/or bands. Based on the observed emission lines, it is apparent that there is not enough energy under the

conditions tested to thermally excite atomic or molecular Cu or Fe species nor O<sub>2</sub>, SO or SO<sub>2</sub> species which would have been useful for monitoring stoichiometry.

### **Flame Flicker**

Frequency fluctuations in a flame are called flicker and can be identified using a Fourier transform, which converts the time domain signal into the frequency domain. A sample of the temperature data from the experiment with Concentrate B with an O<sub>2</sub>/S ratio of 2.5 is shown in Figure 22. The vertical red lines at x = 2420 and x = 4100 shows the section of data that was used in the Fourier analysis. The full temperature profile from this test is shown in Appendix 3 - Figure 55.

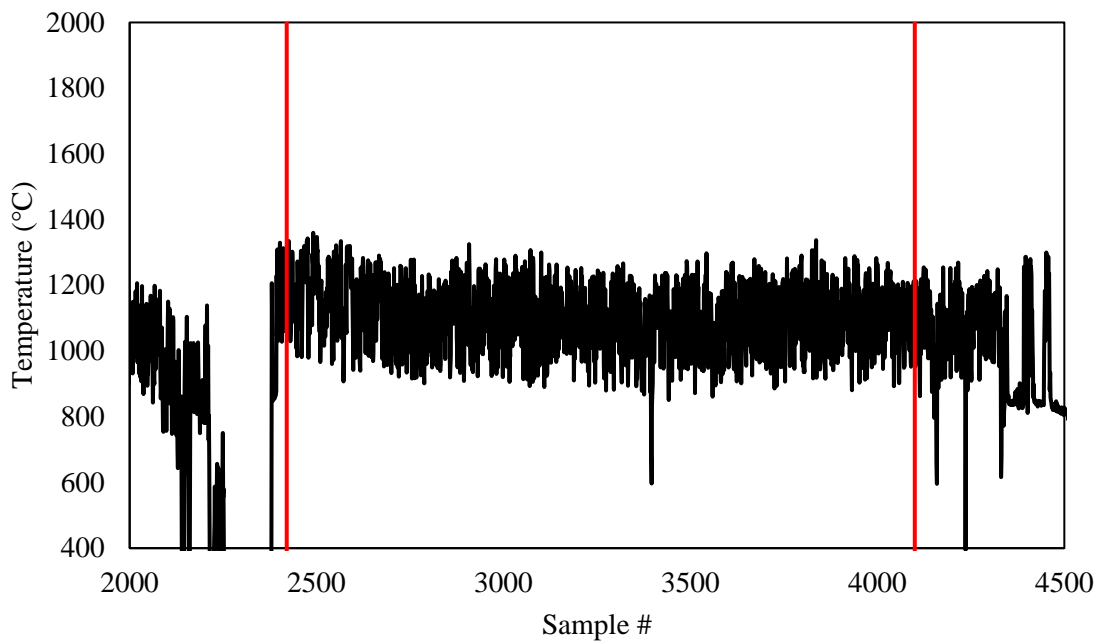


**Figure 22: Flame temperature profile used in the Fourier flicker analysis**

The sample of the temperature profile shown in Figure 22 was measured using a 5-Hz sampling frequency. The `fft()` function in MATLAB was used to convert the time domain signal in

into the frequency domain so that flame flicker components could be identified. Figure 23 shows the Fourier transform of the flame temperature profile.

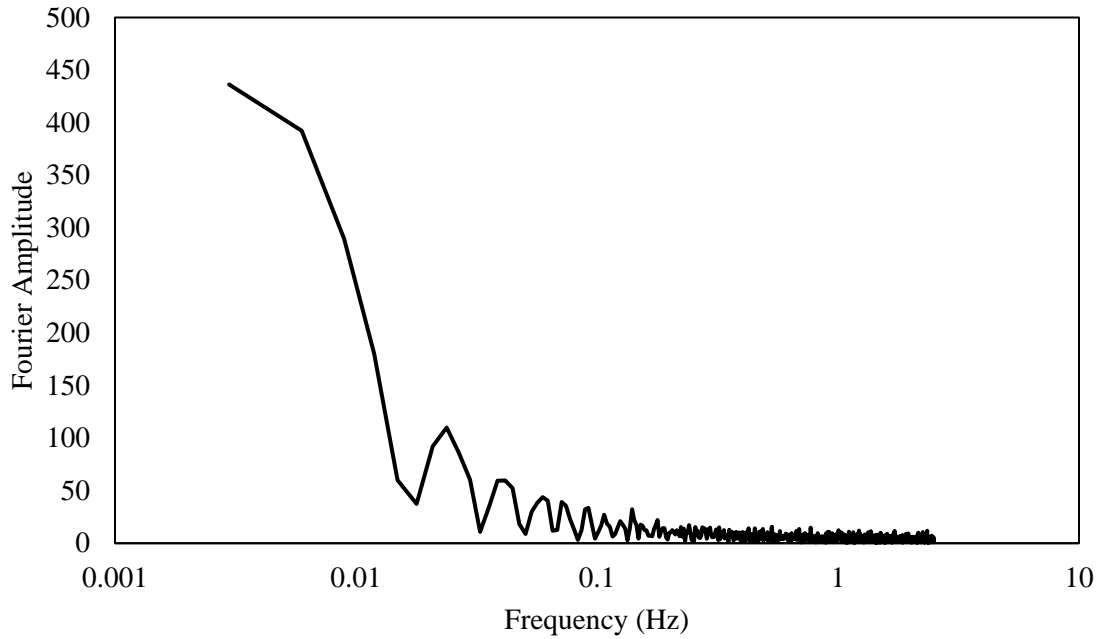


**Figure 23: Fourier transform of the temperature profile (Figure 22)**

There are no dominant frequency components in the Fourier Transform, Figure 23. Thus, the flame does not oscillate with any regularity for periodicity in the range of 1 – 100 seconds. Fourier analyses were done for all experimental conditions and this finding was consistent for all of them. The oscillations apparent in Fig 23 are due to windowing artifacts and may be suppressed by conditioning the data prior to the Fourier transformation.

To characterize the type of noise in the flame temperature signal, an Allan Variance analysis was done using the ALAVAR software. Allan variance analysis of the selected portion of the temperature profile in Figure 22 is shown in Figure 24, where the y-axis is the Allan deviation and the x-axis is the sample time.

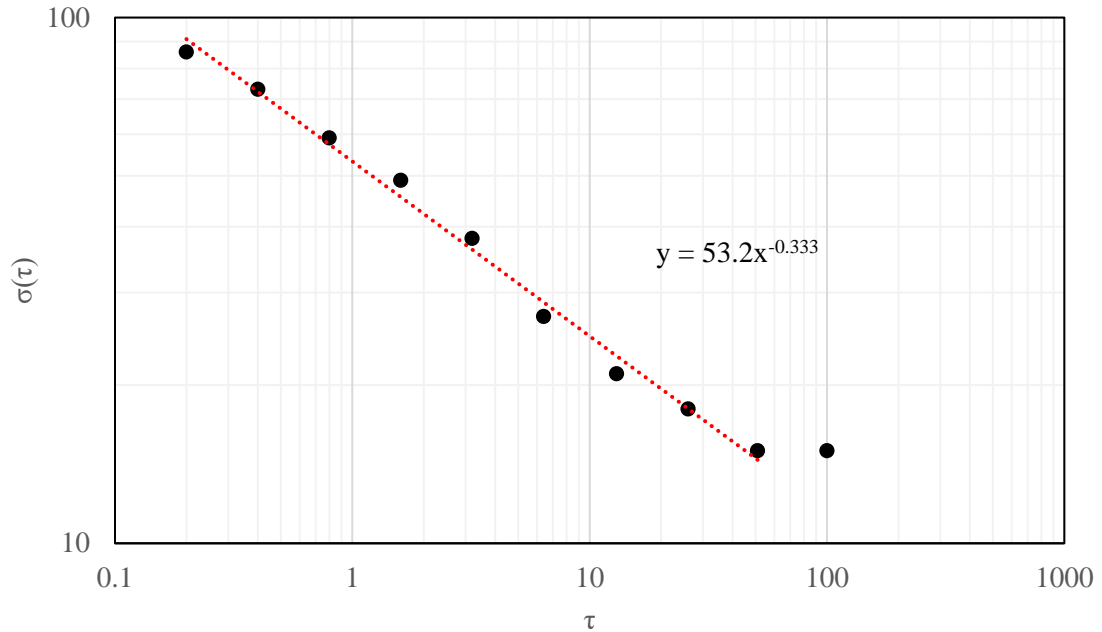


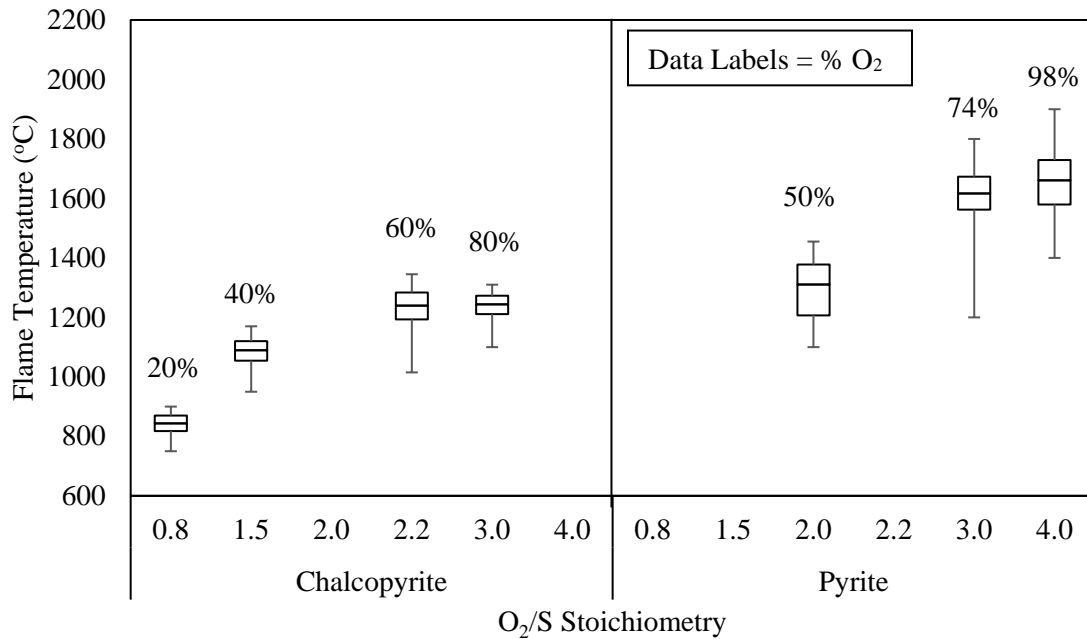
**Figure 24: Allan Variance Analysis**

In Figure 24, the Allan Deviation,  $\sigma(\tau)$ , continues to decrease with  $\tau$  and there is no clear minimum for the Allan Deviation. This suggests that averaging for longer time periods will reduce the noise in the signal and provide a more precise measure. The graph does not show evidence for long-term fluctuations or drifts which would increase the Allan deviation at longer sampling times. For all data collected in this research, integration times between 0.05 – 2 seconds were used without averaging. The Allan Variance diagram in Figure 24 can also be used to characterize the types of noise that give rise to fluctuations in the signal using the slope of the line. The slope of the linear fit in Figure 24 is -0.33. On an Allan Variance plot, a slope of -0.5 is indicative of white noise and a slope of 0 is indicative of flicker noise. Because the slope in Figure 24 is in between -0.5 and 0, the type of noise in the signal is between white and flicker noise. [47] [48] The contribution of these noise sources can be minimized by averaging the signal. If a plant trial of the sensor is conducted, an Allan Variance analysis should be conducted at the start of the trial to determine the

optimum sampling time that should be used. This will ensure a good signal to noise ratio in the data that is collected.

### Combustion Temperatures

Using the two-wavelength technique, the temperature of the combusting particles was calculated from the emission spectrum continuum. The calibration procedure and methodology are summarized in Appendix 1. Temperature profiles are compared for the pure minerals and the concentrates to identify differences in combustion behaviour between feeds. Figure 25 compares the combustion profiles of the pure minerals.



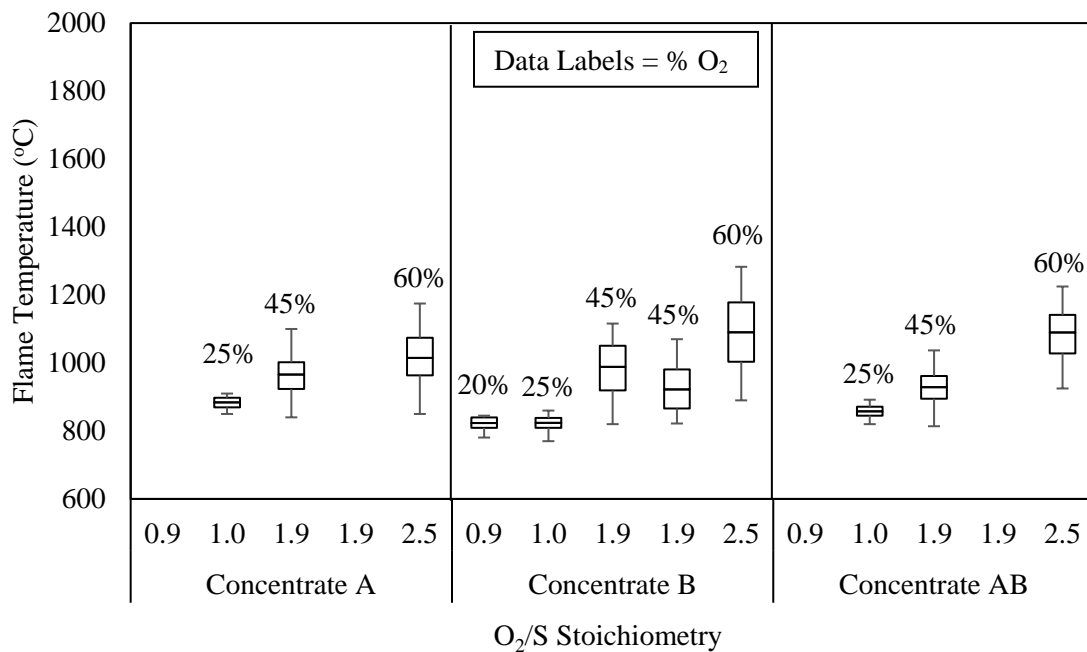
**Figure 25: A comparison of the pure mineral combustion temperature profiles as a function of O<sub>2</sub>/S stoichiometry**

Figure 25 shows that the flame temperature formed from the flash combustion of pure minerals chalcopyrite and pyrite is driven by the O<sub>2</sub>/S stoichiometry. For chalcopyrite, the flame temperature appears to be levelling off at O<sub>2</sub>/S ratios of 2.2 – 3.0. When the O<sub>2</sub>/S condition of 3.0

is considered and the combustion temperatures of chalcopyrite and pyrite are compared, the data shows that pyrite burns ~400° hotter than chalcopyrite.

A measure of stability of the flame temperature is related to its standard deviation. In Figure 26, the standard deviation of the pure mineral temperature profiles increases with O<sub>2</sub>/S stoichiometry. This suggests that flame stability of pure minerals is inversely proportional to flame temperature and the O<sub>2</sub>/S stoichiometry. When comparing the spread of chalcopyrite and pyrite data at an O<sub>2</sub>/S ratio of 3.0, it appears that the pyrite flame is less stable than the chalcopyrite flame in terms of temperature.

The pure mineral temperature profiles are useful for studying concentrates. It was hypothesized that concentrates with higher proportions of pyrite (% Py in Concentrates: Conc. B > Conc. AB > Conc. A) will burn at higher temperatures when compared at the same O<sub>2</sub>/S condition. Figure 26 compares the combustion temperature profiles of the three concentrates.



**Figure 26: A comparison of concentrate combustion temperature profiles as a function of O<sub>2</sub>/S stoichiometry**

Like the pure minerals, the temperature of the flame formed by the combustion of concentrates is driven by the  $O_2/S$  stoichiometry. For the three concentrates tested, the relationship between combustion temperature and  $O_2/S$  stoichiometry appears to be quite similar for a constant  $O_2/S$  stoichiometry and possibly linear over the conditions tested. The combustion temperature profiles are similar for each of the experimental conditions. Differentiation of the concentrates based on their flame temperature is difficult.

Regarding concentrate flame temperature stability, the standard deviation of the concentrate temperature profiles increases with  $O_2/S$  stoichiometry. This suggests that concentrate flame stability is inversely proportional to flame temperature, which is consistent with the pure mineral results.

### **Flame Brightness**

Flame brightness is calculated as the integrated intensity of the emission spectrum. Brightness profiles for all the feeds have been prepared to identify differences in their luminous combustion properties. Figure 27 compares the brightness profiles of the pure minerals.

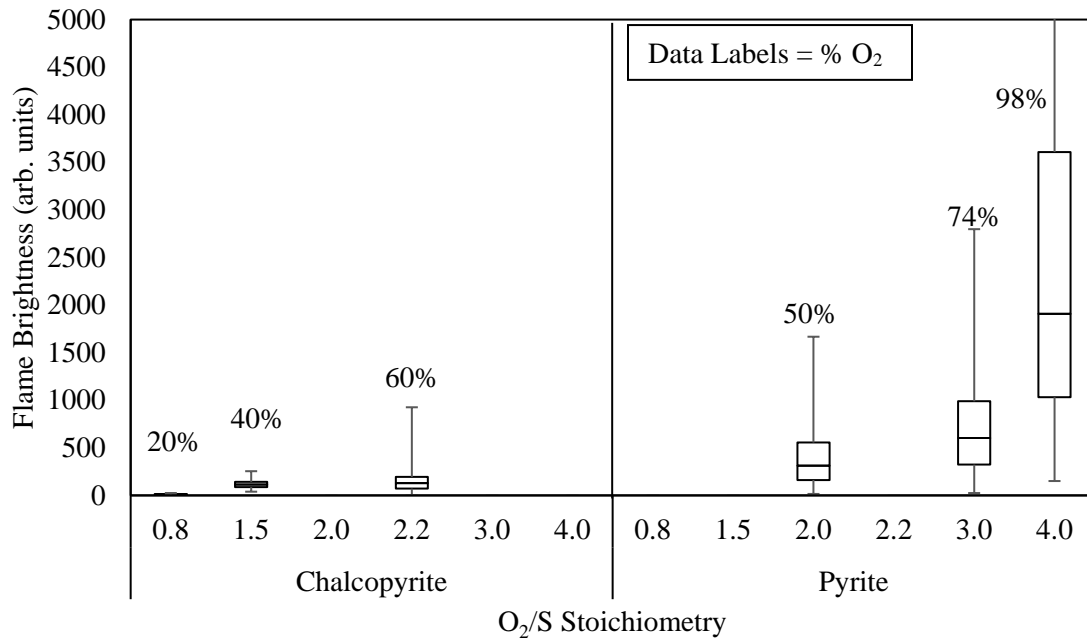


**Figure 27: A comparison of pure mineral combustion brightness profiles as a function of O<sub>2</sub>/S stoichiometry**

Like the flame temperature, brightness is driven by the O<sub>2</sub>/S ratio. In Figure 27, pyrite burns much brighter than chalcopyrite, which suggests that these minerals could be differentiated by the combustion brightness. Despite burning much brighter than chalcopyrite, the pyrite flame is far less stable than that of chalcopyrite as indicated by the standard deviation of the data.

Figure 28 compares the brightness profiles of the concentrates.

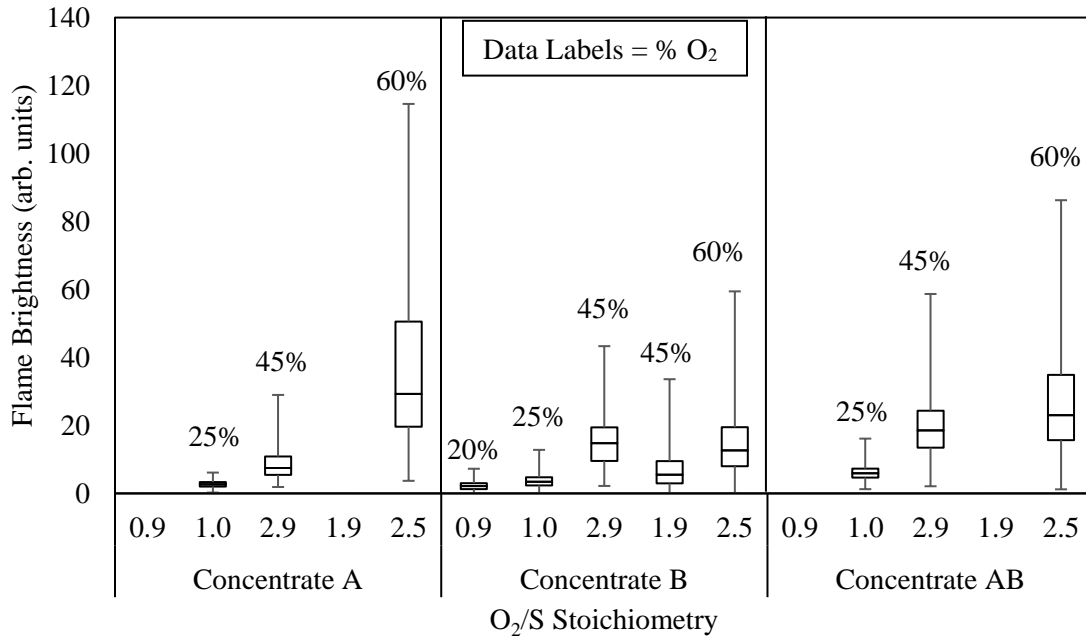


**Figure 28: A comparison of concentrate combustion brightness profiles as a function of O<sub>2</sub>/S stoichiometry**

Like combustion temperature and pure mineral combustion brightness, the concentrate combustion brightness is driven by the O<sub>2</sub>/S stoichiometry. As well, as the stoichiometry is increased, the stability of the flame, as measured by brightness, decreases. At low O<sub>2</sub>/S ratios, the concentrates appear to burn similarly however as the ratio increases, Concentrate A appears to burn brighter than the others. This is contrary to expectations as Concentrate A has the lowest pyrite content in it and it was thought that concentrates with greater proportions of pyrite in them would burn brighter.

## Chapter 5

### Discussion

#### Drop Tower Reaction Products

##### Desulphurization in Flash Smelting – Impact of Mineralogy

To evaluate the scale up potential of the lab results, a mass balance was developed to approximate the sulfur remaining in a 62% Cu matte produced in a commercial furnace. This was done for pure chalcopyrite as well as Concentrates A & B. Assumptions made in developing the models for each of these feeds are:

- 98.5 % of the copper is recovered to the matte in the form of  $\text{Cu}_2\text{S}$
- The matte grade is 62% Cu
- The matte is a binary mixture of  $\text{Cu}_2\text{S}$  and  $\text{FeS}$

With these assumptions and the Cu and S assays of the feed, the % sulphur remaining in the molten products can be approximated. An example calculation is shown for chalcopyrite:

Feed Basis = 100g

Mass S = 34.94g (Chalcopyrite is 34.94% sulphur)

Mass Cu = 34.63g (Chalcopyrite is 34.63% copper)

Mass Cu reporting to the matte =  $34.6 \cdot 0.985 = 34.11$  g

Moles Cu reporting to the matte =  $34.11 / 63.55 = 0.54$  moles

Moles of  $\text{Cu}_2\text{S}$  in the matte =  $0.54 / 2 = 0.27$  moles

Mass  $\text{Cu}_2\text{S}$  in the matte =  $0.27 \cdot 159.1 = 42.71$  g

Moles of S in the matte associated with  $\text{Cu}_2\text{S}$  = 0.27 moles

Mass of S in the matte associated with  $\text{Cu}_2\text{S}$  = 8.66 g

Using the 62% matte grade, the total mass of the matte is calculated to be 55.02 g:

$$\text{Matte Grade (\% Cu)} = 62\% = \frac{\text{Mass of Cu}}{\text{Total Mass of Matte}}$$

Because of the assumption that the matte is a binary mixture of  $\text{Cu}_2\text{S}$  and  $\text{FeS}$ , the difference between the mass of  $\text{Cu}_2\text{S}$  and the total mass of the matte is attributed to the phase  $\text{FeS}$ .

$$\text{Mass FeS in Matte} = \text{Total Mass of Matte} - \text{Mass of Cu}_2\text{S in Matte} = 55.02 - 42.71 = 12.30 \text{ g}$$

$$\text{Moles FeS in Matte} = \text{Moles S in Matte} = 12.30 / 87.91 = 0.14$$

$$\text{Mass of S in the matte associated with FeS} = 0.14 \cdot 32.06 = 4.49 \text{ g}$$

$$\text{Total Mass of S in the matte} = 4.49 + 8.66 = 13.15 \text{ g}$$

$$\% \text{ S Remaining in Matte} = \frac{\text{Total Mass of S in the Matte}}{\text{Total Mass of S in the Feed}} = \frac{13.1}{34.9} = 0.375 = 37.5\%$$

Thus, the sulphur remaining in the molten products of the flash combustion of pure chalcopyrite is 37.5%. The above calculations were carried out for Concentrates A & B. Because these concentrates have nearly identical Cu and S assays, the matte produced from them will have similar compositions. A 62% matte produced from the combustion of Concentrates A & B will have 32% of the feed sulphur remaining in it.

The calculated conditions of the commercial furnace are useful for evaluating the quality of the results acquired in the drop tower. Commercial furnaces typically operate with an  $\text{O}_2/\text{S}$  ratio  $< 1$  (for pure chalcopyrite, an  $\text{O}_2/\text{S}$  of 0.8 is required to produce a 62% matte). The  $\text{O}_2/\text{S}$  conditions used in this test work were in the range 0.8 – 4. Thus, we are in part capturing the industrial operating  $\text{O}_2/\text{S}$  condition.

### Pure Chalcopyrite

Calculations show that an industrial flash furnace, the production of a 62% Cu matte from pure chalcopyrite will result in 37.5% sulphur remaining in the molten products. With this information, the  $O_2/S$  ratio required to produce a product of this composition in the drop tower can be interpolated. Figure 29 shows the chalcopyrite desulphurization curve. The horizontal dashed line represents the amount of sulphur that would remain in a matte with a Cu grade of 62%.

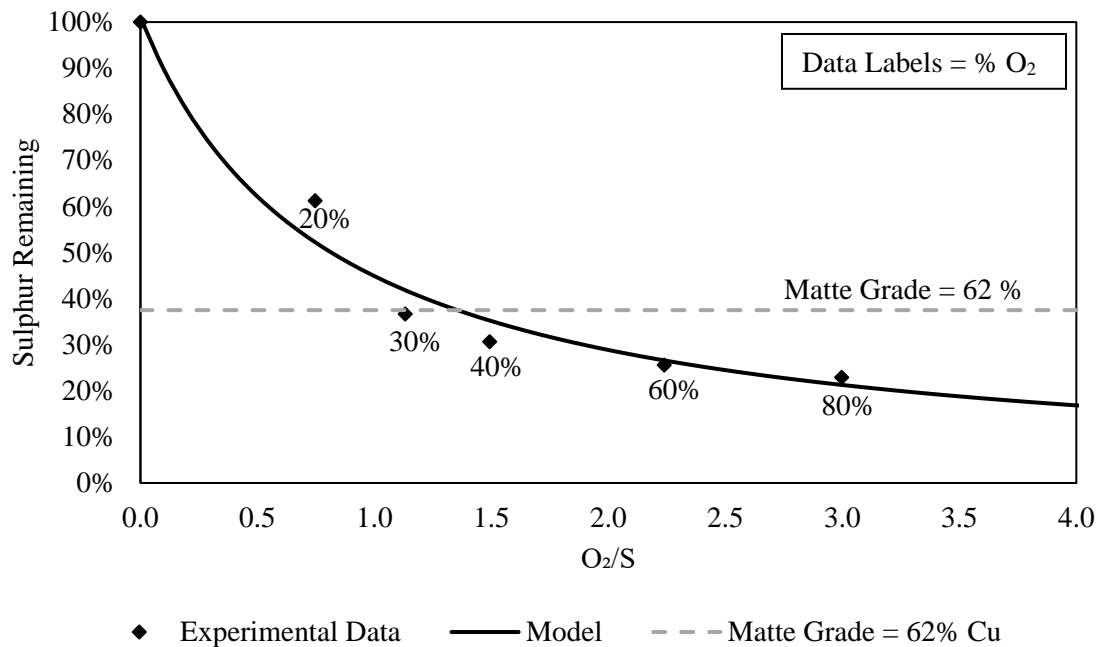


**Figure 29: Chalcopyrite desulphurization to a 62% grade matte**

The intersection of the dashed horizontal line with the modelled desulphurization curve represents the  $O_2/S$  stoichiometry required to desulphurize the feed to a matte grade of 62%. For pure chalcopyrite, the  $O_2/S$  ratio required for this is ~1.35.

### *Concentrates*

Chalcopyrite and pyrite are typical minerals in a copper concentrate. Using the experimental and modelled desulphurization data of the pure minerals, the desulphurization of the concentrates was estimated. Figure 30 and Figure 31 show the experimentally modelled desulphurization curves of Concentrate A & B with the following information mapped onto it:

- The cumulative contributions of the pure minerals, chalcopyrite and pyrite, to the concentrate desulphurization are mapped onto the experimental points as stacked columns below the curve. The sum of the stacked columns represents the amount of sulphur that would be expected to remain in the products if sulphur is only removed from pyrite and chalcopyrite. These values were calculated using the modelled pure mineral desulphurization curves.
- In the top right corner of Figure 30 and Figure 31 the contributions of pyrite and chalcopyrite to the overall mineralogy of the concentrate are presented.
- The horizontal dashed line represents the calculated amount of sulphur that would remain in a matte with a grade of 62% Cu. The O<sub>2</sub>/S ratio at the intersection of this horizontal line with the desulphurization curve is the condition required to produce a matte with 62% Cu.
- The enrichment of O<sub>2</sub> in the reaction gas is shown as a data label above the experimental points.

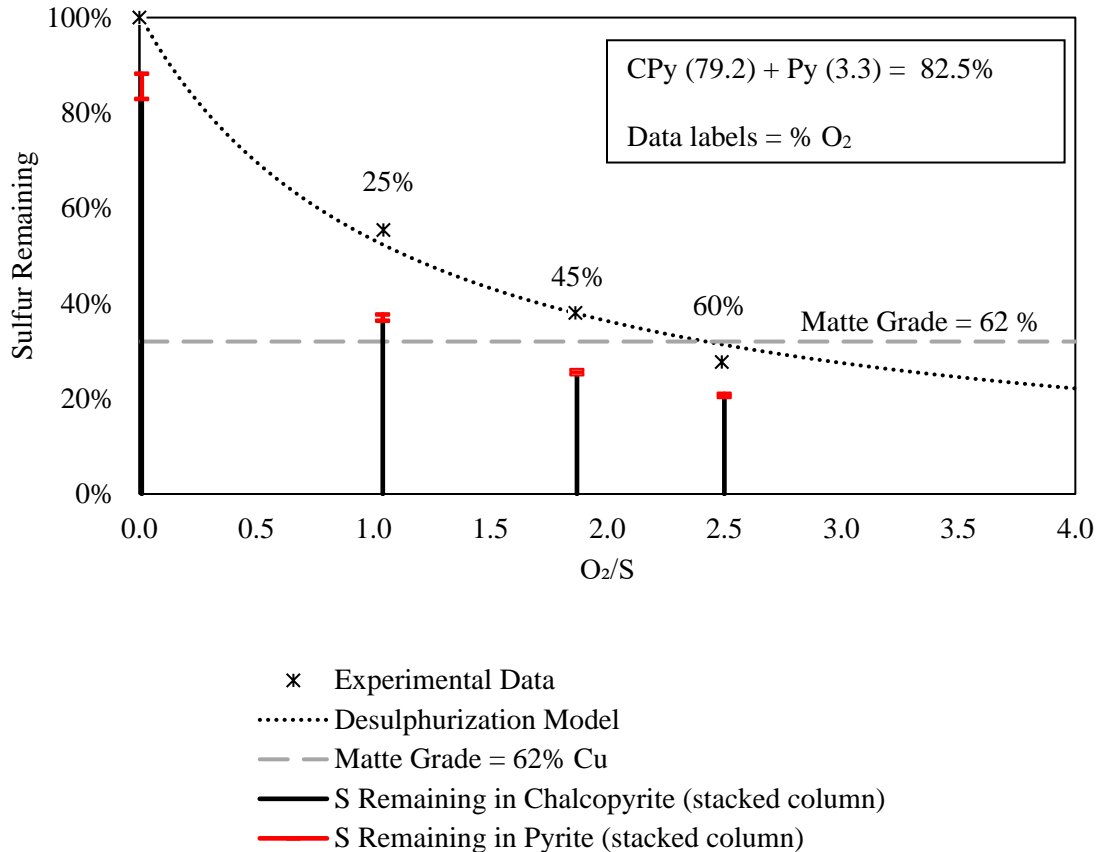


**Figure 30: Pure mineral mapping to the desulphurization of Concentrate A**

The stacked columns in Figure 30 show that chalcopyrite and pyrite alone do not reconstruct the desulphurization curve for Concentrate A. The effect of other minerals and the interaction between minerals is believed to explain the difference between the stacked columns and the experimental data. Through further drop tower testing with other minerals and binary mixtures of minerals, the concentrate desulphurization curve can likely be reconstructed completely.

The % sulphur remaining in a 62% Cu matte produced from Concentrate A was calculated to be 32%. From the Concentrate A desulphurization curve, the O<sub>2</sub>/S ratio required to produce a product of this composition is ~2.4. The enrichments used in these experiments were generally quite low. The industrial furnace operates around a 60% O<sub>2</sub> enrichment. It is thought that with a more enriched reaction gas, especially for the lower O<sub>2</sub>/S ratios, concentrate desulphurization

would be greater. Thus, in future testing, a more enriched reaction gas representative of the commercial furnace should be used.

Figure 31 shows the desulphurization curve for Concentrate B with the cumulative contributions of pure minerals, chalcopyrite and pyrite, mapped onto the experimental points as a stacked column below the curve.

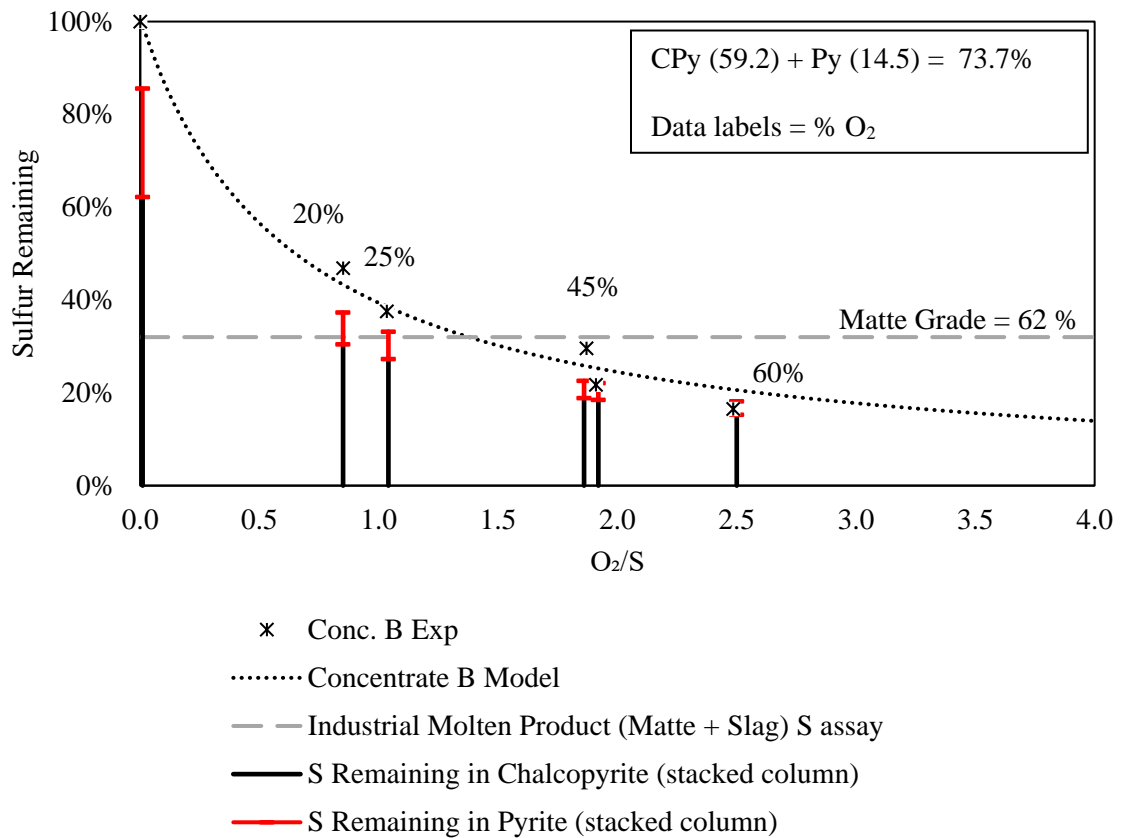


**Figure 31: Pure mineral mapping to the desulphurization of Concentrate B**

Like Concentrate A, the pure minerals chalcopyrite and pyrite alone do not reconstruct the Concentrate B desulphurization curve. Other minerals in the concentrate are contributing to the desulphurization of this concentrate, which were not captured in this experimental campaign.

The % sulphur remaining in a 62% Cu matte produced from Concentrate B was calculated to be 32%. This number is the same as for Concentrate A because these two concentrates have nearly identical Cu/S ratios. From the Concentrate B desulphurization curve in Figure 31, the  $O_2/S$  ratio required to produce a 62% matte is ~1.35. Concentrate B requires a 43.75% lower  $O_2/S$  stoichiometry to be desulphurized to a 62% matte than Concentrate A does. The differences in  $O_2/S$  required for desulphurization between these concentrates is attributed to their mineralogy. It is likely that the pyrite content in Concentrate B drives its increased desulphurization, as pyrite was observed to lose sulphur rapidly as the  $O_2/S$  ratio is increased (see Figure 9).

A comparison of the Concentrate A and B desulphurization curves in Figure 30 and Figure 31, respectively, has interesting implications for the impact of mineralogy on flash combustion processes. Concentrate B requires a significantly lower  $O_2/S$  stoichiometry for matte production. It is the belief of the authors that the difference in  $O_2/S$  conditions required for processing is attributed to differences in mineralogy. When the pure mineral behaviour is considered from Chapter 4 (Figure 9), pyrite requires a lower  $O_2/S$  stoichiometry than chalcopyrite to be desulphurized to a common product sulphur assay. Relative to Concentrate B, Concentrate A has a high proportion of chalcopyrite (79.2%) and a low proportion of pyrite (3.3%); it requires a “high”  $O_2/S$  to be desulphurized. Conversely, Concentrate B has low chalcopyrite (59.1%) and high pyrite (14.5%) mineralization relative to Concentrate A; it requires a lower  $O_2/S$  stoichiometry to be desulphurized. These results make it clear that mineralogy is an important variable for flash combustion processes.

Another consideration for the desulphurization behaviour is that the concentrates did not have the same size distribution. It is interesting to note that Concentrate B, which had the coarsest F80 particle size, was still desulphurized to the greatest extent. Based on single particle experimental results in the literature, it was expected that the desulphurization of Concentrate B would be hindered by its coarser size distribution. [9] It is likely the presence of pyrite in Concentrate B that is driving the desulphurization reactions forward despite the coarse size distribution (measured relative to the other concentrates in this thesis).

Concentrates A and B are almost identical in terms of the Cu, Fe and S assays which allows for the impact of mineralogy on the flash combustion process to be isolated. It is clear from the desulphurization curves in Figure 30 and Figure 31 that mineralogy plays an important role on the flash combustion behaviour of concentrates. A major finding of this thesis is that the mineralogy as well as chemical composition is important to consider when preparing the feed/choosing the conditions for the blend entering a flash furnace. Operations interested in taking feed mineralogy into account would be well-advised to first identify and distinguish concentrates that are easy and hard to process in their flash furnace. By comparing the mineralogy of these blends, it may be possible to identify reasons why some concentrates are challenging to process and others are not. Such work could be further validated with drop tower experiments at conditions that are representative of their furnace. This information could be useful for preparing blends, sourcing new concentrates and/or choosing operating conditions.

In considering the data collected as part of these thesis, there is an opportunity to improve. This could be accomplished by:

- Running multiple tests at each of the experimental conditions to increase the confidence in the results
- Conducting tests at more O<sub>2</sub>/S conditions for each of the feeds to fill out the desulphurization curves and increase the accuracy of results. To have an accurate curve, several data points at different O<sub>2</sub>/S conditions are required.
- The O<sub>2</sub>/S and O<sub>2</sub> enrichments used in this thesis likely do not match the industrial burner for the same matte grade. Future testing should use O<sub>2</sub>/S ratios < 1 with O<sub>2</sub> enrichments > 50% to match conditions in the commercial furnace.

## **Product Mineralogy**

### ***Pure Minerals***

XRD analysis of the pure minerals was done to understand the reaction mechanism that happens in the shaft of the flash furnace. The XRD analysis of the pyrite reaction products was not revealing because the  $O_2/S$  stoichiometric conditions used were too oxidizing; only  $Fe_2O_3$  and  $Fe_3O_4$  were identified through the XRD analysis. These reaction products are consistent with the single particle tests done by Jorgensen. [18] In future tests, lower  $O_2/S$  stoichiometries should be used to better capture intermediate phases. In such tests, it is expected that pyrrhotite as an intermediate phase would be observed. [18]

The products of flash combustion of chalcopyrite all contained appreciable amounts of  $Fe_3O_4$ , regardless of the  $O_2/S$  condition. Only under the highest  $O_2/S$  condition were small quantities of hematite formed. Single particle combustion tests of chalcopyrite by Jorgensen showed that cuprospinel ( $CuFe_2O_4$ ), intermediate solid solution ( $CuFe_2S_3$ ) and  $Fe_2O_3$  are the main reaction products of chalcopyrite flash combustion. [9] [19] In comparing these phases to the ones formed in the drop tower, the only commonality is hematite which was observed in the products formed at an  $O_2/S$  condition of 3.0. These differences may be explained by differences in oxygen supply ( $O_2/S$  ratios) used in single particle tests and drop tower tests. Compared to single particle tests, the  $O_2/S$  stoichiometries used in this research are much lower than what has conventionally been used. It may be that the lower  $O_2/S$  ratios used in the drop tower limited the further oxidation of  $Fe_3O_4$  into  $Fe_2O_3$  compared to the single particle tests. In terms of Cu-Fe-O species, the XRD analysis of chalcopyrite products indicates that delafossite ( $CuFeO_2$ ) is one of the reaction products of its flash combustion which is supported by the concentrate QEMSCAN® analysis. Thus,  $CuFeO_2$  is an intermediate phase formed in the flash combustion of chalcopyrite in addition to the intermediate solid solution and cuprospinel that Jorgensen documented. [19]

**Concentrates**

To analyze the QEMSCAN data, a mass balance using the feed and product silicon assays was done to calculate the mass ratio of products to feed, X. An assumption made in developing the mass balance is that all the of silicon in the feed reports to the solid products. The mass balance of Si was set up as follows:

$$\begin{array}{rcl}
 & \text{Feed} & == & \text{Products} \\
 \text{Mass} & 1 & & X \\
 \%Si & Si_{\text{Feed}} & & Si_{\text{Prod.}}
 \end{array}$$

Assuming a 1-gram basis for the feed, the mass of the products is calculated using the silicon content of the feed and products by:

$$X = \frac{1 \cdot Si_{\text{Feed}}}{Si_{\text{Prod.}}}$$

This calculation was done for each of the products that were analyzed by QEMSCAN® to calculate X. The mass ratio of products to feed, X, for each of the four samples analyzed with QEMSCAN® are summarized in Table 15.

**Table 15: Mass yield to the products for the concentrate QEMSCAN® samples**

	O <sub>2</sub> /S	Feed %Si	Product %Si	X
Concentrate A	1.9	0.96	1.8	0.53
Concentrate AB	1.9	1.61	2.96	0.54
Concentrate AB	2.5	1.61	2.61	0.62
Concentrate B	1.9	2.26	3.03	0.75

The results in Table 15 make sense as concentrates with a higher ratio of products to feed, X, should be desulphurized more. The mass yield fractions agree with the concentrate desulphurization curves whereby the concentrates in order of increasing desulphurization are: Concentrate A, Concentrate AB and Concentrate B.

### Consumption / Production of Sulphur Bearing Minerals

The mass balance in Table 15 was used to evaluate the consumption & production of major sulphide minerals in the feed. Calculations for consumption were done according to:

$$\% \text{ Consumption} = \frac{M_{i,Feed} - M_{i,Prod.}}{M_{i,Feed}} \cdot 100\%$$

where,  $M_{i,Feed}$  is the mass of the mineral in the feed

$M_{i,Prod.}$  Is the mass of the mineral in the products

Percent consumption can assume a positive value with an upper limit of 100%. A positive consumption means that there is less of that mineral in the products than in the feed. Percent consumption can also assume a negative value which would mean that there is more of that mineral in the products than was originally present in the feed. Figure 32 shows the % consumption of major sulphide minerals during drop tower testing. In Figure 32, the chalcopyrite phase and bornite phase categories includes the pseudo forms of these minerals.

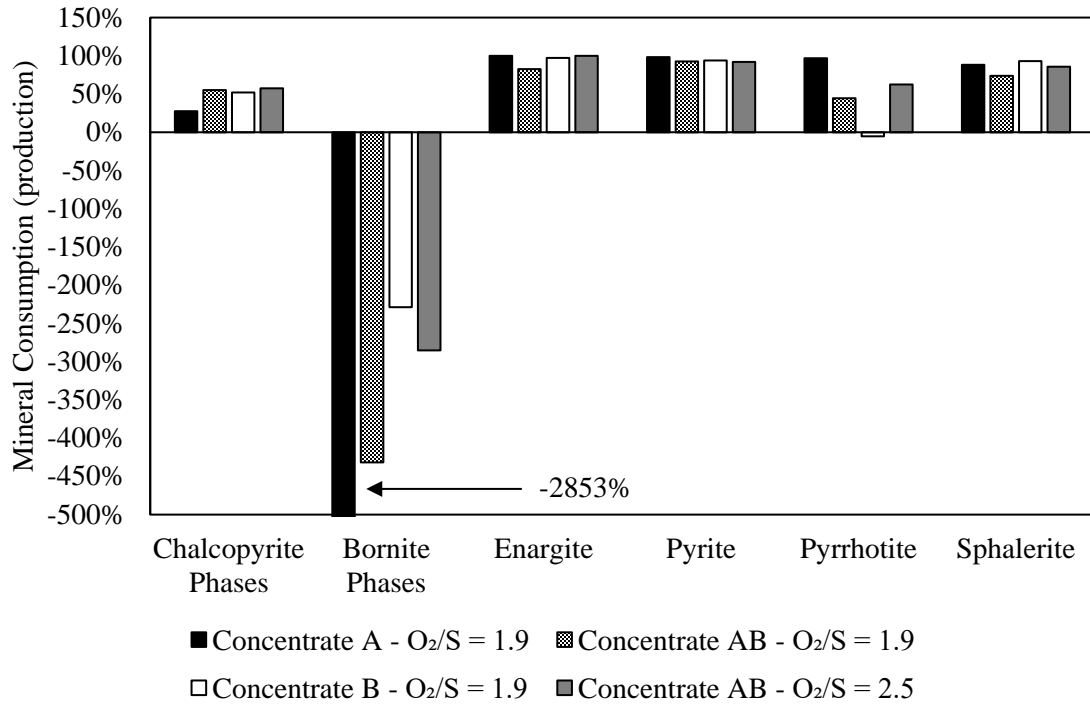


**Figure 32: Consumption (production) of major sulphide minerals in concentrate flash combustion**

Figure 32 shows that chalcopyrite was only partially consumed for each of the concentrates and O<sub>2</sub>/S conditions. The reason for this is that it forms intermediate decomposition products, pseudochalcopyrite and pseudobornite. Concentrate A, which had the greatest consumption of chalcopyrite had the highest production of bornite phases. Because bornite phases are present in high quantities in the products, the further reaction of this mineral is likely not favourable (otherwise it would have reacted into other phases). Thus, in future tests with the drop tower, if bornite is used as the feed, it is expected that the desulphurization of bornite will be less than it was for chalcopyrite and pyrite. Bornite has a higher ignition temperature than chalcopyrite and pyrite [18], likely due to the lower concentrations of Fe and S in the mineral. Because of this, ignition takes longer and oxygen will preferentially react with minerals such as chalcopyrite and pyrite.

The consumption of pyrite, enargite and sphalerite was nearly 100% for each of the concentrates and O<sub>2</sub>/S conditions. This suggests that the desulphurization of these minerals is favourable and that they will react preferentially over phases such as chalcopyrite and bornite.

The QEMSCAN® maps in Chapter 4, combined with the data in Figure 32, provide some interesting insights into the reaction mechanisms that minerals underwent.

- Chalcopyrite decomposes to pseudochalcopyrite which is the partially oxidized form of chalcopyrite. It seems that further reaction of pseudochalcopyrite is limited as the morphology of these particles are almost all non-spherical and their composition is generally uniform throughout the particle. The non-spherical nature of these particles and the uniform composition of these particles suggest that they did not melt and oxidation of other minerals occurred preferentially over pseudochalcopyrite. Thus, chalcopyrite decomposes readily into its partially oxidized form, pseudochalcopyrite, however further reaction of these mineral species is not favourable.
- The morphology of pseudobornite particles are highly irregular and fragmented. As well, pseudobornite seems to associate with the phase magnetite-hematite, which tends to form on the outside of the particles. The magnetite-hematite encapsulation of these particles and the highly irregular particle morphologies would support the dusting mechanism proposed by Jokalaikso whereby pressure buildup inside an encapsulated particle eventually leads to a pressure burst and particle fragmentation. [45] The concentration of pseudobornite in the products appears to correlate with the original chalcopyrite concentration in the feed; concentrates with high chalcopyrite mineralization seem to produce high amounts of pseudobornite as an intermediate phase. This may suggest that concentrates with high chalcopyrite mineralization are more prone to dusting through production of this intermediate phase.

### Minor Element Behaviour

In Chapter 4, a trend was identified whereby minor metal impurities tend to associate in increasing concentrations with species that have high atomic proportions of oxygen. Table 16 shows the pseudo species and the concentrations of minor metal impurities in each. Moving down the table, the atomic % of sulphur decreases and that of oxygen increases.

**Table 16: Impurity composition of pseudo species from the QEMSCAN® Analysis**

Phase	Si	Al	Ca	Mg	Zn	Total Impurities
Pseudochalcocite	0.0 ± 0.0	0.0 ± 0.0	0.0 ± 0.0	0.0 ± 0.0	0.0 ± 0.0	0.0 ± 0.0
Pseudobornite	0.0 ± 0.0	0.0 ± 0.0	0.0 ± 0.0	0.0 ± 0.0	1.3 ± 2.8	1.3 ± 2.8
Pseudochalcopyrite	0.0 ± 0.0	0.0 ± 0.0	0.0 ± 0.0	0.0 ± 0.0	1.5 ± 2.4	1.5 ± 2.4
FeOx + Cu	4.8 ± 1.4	1.6 ± 0.4	1.3 ± 0.9	1.9 ± 1.7	0.3 ± 0.7	9.9 ± 3.0
FeOx Impure	5.3 ± 3.3	1.2 ± 1.1	2.2 ± 1.4	3.3 ± 3.3	0.5 ± 0.9	12.6 ± 7.6

Si, Al, Ca, Mg and Zn were the main minor metal impurities that associated with the pseudo species. For each of these species except Zn, the concentration was positively correlated with the atomic % of oxygen in the phase. For Zn, the opposite was true whereby Zn tends to associate with phases that have a high atomic % sulphur and low oxygen. These results suggest that in flash combustion, Zn will be recovered to the matte and Si, Al, Ca, and Mg will be recovered to the slag.

### **Particle Size Analysis**

The products of drop tower experiments were subjected to particle size analysis to evaluate the impact of O<sub>2</sub>/S stoichiometry and feed mineralization on the product particle size distribution. The cumulative particle size distributions in Chapter 4 were used to interpolate the P80 particle size and dust fractions for each feed and experimental condition. For the purposes of this study, dust is defined as particles in the size range 0 – 20 µm and the dust fraction is the cumulative volume % of material in this size range. [40] Figure 33 compares the evolution of products for the pure minerals, where the dust fraction is represented by the columns on the primary y-axis and the P80 particle size is captured by the line on the secondary y-axis. The “Feed” represents pure,

unreacted material while the numerical  $O_2/S$  condition on the x-axis represents the analysis of products for that experimental condition.

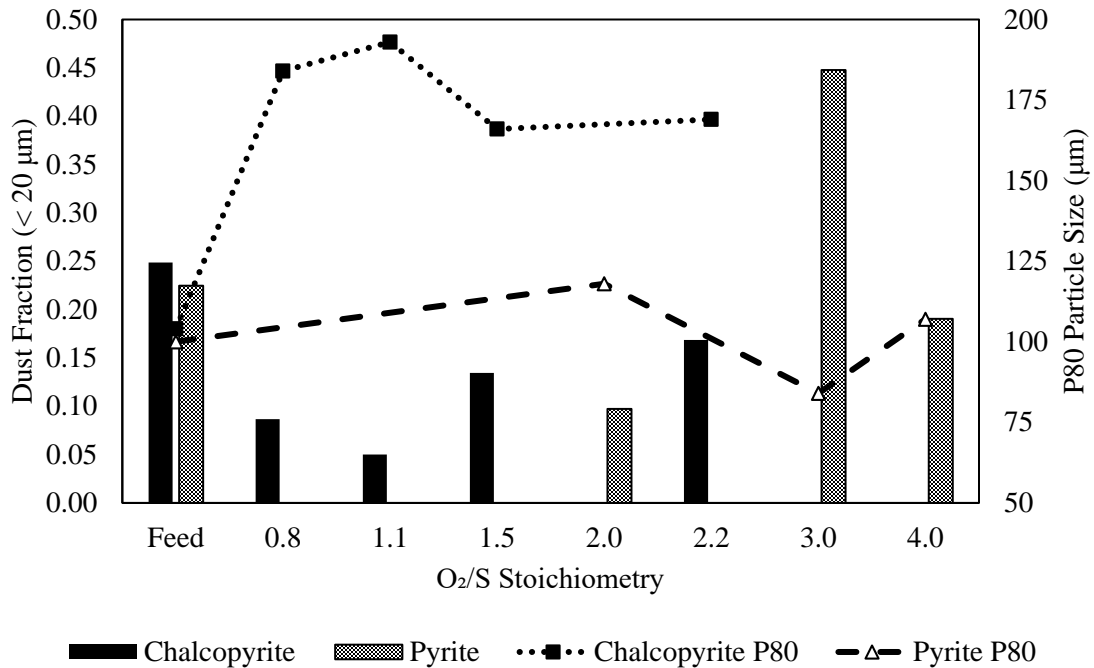


**Figure 33: Evolution of products – Dust fraction in the products (bars on primary y-axis) and P80 particle size (line on secondary y-axis)**

It is clear from Figure 33 that chalcopyrite and pyrite behave differently in terms of how the particles evolve. When considering chalcopyrite, the P80 increased relative to the feed for all test conditions and the dust fraction appears to increase with the  $O_2/S$  stoichiometry. The increase in the dust fraction at higher  $O_2/S$  stoichiometry suggests that  $O_2/S$  drives dusting of chalcopyrite. In terms of the data collected at an  $O_2/S$  ratio of 0.8, which is in line with where the commercial furnace operates, the dust fraction in the decreased from 24.6% in the feed to 8.7% in the products. This reduction in dust at low  $O_2/S$  stoichiometries is good for commercial operations as dust in the feed will be consumed rather than generated in the flash combustion process.

Regarding the behaviour of pure pyrite in the drop tower, the data in Figure 33 suggests that flash combustion of pyrite does not significantly change the P80 particle size. As for

chalcopyrite, the dust fraction in the products is reduced post combustion and the dust fraction appears to increase with  $O_2/S$  stoichiometry. Other researchers have shown that dust production and particle fragmentation increases in higher oxidizing environments. [45]

The single particle behaviour of pyrite and chalcopyrite has been previously studied in the lab, however the documented results do not compare well with those in this thesis. In studies by Jorgensen, flash combustion of chalcopyrite and pyrite resulted in a reduction in the particle size. [9] [16] These experiments used very low feed rates to simulate single particle behaviour. Stefanova states that the mechanism for particle expansion is the collision and fusion of particles during oxidation processes. [49] In these early flash combustion studies, particle expansion was unlikely because of the very low feed rates and dilute ratio of solids:reaction gas. [40] This is likely why only a reduction in the particle size was observed in Jorgensen's pure mineral experiments. In the current research, a higher feed rate is used and thus particle-particle interactions cannot be discounted. Thus, the differences in results between single particle literature and the current study may be attributed to the solids feed rate and the density of solids in the reacting gas stream.

The behaviour of pure minerals is useful for evaluating the concentrates that were tested in this research. Based on the pure mineral results, the expected behaviour of the concentrates is that ones with more chalcopyrite will see a greater increase in the P80 and the fraction of dust in the products should correlate positively with the  $O_2/S$  stoichiometry. Figure 34 compares the change in dust fraction and P80 particle size for each of the three concentrates.

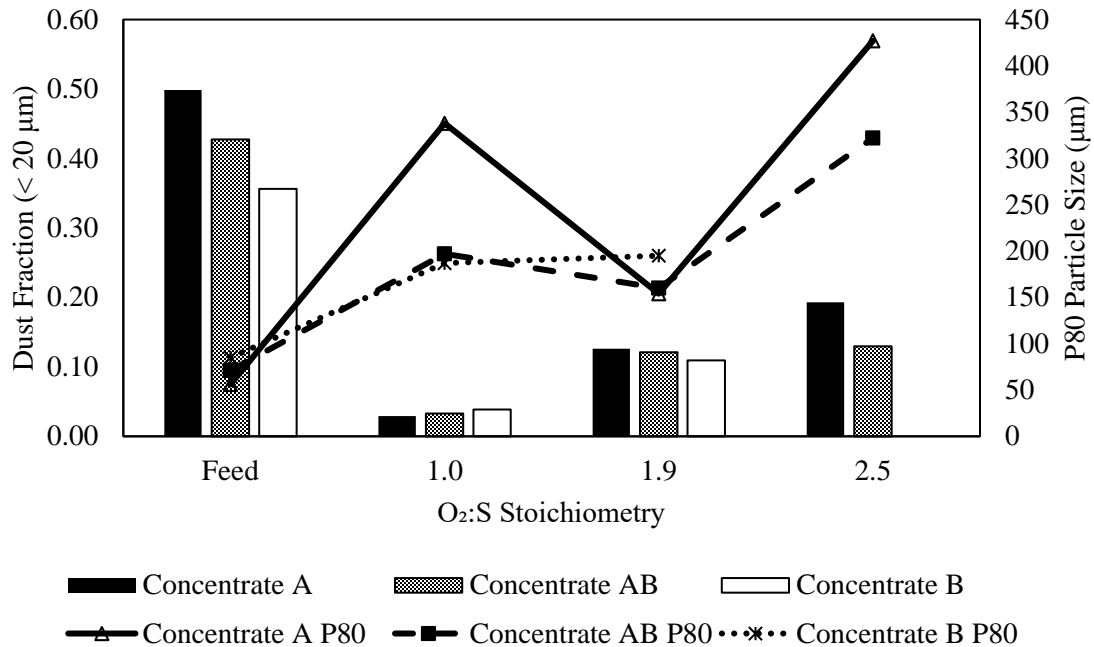


**Figure 34: Evolution of products – Dust fraction in the products (bars on primary y-axis) and P80 particle size (line on secondary y-axis)**

Judging by the feed columns in Figure 34, the unsieved concentrates originally contained a significant amount of very small particles (dust). For all concentrates, flash combustion in the drop tower resulted in a reduction in the dust fraction in the products; however, as the O<sub>2</sub>/S stoichiometry is increased, the dust fraction appears to increase. This result is consistent with the pure mineral results, in which there appeared to be a positive correlation between the dust fraction and the O<sub>2</sub>/S ratio. In a recent paper by Dr. Parra, his group found that particles <45 μm tended to coalesce together and increase their mean size thus reducing the fraction of dust in the products. [40] The reason for this is the particle-particle interactions in the reaction gas solid stream cause particles to fuse together. [40] This mechanism is elucidated in Figure 35, which is an SEM image of a pseudochalcopyrite particle with smaller particles fused to its exterior.

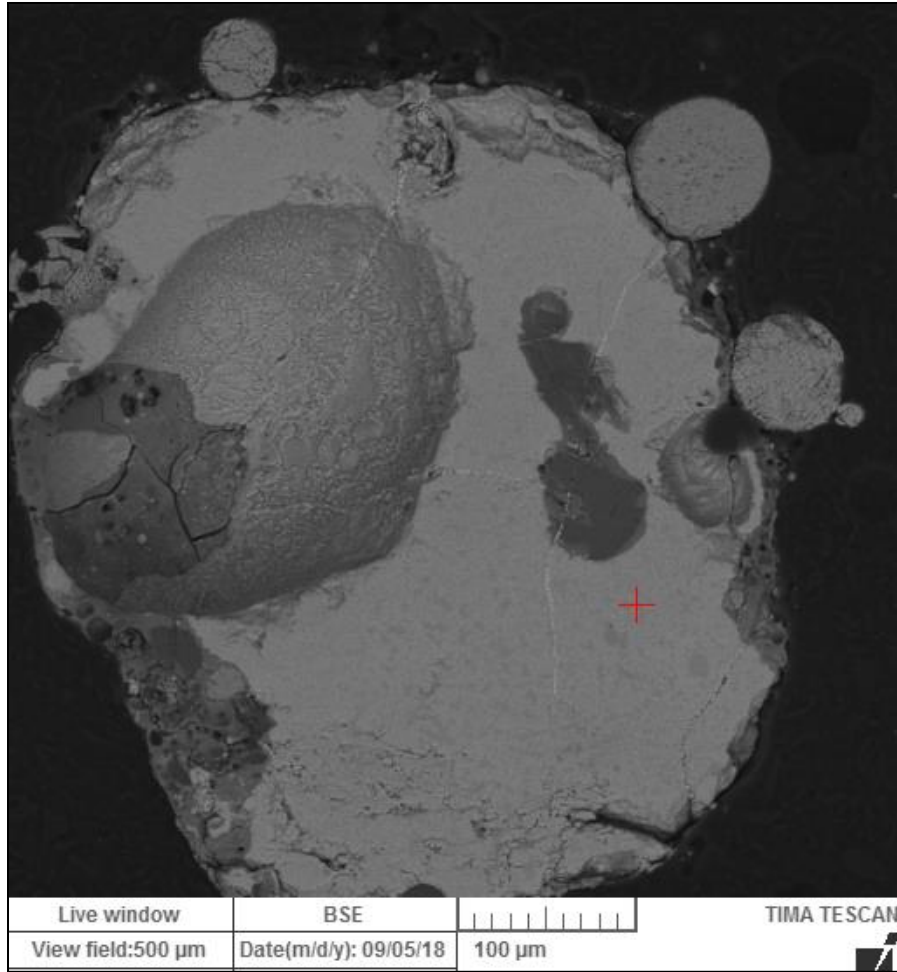


**Figure 35: SEM-EDX image of a pseudochalcopyrite particle with fused particles on the exterior**

Figure 35 validates the theory that particles are fusing together as the mechanism for particle expansion for higher density gas-solid mixtures, which Dr. Parra proposed. [40] In this SEM image, the individual particles can be identified which suggests that fusion took place in a semi-molten state. Dr. Parra's research group used a very similar experimental setup and thus the particle expansion results are consistent with his observations.

In terms of particles  $> 45 \mu\text{m}$ , Dr. Parra's group observed minimal change or a reduction in particle size. [40] In the current study, an increase in the P80 particle size was observed. These

differences could be caused by differences in the feed composition between Dr. Parra's study and the current one or by the O<sub>2</sub>/S ratio, which was much higher in Dr. Parra's experiments. [40]

## **Emission Spectroscopy in Flash Furnace Smelting**

### **Emitting Species**

One of the main thrusts of this thesis was to use emission spectroscopy to identify changes in feed composition in flash furnace smelting in real time using atomic and molecular emissions. For all feeds, only alkali metal emissions were observed, which were not quantified, as they do not provide a useful information on the oxidation of Cu and Fe species. The reason that only alkali metal emissions were induced is related to the temperature of the reactor and flame, which was not high enough to thermally excite other species such as Cu or Fe. Alkali metal species have low melting points, are easily ionized and have a high transition probability which results in the strong emissions that were observed. [46] The temperature of the flame formed in the laboratory reactor was less than 2000°C for all feeds that were tested. To induce atomic or molecular emissions that can be used to differentiate the blends, a much hotter flame is needed. It is possible that in the commercial furnace, with a greater feed rate and higher furnace temperature, emission lines or bands from species other than the alkali metal group will be observable. This represents an opportunity associated with scaling up the sensor to the commercial furnace. Alternatively, an auxiliary, intermittent, high-temperature flame (based on e.g. an acetylene flame or hydrogen flame) may be used to induce atomic emission. With a hotter flame, opportunities for new emissions includes SO, O<sub>2</sub>, FeO, CuOH, CuCl and CO<sub>2</sub>, all of which happen in the range 244 to 576 nm, to be observed. [28] As well as these molecular emissions, Cu, Fe and other transition metal emissions may be induced in 500 – 900 nm region of the spectrum, which is already being monitored by the Avantes spectrometer. Another opportunity for monitoring flash combustion processes is through absorption spectroscopy. Within the flame emission spectrum there may be absorption bands from gaseous molecules. H<sub>2</sub>O, NO<sub>x</sub>, CO and CO<sub>2</sub> absorb in the near IR. [50] O<sub>2</sub> and SO<sub>2</sub> absorptions

occur in the UV in the ranges 167 – 244 nm and 265 – 319 nm respectively. [28] The use of a pen light and extending the measurement range of the spectrometer may allow for such absorptions to be measured.

### **Flame Temperature**

Using the two-wavelength method, the combustion temperature of different feeds in the drop tower was calculated during experimental tests. For both pure minerals and concentrates, the temperature of the flame is governed by the  $O_2/S$  stoichiometry. It was possible to differentiate chalcopyrite and pyrite at a common  $O_2/S$  stoichiometry based on their combustion temperatures, as pyrite was observed to burn at higher temperatures than chalcopyrite. This result is consistent with existing literature. [9] [17] [51] When considering the concentrate temperature profiles, it was hypothesized that concentrates with higher proportions of pyrite in them would burn hotter. This hypothesis was not proven to be true, as the concentrates had very similar temperature profiles at a constant  $O_2/S$  stoichiometry. The concentrate flame temperatures were in the range of 900 – 1500°C across the  $O_2/S$  conditions tested (0.8 to 2.5). This is lower than what was measured by Dr. Parra in [14] with the same instrument, however the tests in his paper used  $O_2/S$  stoichiometries on the order of 100. In Dr. Parra's study, the impact of  $O_2$  enrichment on flash combustion reactions, in the absence of  $O_2$  mass transport, was isolated. This thesis aimed to do the opposite, which was to study the impact of  $O_2/S$  stoichiometry when mass transport may be limiting to the reaction progress.

The experimental conditions used in this thesis had lower  $O_2/S$  stoichiometries than anything currently documented in the literature. Flash combustion research typically isolates the enrichment of the gas at  $O_2/S$  conditions that are not representative of the commercial furnace. This is done to remove mass transport limitations on the reactions. The temperatures measured in this research are lower than what the single particle combustion studies found, which is thought to be a result of mass transport of  $O_2$ . [9] [17] [51] It will be interesting to test the sensor in a commercial

furnace and see how the flame temperature measured in the lab compares with the flame formed in a plant. Such results may be useful for researchers developing flash combustion models as they may be able to use more representative temperatures to capture the phenomena which happen in a flash furnace.

### **Flame Brightness**

The brightness of the flame formed for different feeds was calculated as the integrated intensity of the emission spectrum. In an ideal case one would want to integrate the entire blackbody emission spectrum. Unfortunately, a very large fraction of the emission is at wavelengths longer than about 1000 nm and could not be captured with the spectrometer. This explains why the expected temperature dependence of the brightness  $B = a T^4$ , was not observed. Like the flame temperature, the brightness of the flame is driven by the O<sub>2</sub>/S stoichiometry and the pure minerals could be differentiated based on the brightness of the flame at a fixed O<sub>2</sub>/S condition. Pyrite was observed to burn brighter than chalcopyrite. When considering the concentrate brightness profiles, it was hard to differentiate the concentrates based on their brightness at a fixed O<sub>2</sub>/S condition. It was hypothesized that concentrates with a great proportion of pyrite in them would burn brighter, however this was not observed to be true when the brightness profiles were compared at a constant O<sub>2</sub>/S stoichiometry. These results suggest that changes in the feed composition with fixed O<sub>2</sub>/S conditions in a furnace will not be able to be identified in real time using the flame brightness. It will be interesting to see how this result scales up to the commercial furnace if a plant trial is executed. Importantly, a spectrometer that extends to wavelengths longer than 1000 nm would be very useful.

### **Flame Flicker**

Flame flicker represents the oscillation frequency of the flame. In the laboratory, there were no dominant frequency components in the temperature nor brightness signals. It is possible that

there are some very high frequency components in the signal and that the sampling rate used in the lab was not fast enough to capture these. It is also possible that experiments were not conducted for long enough to identify low frequency components in the data. When plant data is collected over extended periods of time, it will be interesting to revisit flicker and see if there are any underlying frequency components and to see if these can be used to identify changing conditions in the furnace.

### **Opportunities for Process Monitoring & Control in a Plant**

Some practical and immediate applications of the optical sensor used in this research for a commercial operation have been identified. Such applications include:

- Monitoring the temperature of the flame
- Monitoring of feed distribution using the brightness/temperature ratio
- Monitoring dusting with the standard deviation of the flame temperature or brightness

All the aforementioned monitoring applications are novel for the commercial flash furnace. In terms of monitoring feed distribution, the flame brightness/temperature ratio was useful in the lab for identifying clogs in the solids feed line. Conversations with operations teams of commercial furnaces were very useful as it was learned that commercial furnaces can also have feed distribution problems in their concentrate burners. Such problems arise when foreign material (a piece of conveyor belt, tools, gloves, etc) gets caught in the concentrate burner. The principle of this problem is the same as what was experienced during operation of the drop tower. Thus, it is possible that the brightness/temperature ratio may be useful for identifying such operational upsets in the commercial furnaces.

### **Flame Temperature Monitoring**

Flash furnace operations currently do not monitor the temperature of the flame. Thus, the sensor that was used in this thesis can already offer more information to a commercial operation for process monitoring than currently exists. In this research the experimental conditions were controlled which allowed for the impact of O<sub>2</sub>/S stoichiometry on the flame temperature to be isolated. Such controlled and regular conditions will not exist in the commercial furnace which will make it more complicated to identify correlations in the data. It is possible that the flame temperature may be useful for monitoring desulphurization of concentrates in the commercial furnace.

The sensor may struggle to capture changes in feed composition entering the furnace. Once the product composition and ideal operating conditions are set, it is thought that the flame temperature could be a useful variable for maintaining product composition in the furnace. The reason that this sensor may struggle to capture changes in feed composition in real time is related to O<sub>2</sub>/S condition; if a change in the feed composition occurs without a change in the O<sub>2</sub>/S condition, the temperature of the flame will likely not change (Figure 26). This theory is based on data in Figure 25 (Chapter 4), which compares the combustion temperatures of the concentrates. At a fixed O<sub>2</sub>/S condition, the concentrates could not be differentiated based on temperature. The ability of the sensor to differentiate concentrates in real time will also require a plant trial.

### **Monitoring Feed Distribution**

The ratio of flame brightness / temperature was useful for monitoring feed distribution in the drop tower and identifying clogs in the feed lance in real time. The relationship between temperature and brightness from one of the experiments is shown in Figure 36.

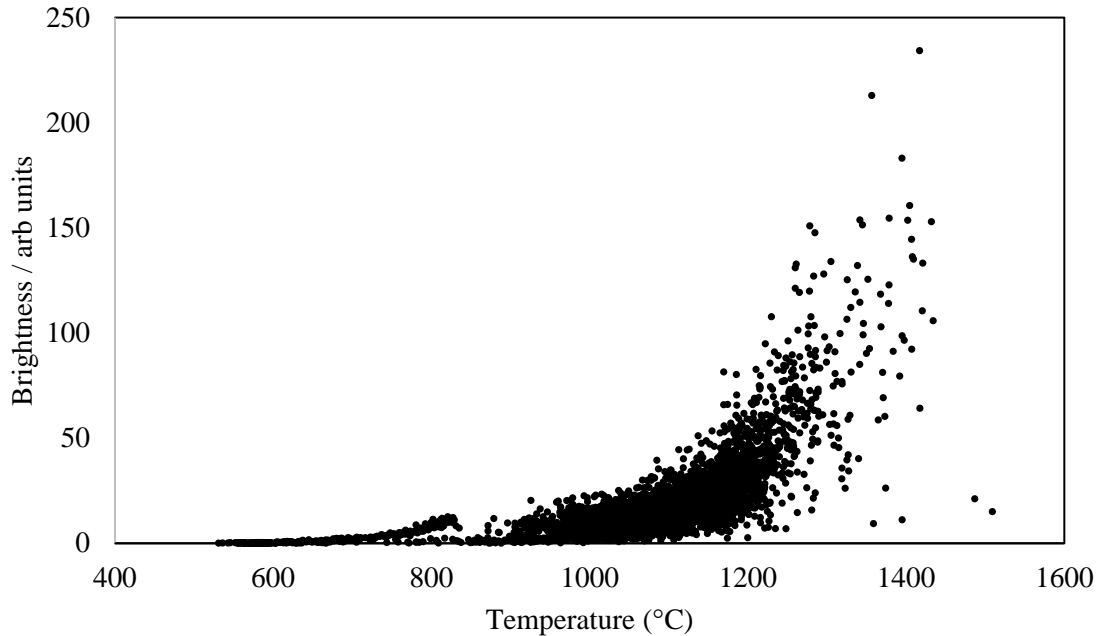


**Figure 36: Relationship between flame temperature and brightness**

The relationship between flame temperature and brightness in Figure 36 is consistent for all feed materials, however the curve scales vertically depending on the O<sub>2</sub>/S test condition. The relationship between temperature and brightness suggests two things:

1. Hot flames are not always bright
2. Bright flames are always hot

This information is useful for identifying issues with feed rate to the furnace. In the lab, clogging of the feed lance was a common issue, however the problem could be identified by monitoring the ratio of flame brightness:temperature. Similar feeding issues are also encountered in commercial flash furnaces when foreign objects (tools, conveyor belt pieces, etc) create blockages in the concentrate burner. In these situations, the furnace operation needs to be stopped so that the clog can be alleviated, which affects furnace availability. Based on experience in the lab and the relationship in Figure 36, such a blockage would affect the ratio of flame brightness:temperature, however the upset may not be noticeable based solely on measurements of

the flame temperature. Thus, the measures of flame temperature and the ratio of flame brightness:temperature from the emission spectrum may provide a powerful diagnostic tool for flash furnace smelting. An example of how the ratio of flame brightness:temperature and temperature can be used together to monitor a flash process is shown in Figure 37.

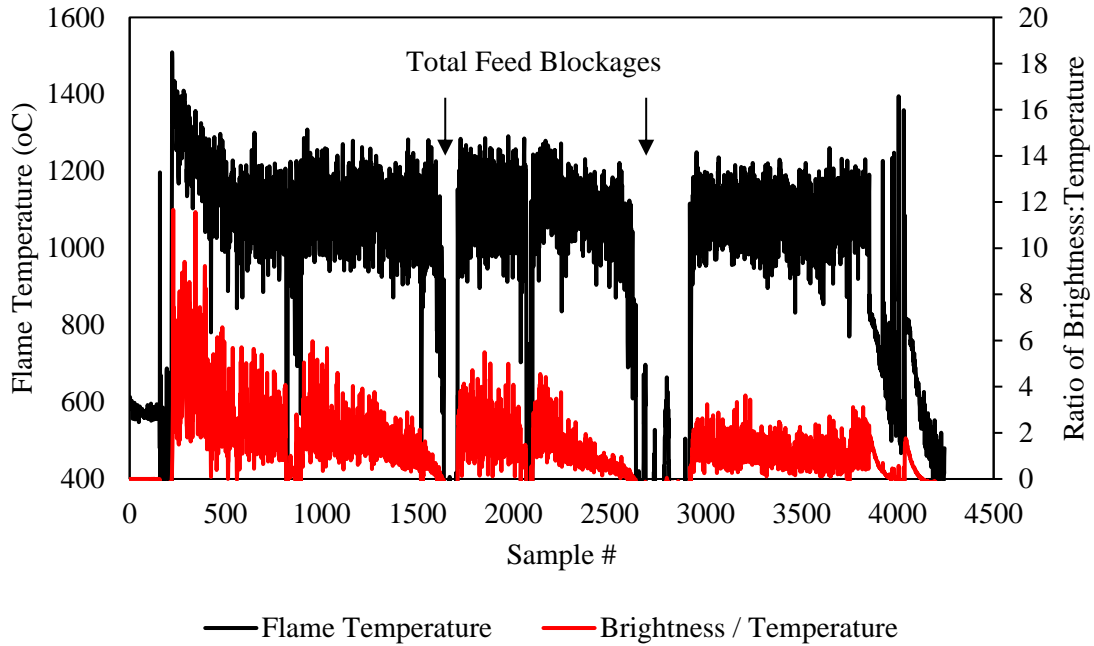


**Figure 37: Flame temperature and brightness profiles for the test with Concentrate AB**

**( $O_2/S = 2.49$ , %  $O_2 = 60\%$ )**

The data in Figure 37 shows that the flame brightness can be used as an early indicator of problems with feed distribution. The flame brightness data begins trending down much earlier than the flame temperature does. The proposed reason for this is that, with reduced feed rate, the feed particles that enter the reactor have more oxygen available to them for reaction, which causes them to maintain or increase their combustion temperature. Thus, to be able to identify problems with feed distribution, both temperature and brightness are important to measure. These variables were very useful for operating the drop tower experiment and it is thought that similar benefit can be realized at the commercial scale. These measures from the burner may be very useful for improving

furnace availability associated with early identification of feed distribution issues through the burner.

### **Dusting**

Flame temperature and stability measures may be useful for identifying conditions that give rise to dusting in the flash furnace. The standard deviation in temperature and brightness measurements of the flame increases with the  $O_2/S$  stoichiometry (this means that the stability is negatively correlated to  $O_2/S$ ). As well, the dust fraction in the products appears to positively correlate with the  $O_2/S$  stoichiometry. Thus, flames with high standard deviation in their temperature and/or brightness are thought to be more prone to dusting. From the desulphurization curves, it is known that concentrates with high chalcopyrite require a greater  $O_2/S$  ratio to be desulphurized to the target matte composition. Because these concentrates require a greater  $O_2/S$  stoichiometry, they may be more prone to dust production.

## Chapter 6

### Conclusions

The goals of this thesis were to evaluate the impact of concentrate mineralogy on the flash combustion behaviour of concentrates and to complete proof of concept testing of a novel sensor for combustion monitoring. This was done using an experimental campaign in a drop tower flash furnace using five different feeds: pure pyrite, pure chalcopyrite and 3 mineralogically distinct copper concentrates. Because the concentrates all had similar Cu, Fe and S content, the impact of mineralogy on the combustion processes was isolated. For each feed  $O_2/S$  stoichiometries between 0.8 – 4.0 at an experimental temperature of 950°C were executed resulting in 21 different operating conditions. These experimental conditions are unique in the literature, since most or all previous studies used  $O_2/S$  stoichiometries far greater than what is used in the commercial furnace ( $O_2/S < 1$ ). This is important as the results of this thesis may better represent the reaction conditions in a commercial furnace. The main observations from the work done in this thesis are summarized as follows:

- Desulphurization data provides an excellent and expected track of the effect of  $O_2$  enrichment and  $O_2/S$  stoichiometry on the desulphurization of feed. This indicates that the drop tower can be used for quantitative experimental work.

Pyrite requires a lower  $O_2/S$  stoichiometry than chalcopyrite to be desulphurized to a target sulphur composition (Chapter 4 - Desulphurization). This is supported by the kinetic models of the desulphurization behaviour of these minerals, which show that desulphurization is driven by the  $O_2/S$  ratio and that the rate constant for the desulphurization of pyrite is greater than that of chalcopyrite (Chapter 4 - Desulphurization). The desulphurization behaviour of these pure minerals was used to estimate the behaviour of concentrates. It was found that the proportions of pyrite and

chalcopyrite in the concentrate impact the  $O_2/S$  stoichiometry required for concentrate desulphurization; concentrates that lack pyrite seem to require a higher  $O_2/S$  stoichiometry to be desulphurized to the target bulk product composition (Chapter 5 – Concentrate Desulphurization – Impact of Mineralogy). For example, the high pyrite Concentrate B required a 43.75% lower  $O_2/S$  ratio to be desulphurized to a 62% matte compared to Concentrate A. Although the impact of pure minerals could be quantified, the concentrate desulphurization curves could not be reconstructed solely with pyrite and chalcopyrite. Thus, future experimental work in the drop tower should explore the impact of other minerals on the desulphurization behaviour of concentrates. When the impact of all minerals in a concentrate are understood, it is hoped that a blending “recipe” may be developed which optimizes the chemical and mineralogical inputs to the flash furnace. Such an optimization may help maintain product quality as well as the furnace heat balance. Another route would be to provide operations teams with an empirical relationship between concentrate mineralogy and the necessary  $O_2/S$  conditions for optimal processing.

The desulphurization results elucidate that mineralogy is an important variable to consider during the blending process and that non-Cu containing minerals influence the optimal reaction conditions. Operations should consider the mineralization as well as the chemical analyses of the blends that they prepare for their flash furnace and for selecting the  $O_2/S$  conditions needed for processing to a target matte grade.

- Particle size analysis of the combustion products for all feeds and experimental conditions was done to understand how particles evolve in flash combustion (Chapter 4 – Product Particle Size Analysis). Like Dr. Parra’s recent drop tower studies, the experiments in this thesis used higher density gas-solid mixtures than conventionally used and it was found that particle expansion prevails over particle fragmentation for chalcopyrite and the

concentrates (Chapter 5 – Particle Size Analysis). [40] This is reflected in the increase in P80 particle size for these four feeds. PSA analysis of pyrite combustion products showed minor changes in the P80 particle size. SEM imaging of combustion products was used to support the particle expansion mechanism. Particles in the reaction products were observed to coalesce and fuse together into larger particles (Chapter 5 – Particle Size Analysis). Dr. Parra proposed a mechanism whereby collision and coalescence of particles midflight drives particle expansion for higher density gas-solid mixtures; the results of this study are consistent with his groups findings. [40]

The fraction of dust in the products (cumulative volume % of particles  $<20 \mu\text{m}$ ) was interpolated from the particle size distributions. The results indicate that flash combustion for  $\text{O}_2/\text{S}$  stoichiometries between 0.8 – 4.0 results in a reduction in fraction of dust of the products. A positive correlation was identified for all feeds between the dust fraction and the  $\text{O}_2/\text{S}$  stoichiometry; dusting seems to increase with  $\text{O}_2/\text{S}$  (Chapter 5 – Particle Size Analysis). This is consistent with previous observations whereby higher oxidizing conditions cause more dust to be generated. [45]

- QEMSCAN® analysis was used to study the reaction products from the flash combustion of the concentrates. It seems that pseudochalcopyrite and pseudobornite are the main combustion products of chalcopyrite (Chapter 4 – QEMSCAN® Analysis). To the best knowledge of the author, these phases have not been identified before as combustion products of chalcopyrite in experimental tests (in part due to the overoxidation of these other test feeds). These pseudo phases are partially oxidized products of their minerals (chalcopyrite and bornite).

In each of the concentrates analyzed by QEMSCAN®, significant proportions of pseudobornite were produced. The morphology of this phase was heavily fragmented, and the rims of the particles were commonly covered with hematite-magnetite which suggests particle encapsulation. This suggests that pseudobornite is a significant contributor to dust in flash combustion reactions as the encapsulation likely caused particle boiling and explosion of the particles according to the accepted dusting mechanism. [45] Because pseudobornite appears to be a significant intermediate combustion product, future tests with the pure mineral bornite could be conducted in the drop tower. Given the above mechanism, one might expect that the desulphurization of bornite would be limited as its production far outweighed its consumption in tests done in this thesis.

The analysis of the QEMSCAN® results in this thesis are quite limited in their scope. There is likely a lot more mechanistic information that could be extracted from these results. Future work on this project should revisit the QEMSCAN® results so that a detailed and complete analysis can be completed.

- Emission spectroscopy was selected to study the flame because it was thought that the composition of reaction products could be analyzed in real time using Cu, Fe, S or O emission lines or bands (Chapter 4 – Characteristic Emission Spectrum & Emitting Species). Unfortunately, the temperature of the flame, which was between 900 – 1500°C, was not hot enough to induce emissions from these species and only atomic emissions from alkali metals Na (589.4 nm), K (766.5, 769.9, 779.6 & 795.6 nm) and Li (670.8 nm) were observed. [27] [46] These emissions were not quantified as they have no bearing on the oxidation state of Cu, Fe and S species. Commercial testing of the sensor may yield different results as the furnace temperature is hotter and the feed rate is much higher. With

a higher feed rate, the probability of exciting a Cu, Fe, S or O species is increased. This represents an opportunity for future testing of the sensor.

Other than emitting species, information that could be extracted from the emission spectrum includes the flame's temperature and its brightness (Chapter 5 – Emission Spectroscopy in Flash Furnace Smelting). Flame temperature was calculated using the two-wavelength method in the black body emission approximation and the brightness was measured as the integrated intensity of the emission spectrum. It was found that both the flame temperature and brightness are driven by the  $O_2/S$  stoichiometry and the  $O_2$  enrichment. These measures did not increase linearly with the  $O_2/S$  stoichiometry. Flames that form under higher  $O_2/S$  stoichiometries have a higher standard deviation in these measures, which reflects stability. Thus, as the  $O_2/S$  stoichiometry is increased, the stability of the flame decreases. This may be useful for identifying conditions that cause dust as the dust fraction in the products was also correlated to the  $O_2/S$  stoichiometry. Flame temperature and brightness as well as desulphurization was driven by the  $O_2/S$  stoichiometry. Thus, it may be possible to use one of the measures from the optical sensor to gauge the extent of feed desulphurization in the lab. To accomplish this, it would be necessary to complete further experimental studies and it is unclear whether this application would scale to the commercial furnace. Developing a relationship between flame brightness and/or temperature and the desulphurization could be done as a next step in this research project.

A potential application of the optical sensor used in this research is to monitor feed distribution with the brightness:temperature ratio (Chapter 5 – Monitoring Feed Distribution). In the lab, feed distribution was the main experimental issue, and this ratio was very useful for the early identification of clogs forming in the solids feed line. In

commercial flash furnaces, the solids feed distribution through the concentrate burner can sometimes be clogged with foreign material such as pieces of conveyor belt, gloves or tools. Cleaning requires the removal of the concentrate burner which impacts the furnace availability. Thus, early identification of clogs through monitoring of the brightness/temperature ratio could help improve furnace availability.

Overall, the product analysis using the drop tower and the observations with the optical sensor together were very useful tools for studying flash combustion processes. Differences in feed composition can be captured in the solid analysis of drop tower products and the sensor provides a useful diagnostic tool for running the experiment. It is thought that the benefits provided by the sensor in the lab will scale up to the industrial furnace. It is thus recommended that commercialization of the sensor proceed through further lab work and commercial testing. Future experimental work should investigate the behaviour of pure minerals other than chalcopyrite and pyrite, as well as the binary interactions between minerals using  $O_2/S$  conditions  $< 1$  and with  $O_2$  enrichments in excess of 50%. Selection of experimental conditions should be done to match the conditions of the commercial furnace to try to achieve results that are as close to the actual process as possible.

## Chapter 7

### References

- [1] M. Shamsuddin, *Physical Chemistry of Metallurgical Processes*, Salt Lake City: TMS & Wiley, 2016.
- [2] W. Davenport and E. Partelpoeg, *Flash Smelting Analysis, Control and Optimization*, Oxford: Pergamon Press, 1987.
- [3] W. Davenport, M. King, M. Schlesinger and A. Biswas, *Extractive Metallurgy of Copper* 4th Edition, Oxford: Pergamon, 2002.
- [4] P. Mackey, "Evolution of the large copper smelter - 1800s to 2013," in *Symposium on Pyrometallurgy in honor of David G.C. Robertson*, 2014.
- [5] Y. Maeda, H. Inoue, Y. Hoshihikawa and T. Shirasawa, "Current operation in Kosaka Smelter," in *Sulfide Smelting '98: Current and Future Practices*, 1998.
- [6] I. Kojo and H. Storch, "Copper Production with Outokumpu Flash Smelting: An Update," in *International Symposium on Sulfide Smelting*, 2006.
- [7] C. Ortiz, R. Fernandez-Gil, J. C. Moreno and I. Perez, "Improvements carried out at Huelva smelter in the 2007 general shutdown: A Review," in *Proceedings of the Extractive and Processing Division*, 2008.
- [8] W. Davenport and E. PartelPoeg, *Flash Smelting Analysis, Control and Optimization*, Oxford: Pergamon Press, 1987.
- [9] F. Jorgensen, "Single particle combustion of chalcopyrite," in *Australasian Institute of Mining and Metallurgy*, Parkville, 1983.
- [10] F. Jorgensen, "The ignition of sulfide flotation concentrates in flash smelting," in *Sulfide smelting 2002*, Seattle, 2002.
- [11] F. Jorgensen, F. Moyle and M. Wadsley, "Structural changes associated with the ignition of pyrite and chalcopyrite during flash smelting," in *Process Mineralogy IX, International symposium of Applied Mineralogy*, Montreal, 1989.
- [12] N. Tuffrey, G. Richards and J. Brimacombe, "Two-wavelength study of the combustion of sulfide minerals: Part II. Galena and commercial lead concentrates," *Metallurgical and Materials Transactions B*, pp. 943-58, 1995.

- [13] A. Warczok, T. Utigard, W. Mroz and J. Kowalczyk, "Oxidation of Copper Sulphide Minerals in Suspended State," 1992.
- [14] R. Parra-Figueroa, C. Parra-Sanchez, E. Balladeres-Valera, C. Loeza-Arqueros, C. Villagran-Flores and M. Perez-Tello, "Online Temperature Measurements during Copper Concentrate Flash Combustion at Laboratory Scale by a Spectral Technique," in *Copper 2016*, Kobe, 2016.
- [15] N. Kemori, Y. Kondo and K. Fujita, "Flash smelting behaviour of various copper concentrates in a pilot scale furnace," in *Sulphide Smelting '98: Current and Future Practices*, San Antonio, 1998.
- [16] F. Jorgensen, "Combustion of pyrite concentrate under simulated flash -smelting conditions," *Institution of Mining and Metallurgy Section C: Mineral Process. Extr. Metall.*, pp. 1 - 9, 1981.
- [17] N. Tuffrey, G. Richards and J. Brimacombe, "Two-wavelength pyrometry study of the combustion of sulfide minerals: Part III. The influence of oxygen concentration on pyrite combustion," *Metallurgical and Materials Transactions B*, vol. 26, no. B, pp. 959-70, 1995.
- [18] F. Jorgenson, "Combustion of chalcopyrite, pyrite, galena and sphalerite under simulated suspension smelting conditions," in *Australia Japan Extractive Metallurgy Symposium*, Sydney, 1980.
- [19] E. Segnit and F. Jorgensen, "Copper flash smelting simulation experiments," *Australasian institute of mining and metallurgy*, vol. 261, pp. 39 - 46, 1977.
- [20] L. Arias, S. Torres, C. Toro, E. Balladares, R. Parra, C. Loeza, C. Villagran and P. Coelho, "Flash Smelting Copper Concentrates Spectral Emission Measurements," *Sensors*, vol. 18, no. 7, 2018.
- [21] E. Evenson, H. Goodfellow and M. Kempe, "EAF Process optimization through off-gas analysis and closed-loop process control at Deacero, Saltillo, Mexico," in *58th Electric Furnace Conference and 17th Process Technology Conference proceedings*, Orlando, 2000.
- [22] Sustainable Development Technology Canada, "Development and Demonstration of Goodfellow EFSOP(TM) Technology," 2018. [Online]. Available: <https://www.sdte.ca/en/portfolio/projects/development-and-demonstration-goodfellow-efsopm-technology>.
- [23] D. Zuliani, H. Goodfellow and M. Ferri, "EFSOP(R) Holistic Optimization(TM) of Electric Arc Furnaces - Past, Present and Future," *Archives of Metallurgy and Materials*, pp. 323-329, 2008.

- [24] W. Wendt and W. Persson, "Use of optical on-line production control in copper smelters," in *Copper 99 - Cobre 99*, Ottawa, 1999.
- [25] G. Bezuidenhout, J. Ekstenn, G. Akdogan, B. Van Beek, W. Wendt and W. Persson, "Implementation of flame optical emission spectroscopy system for converter Fe end-point control associated with Ni-Cu-S-PGM converter mattes," *Minerals Engineering*, vol. 100, pp. 132-43, 2017.
- [26] W. Persson and W. Wendt, "From Research to Reality - 15 years with optics for production control in metallurgical industry," in *New Technology Implementation in Metallurgical Processes*, Montreal, 2002.
- [27] National Institute of Science and Technology, "NIST Atomic Spectra Database Lines Form," [Online]. Available: [https://physics.nist.gov/PhysRefData/ASD/lines\\_form.html](https://physics.nist.gov/PhysRefData/ASD/lines_form.html).
- [28] A. Gaydon, *The Spectroscopy of Flames* (2nd Ed.), London: Chapman and Hall, 1974.
- [29] P. Atkins and J. De Paula, *Physical Chemistry - 9th Ed.*, New York City: Oxford University Press, 2010.
- [30] G. Lu, Y. Yan, S. Cornwell, M. Whitehouse and G. Riley, "Impact of co-firing coal and biomass on flame characteristics and stability," *Fuel*, pp. 1133-40, 2007.
- [31] J. Ballester and T. Garcfa-Armingol, "Diagnostic techniques for the monitoring and control of practical flames," *Progress on Energy and Combustion Science*, pp. 375-411, 2010.
- [32] G. Nathan, P. Kalt, Z. Alwahabi, B. Dally, P. Medwell and Q. Chan, "Recent advances in the measurement of strongly radiating, turbulent reacting flows," *Prog. in Energy and Combustion Science*, pp. 41-61, 2012.
- [33] A. Gonzalez-Cencerrado, A. Gil and B. Pena, "Characterization of PF flames under different swirl conditions based on visualization systems," *Fuel*, pp. 798-809, 2013.
- [34] G. Lu, Y. Yan, M. Colechin and R. Hill, "Monitoring of oscillatory characteristics of pulverized coal flames through image processing and spectral analysis," *IEEE*, pp. 226-31, 2006.
- [35] M. Lombardi, "Fundamentals of Time and Frequency," in *Encyclopedia of Science and Technology*, National Institute of Science and Technology, 2002, pp. 783-801.
- [36] E. Ferre-Pikal, J. Vig, J. Camparo, L. Cutler, L. Maleki, W. Riley, S. Stein, C. Thomas, F. Walls and J. White, "Draft revision of IEEE STD 1139-1988 standard definitions of physical quantities for fundamental frequency and time metrology - Random instabilities," in *IEEE International Frequency Control Symposium*, Orlando, 1997.

- [37] J. Rutman, "Characterization of Phase and Frequency Instabilities in Precision Frequency Sources: Fifteen Years of Progress," *IEEE*, vol. 66, no. 9, pp. 1048-75, 1978.
- [38] D. Allan, "Time and frequency (Time-Domain) characterization, estimation and prediction of precision clocks and oscillators," *IEEE Transactions on Ultrasonics, Ferroelectrics and Frequency Control*, vol. 34, no. 6, pp. 647-54, 1987.
- [39] C. Romero, X. Li, S. Keyvan and R. Rossow, "Spectrometer-based combustion monitoring for flame stoichiometry and temperature control," *Applied Thermal Engineering*, pp. 659-76, 2005.
- [40] M. Perez-Tello, V. Parra- Sanchez, V. Sanchez-Corrales, A. Alvarez, F. Bojorquez, R. Parra-Figueroa, E. Balladares-Varela and E. Araneda-Hernandez, "Evolution of size and chemical composition of copper concentrate particles oxidized under simulated flash smelting conditions," *Metallurgical and Materials Transactions B*, vol. 49, no. 2, pp. 627-43, 2018.
- [41] ELTRA, "Carbon / Sulfur Analyzer CS-2000," 08 2018. [Online]. Available: <https://www.eltra.com/products/chs-analyzers/cs-2000/information-downloads/>. [Accessed 30 9 2018].
- [42] FEI Natural Resources, "Automated Mineralogy & Petrography," [Online]. Available: <https://www.fei.com/materials-science/minerals-mining/>. [Accessed 1 10 2018].
- [43] D. Pirrie, A. Burcher, M. Power, P. Gottlieb and G. Miller, "Rapid quantitative mineral and phase analysis using automated scanning electron microscopy (QemSCAN); potential applications in forensic geoscience," *Forensic Geoscience*, vol. 232, pp. 123-36, 2004.
- [44] Malvern, "Mastersizer 3000 - Smarter Particle Sizing," 2018. [Online]. Available: [https://www.malvernpanalytical.com/en/products/product-range/mastersizer-range/mastersizer-3000/?gclid=Cj0KCQjwuafdB RDmARIsAPpBmVXvpa2zOrfoJC1xWv1on\\_8DNJDXV0o3cYpZSylTCWPgovqIGbNVUVEaAICZEALw\\_wcB](https://www.malvernpanalytical.com/en/products/product-range/mastersizer-range/mastersizer-3000/?gclid=Cj0KCQjwuafdB RDmARIsAPpBmVXvpa2zOrfoJC1xWv1on_8DNJDXV0o3cYpZSylTCWPgovqIGbNVUVEaAICZEALw_wcB). [Accessed 1 10 2018].
- [45] A. Jokilaakso, R. Suominen, P. Taskinen and K. Lilius, "Oxidation of chalcopyrite in simulated suspension smelting," *Transactions of the Institution of Mining and Metallurgy, Section C: Extractive Metallurgy*, vol. 100, 1991.
- [46] B. Steward, G. Perram and K. Gross, "Visible and near-infrared spectra of the secondary combustion of a 152 mm Howitzer," *Applied Spectroscopy*, pp. 1363-71, 2011.
- [47] D. Allan, "Statistics of Atomic Frequency Standards," *Proc. of the IEEE*, vol. 52, no. 2, pp. 221-30, 1966.

- [48] P. Werle, R. Mucke and F. Slemr, "The Limits of signal averaging in atmospheric trace-gas monitoring by tunable diode-laser absorption spectroscopy (TDLAS)," *Appl. Phys. B*, vol. 57, pp. 131-39, 1993.
- [49] V. Stefanova, "Phase composition of spinel melts obtained during flash smelting of the mineral chalcopyrite," *Russian Journal of Non-Ferrous Metallurgy*, vol. 49, pp. 148-55, 2008.
- [50] N. Docquier and S. Candel, "Combustion control and sensors: a review," *Progress in Energy and Combustion Science*, vol. 28, no. 2, pp. 107-150, 2002.
- [51] F. Jorgensen and M. Zuiderwyk, "Two-colour measurement of the temperature of individual combusting particles," *J. Phys. E: Sci. Instrum.*, vol. 18, pp. 486-91, 1985.

## Chapter 8

### Appendices

#### Appendix 1: Temperature Calibration

Calibration factors need to be applied to the raw emission spectrum to calculate the temperature of the combusting particles. Wavelength dependent calibration factors to convert the raw emission spectrum into a blackbody distribution were calculated using a tungsten-halogen lamp, which was assumed to be an ideal blackbody emitter. The experimental set up used to measure the calibration factors is show in Figure 38.

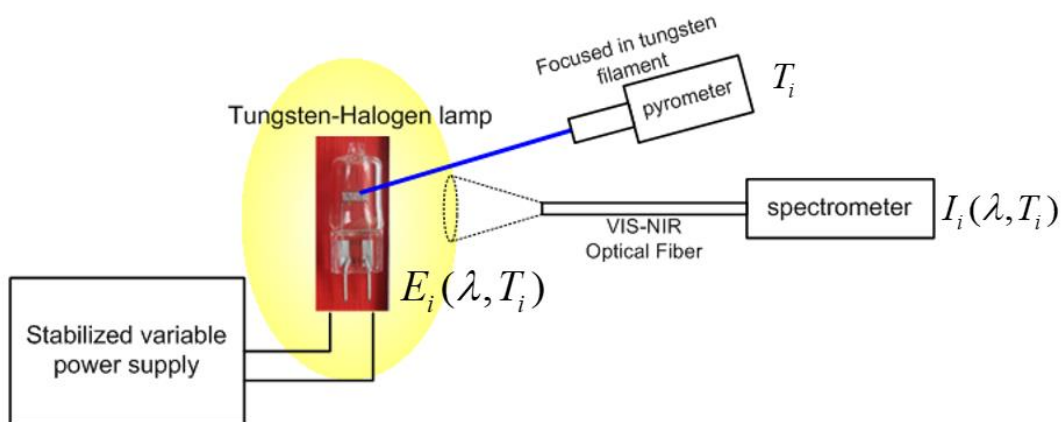


**Figure 38: Two-wavelength temperature calibration experimental setup**

A variable DC voltage supply was used to control the power and temperature of the tungsten-halogen lightbulb. As the power supplied to the lightbulb increases, the temperature of the filament does as well. The temperature of the filament was measured using a high-speed compact radiation thermometer (Chino Corporation IR-CA Series) which validated the modelled temperatures of the filament. The raw emission spectrum was first normalized using the intensity

at 550 nm to remove the effect of integration time on the calibration process. Calibration factors at all wavelengths were calculated using Equation 8-1.

$$\text{Correction Factor}(\lambda) = \frac{\text{Intensity}(\lambda)_{\text{measured}}}{\text{Intensity}(\lambda)_{\text{calculated, BB}}} \quad 8-1$$

Figure 39 shows the correction factors as a function of wavelength and temperature.

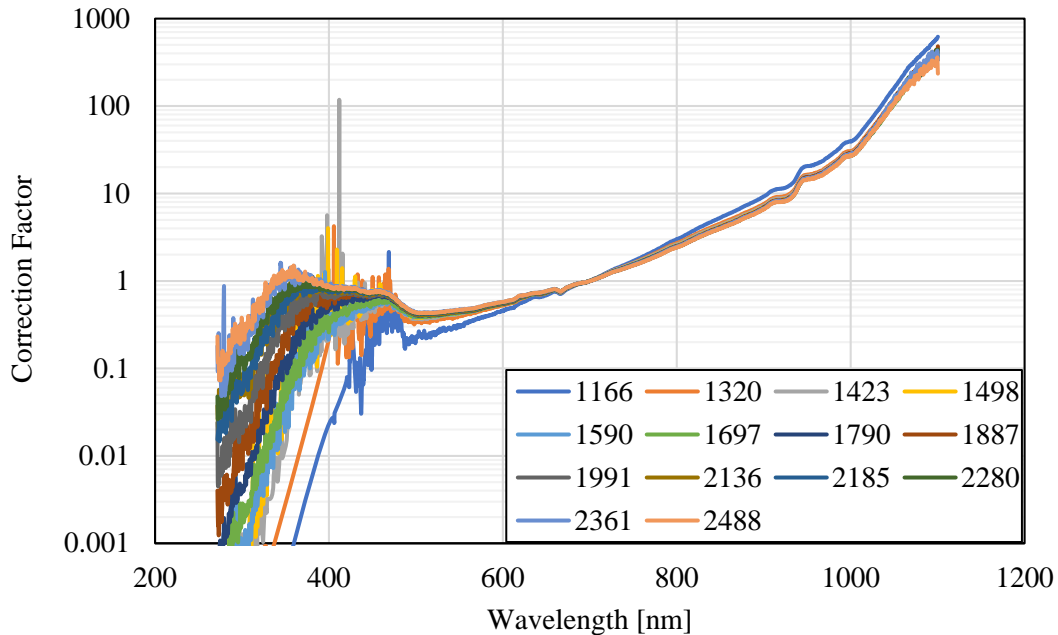


**Figure 39: Wavelength and temperature dependence of correction factors (°C)**

Figure 39 shows that the correction factors are temperature dependent for wavelengths in the lower end of the spectrometer’s detection limit. Further, the correction factors become very large at wavelengths greater than 900 nm. In the spectral range of 500 – 900 nm, the correction factors are close to 1, which means the signal is close to a blackbody distribution. When applying the two-wavelength method, an average of the correction factors in Figure 39 at each wavelength is used.

To select the wavelengths used for the two-wavelength temperature calculations, a least of squares fit of the Planck distribution was fit to the corrected blackbody curve and is shown in Figure 40.

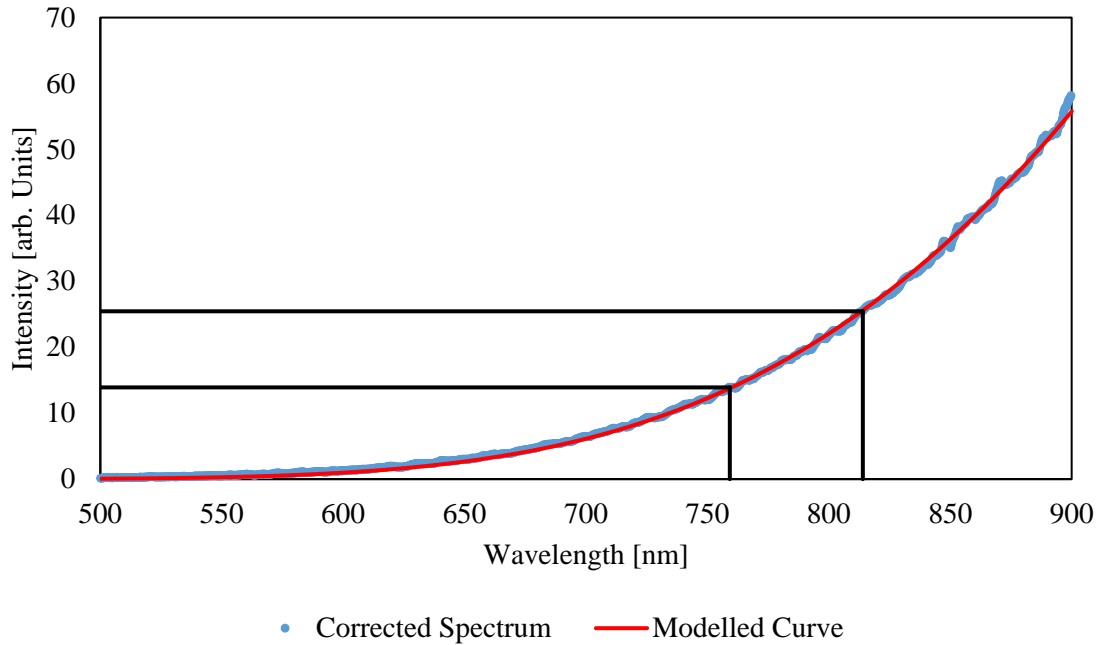


**Figure 40: Least of squares fit of the Planck Distribution to the corrected blackbody spectrum**

From the least of squares fit, the modelled flame temperature was determined to be 1047°C. A Solver optimization in Excel was created to vary the wavelengths used in the two-wavelength method and minimize the error in temperature between the model and the two-wavelength method. The wavelengths that minimize the difference between the modelled temperature and the two-wavelength calculated temperature were found to be 759 and 814 nm, which are identified in Figure 40. The error in measurement is 1.3% (two-wavelength temperature = 1061°C, least of squares modelled temperature = 1047°C) which was deemed acceptable. Comparisons were made between the least of squares modelled and two-wavelength temperatures for multiple emission spectra, and it was found that the error between measurements was less than 2% in all cases thus validating the selection of the wavelengths.

## Appendix 2: Experimental Heat Model

The solids feed lance has a cooling jacket around it to protect the fibre optic probe, which passes through it. In the commissioning work, water was used as the cooling medium through the lance, however operational issues were encountered due to condensation on the inside of the lance and heat removal affecting the reactor heat balance. Condensation on the inside of the solids feed lance caused solid feed particles to stick to the walls of the feed lance, accumulate and eventually block the lance entirely which prevented the execution of experiments over extended periods of time (>2 minutes). As well, the water was removing too much heat from the reactor. The impact of oxygen on the combustion reactions and flame temperature was not measurable because the water was removing such a large amount of heat, that the desired flash reactions were not occurring. A heat model around the process was built to justify a change from water to air as the cooling medium. Table 17 and Table 18 show the heat model outputs for air and water cooling through the solids feed lance.

**Table 17: Heat model output with a water-cooled solids feed lance**

				% of Heat
Heat Sinks	Heat removal by the cooling water	-	92,263 J/min	92%
	Heat carried by the solids	-	572 J/min	1%
	Heat carried by the gas	-	7,404 J/min	7%
Heat Sources	Heat of Reaction		16,299 J/min	16%
	Net Heat Transfer through reactor		83,941 J/min	84%

**Table 18: Heat model output with an air-cooled solids feed lance**

				% of Heat
Heat Sinks	Cooling Air	-	17,856 J/min	69%
	Solids Heat	-	572 J/min	2%
	Gas Heat	-	7,404 J/min	29%
Heat Sources	Heat of Reaction		16,299 J/min	63%
	Net Heat Transfer through reactor		9,534 J/min	37%

As can be seen by Table 17 and Table 18, a water-cooled solids feed lance removes 5-times more heat than an air-cooled lance does. When the switch was made from water to air as the cooling medium, the effect was very pronounced. It was immediately apparent that a flame was forming from the optical signal and supported by product sulphur analysis. Using air as the cooling medium allowed experiments to be run over indefinite periods of time with measurable differences in the flash combustion reactions that were occurring at different conditions. Air-cooling through the feed lance was used for all tests included in this report.

### Appendix 3: Raw Experimental Data (Temperature and Brightness)

This section contains the raw experimental data calculated from the emission spectrum. For a given feed material, the y-axis scales are maintained the same, however the axis limits change between feeds which should be paid attention to.

#### Chalcopyrite

The experimental temperature and brightness data collected from tests with chalcopyrite is presented in Figure 41 to Figure 44. Data for the test at  $O_2/S = 1.49$  with 30%  $O_2$  is omitted as the optical signal was compromised. The brightness data for the test at  $O_2/S = 3.0$  with 80%  $O_2$  was erroneous and is thus omitted from Figure 44.

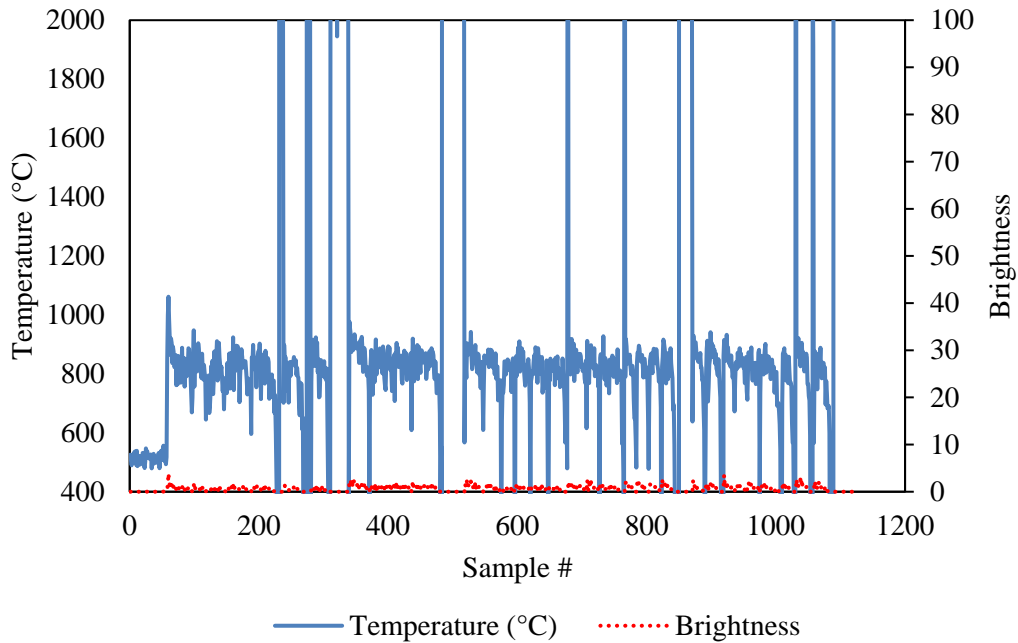


**Figure 41: Chalcopyrite,  $O_2/S = 0.8$ , %  $O_2 = 20$**

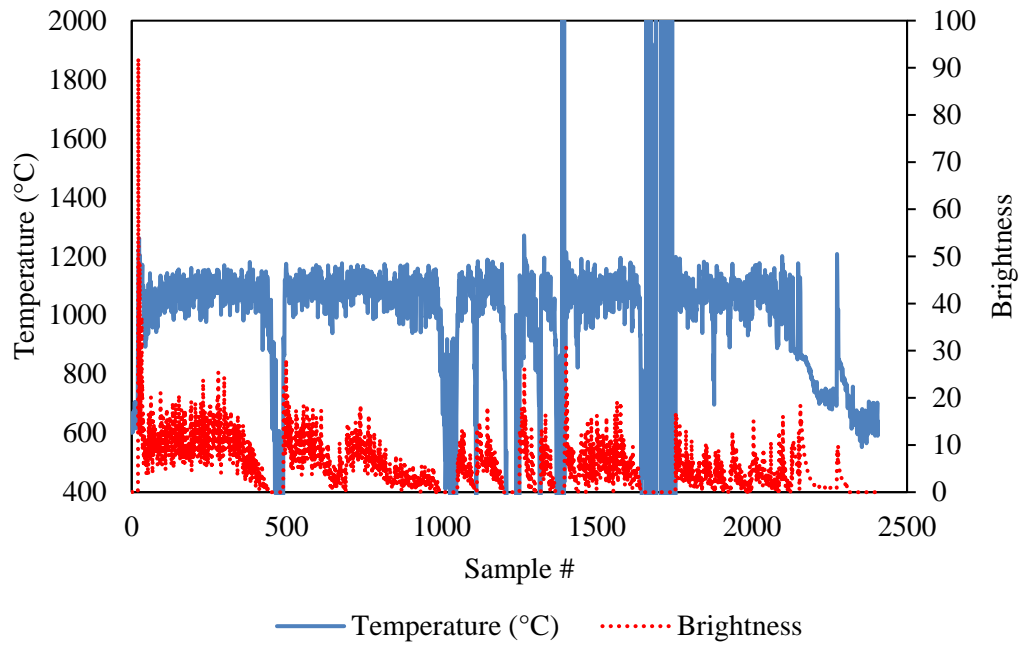


**Figure 42: Chalcopyrite,  $O_2/S = 1.5$ , %  $O_2 = 40$**

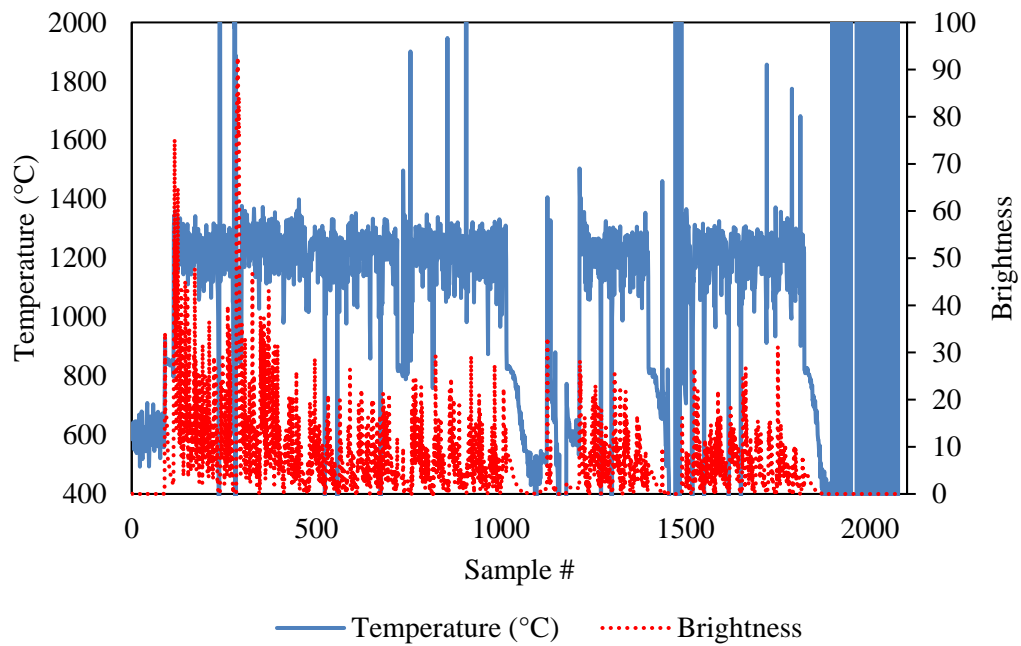


**Figure 43: Chalcopyrite,  $O_2/S = 2.2$ , %  $O_2 = 60$**

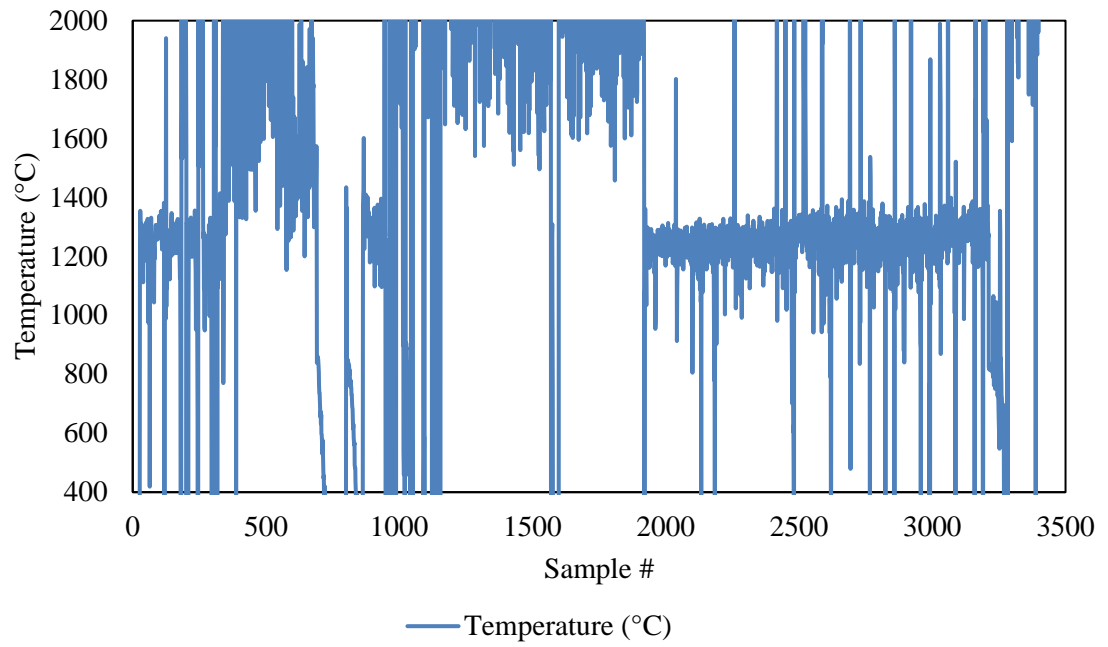


**Figure 44: Chalcopyrite,  $O_2/S = 3.0$ , %  $O_2 = 80$**

## Pyrite

The experimental temperature and brightness data from tests with pyrite is presented in

Figure 45 to Figure 47.

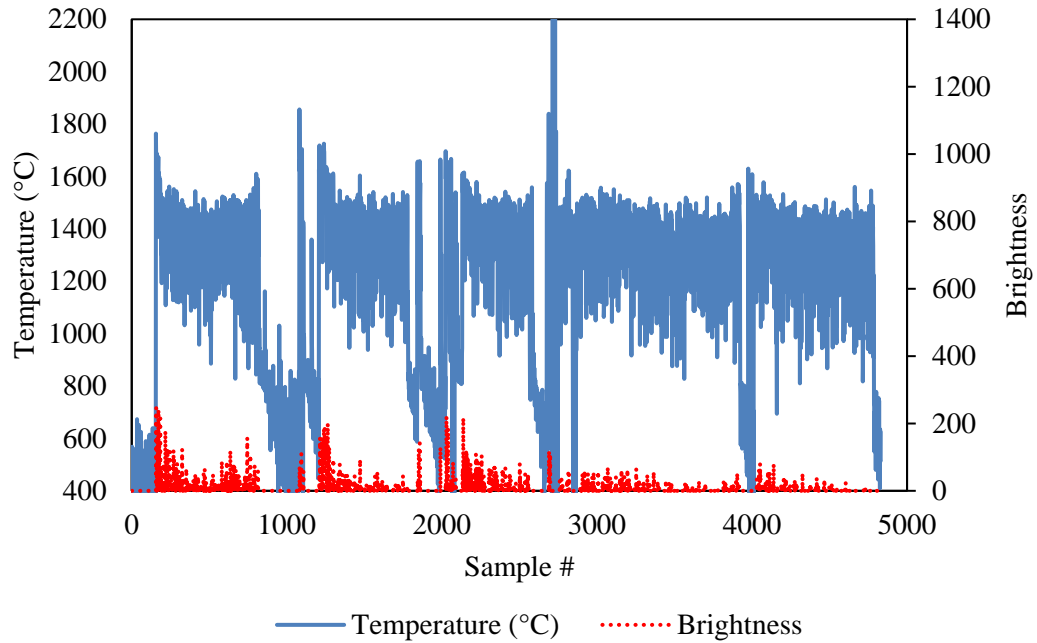


**Figure 45: Pyrite,  $O_2/S = 2.0$ , %  $O_2 = 50$**

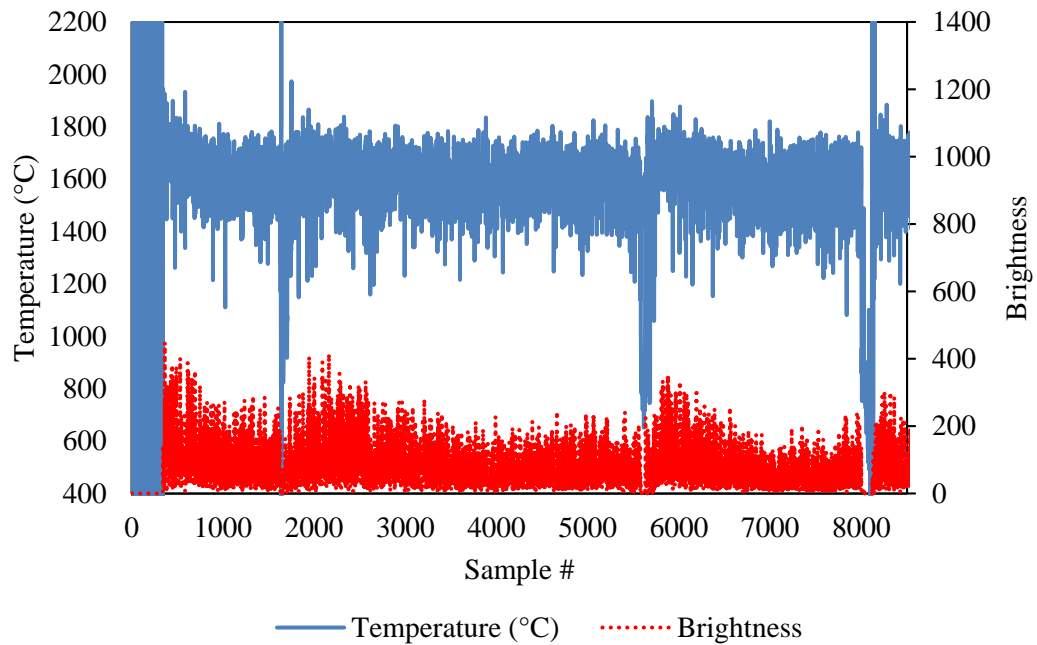


**Figure 46: Pyrite,  $O_2/S = 3.0$ , %  $O_2 = 74$**

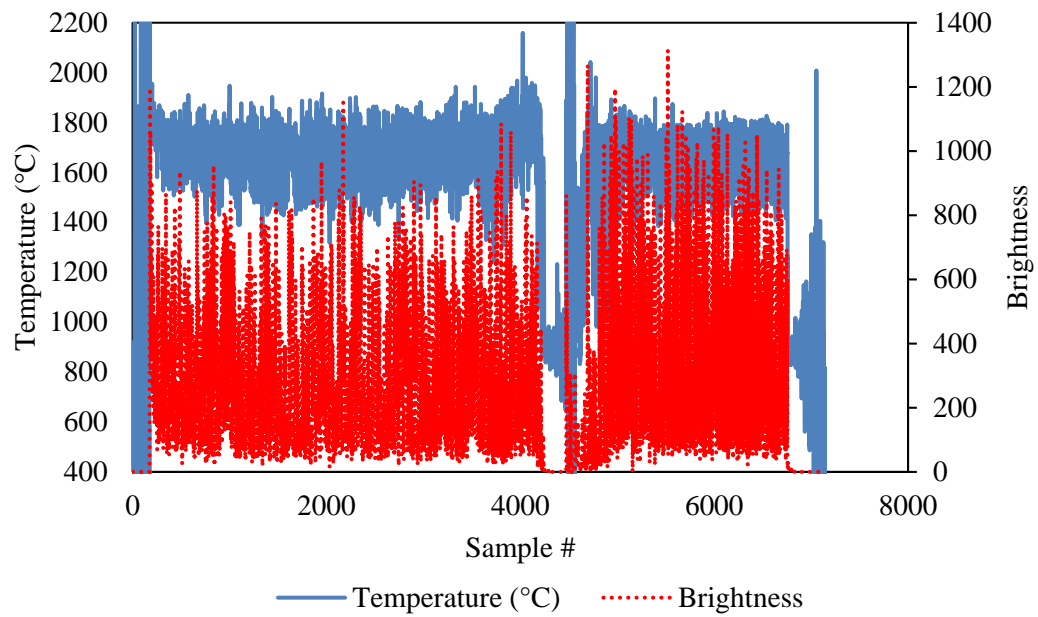


**Figure 47: Pyrite,  $O_2/S = 4.0$ , %  $O_2 = 98$**

### Concentrate A

The experimental temperature and brightness data from tests with Concentrate A is presented in Figure 48 to Figure 50.

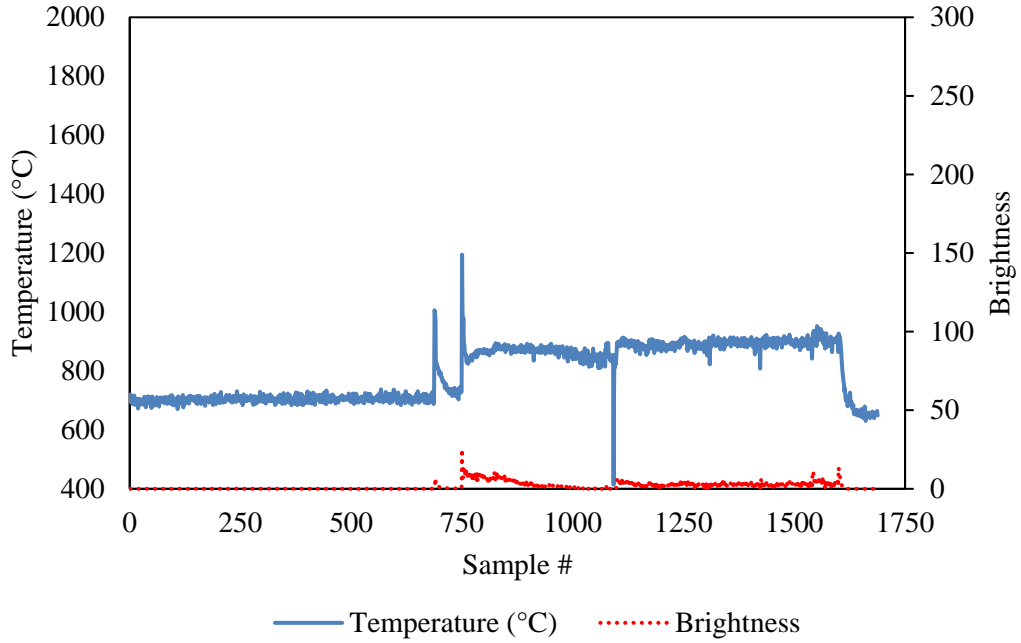


**Figure 48: Concentrate A,  $O_2/S = 1.0$ , %  $O_2 = 25$**

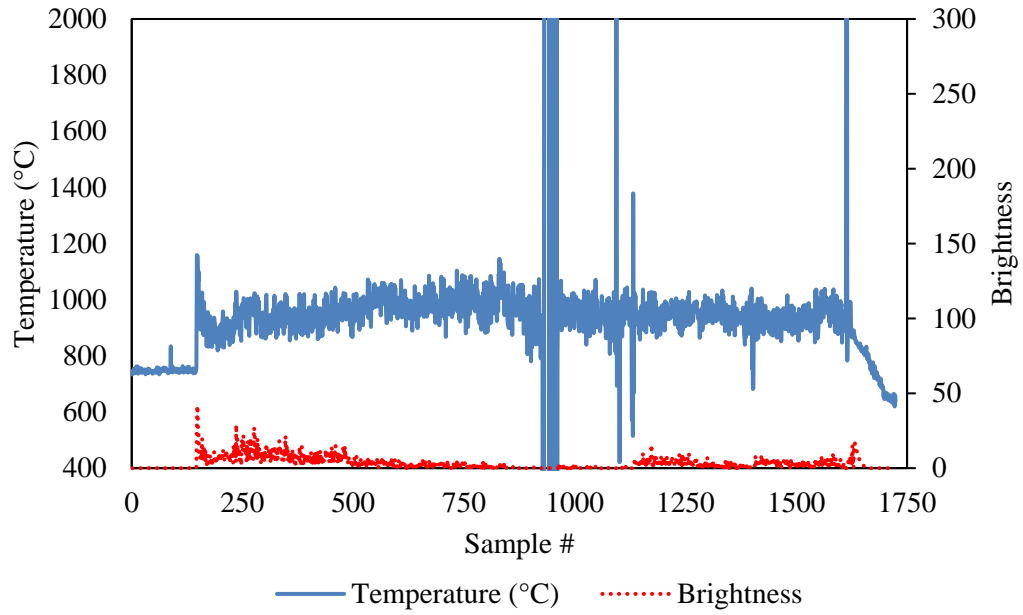


**Figure 49: Concentrate A,  $O_2/S = 1.9$ , %  $O_2 = 45$**

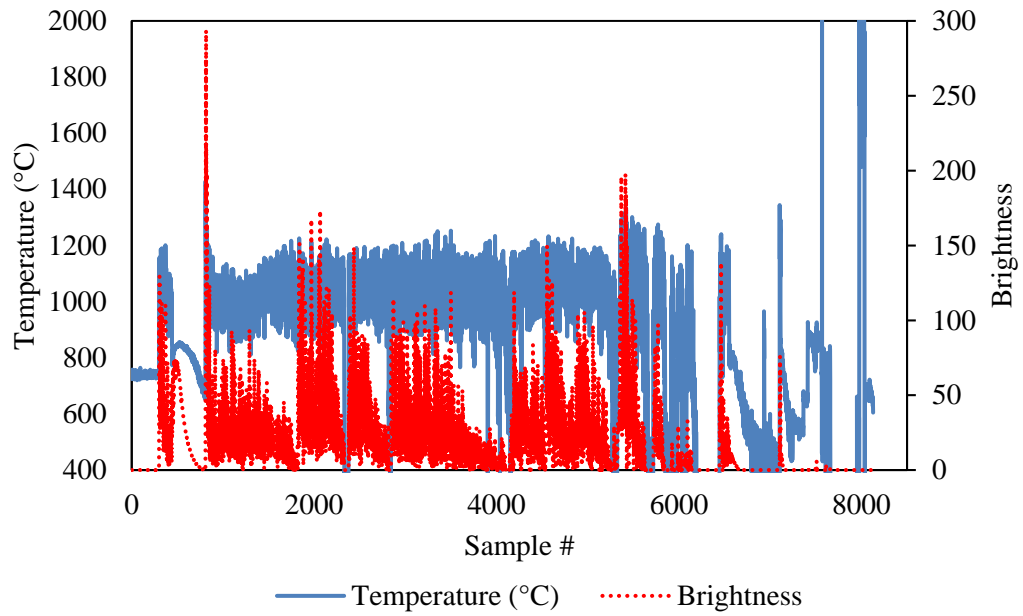


**Figure 50: Concentrate A,  $O_2/S = 2.5$ , %  $O_2 = 60$**

### Concentrate B

The experimental temperature and brightness data from tests with Concentrate B is presented in Figure 51 to Figure 55.

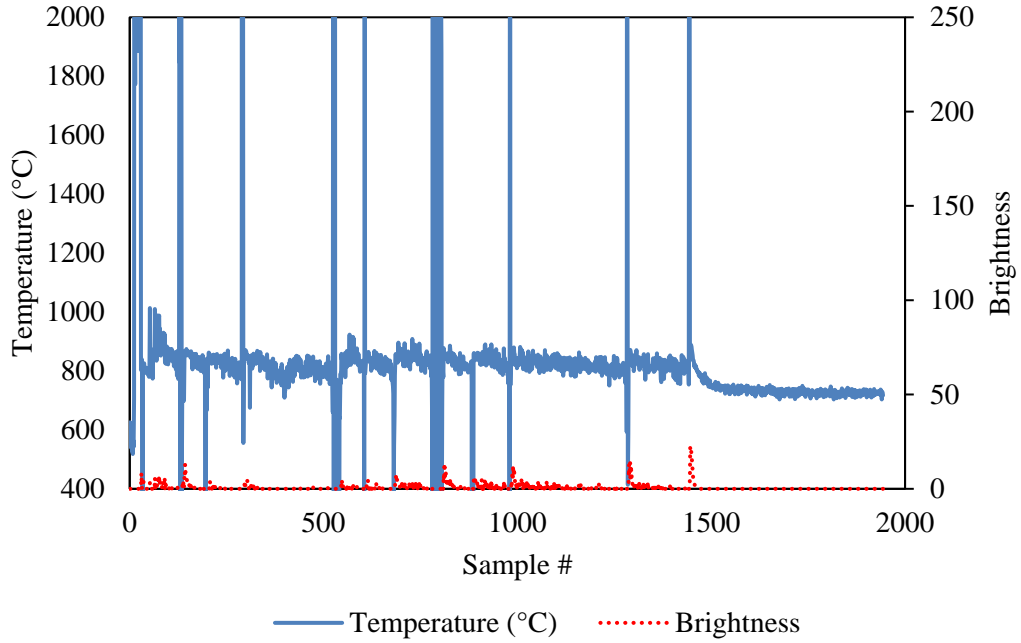


**Figure 51: Concentrate B,  $O_2/S = 0.9$ , %  $O_2 = 20$**

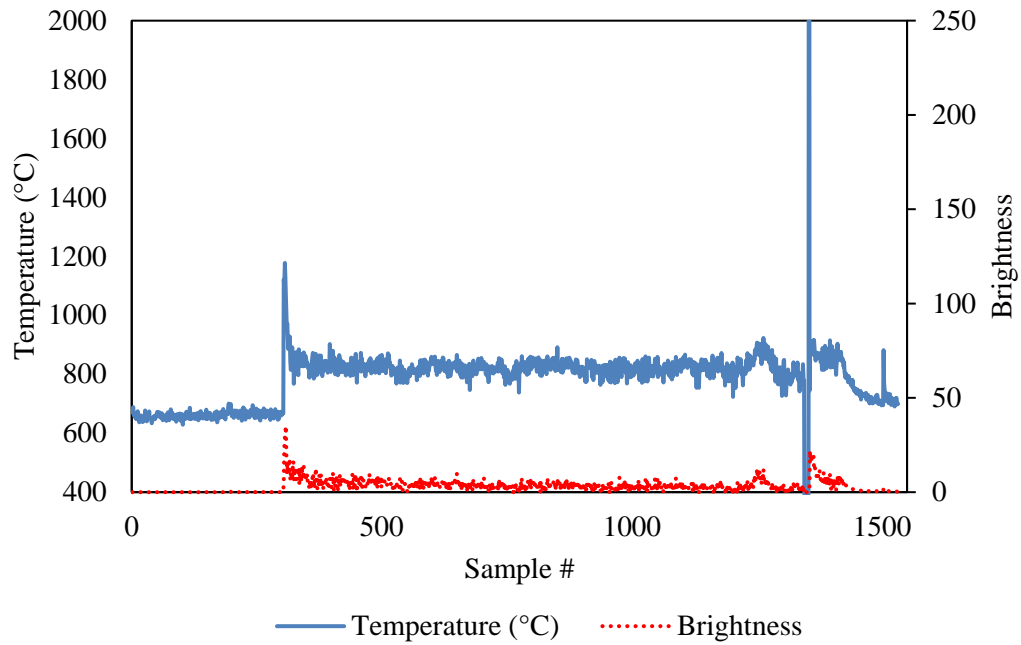


**Figure 52: Concentrate B,  $O_2/S = 1.0$ , %  $O_2 = 25$**

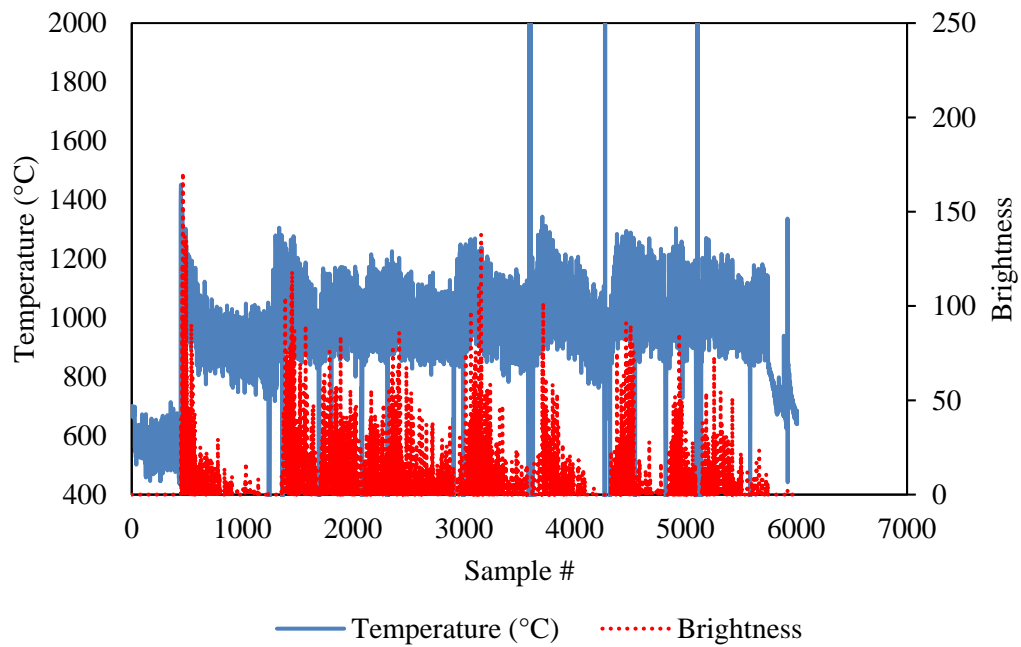


**Figure 53: Concentrate B,  $O_2/S = 1.9$ , %  $O_2 = 45$**

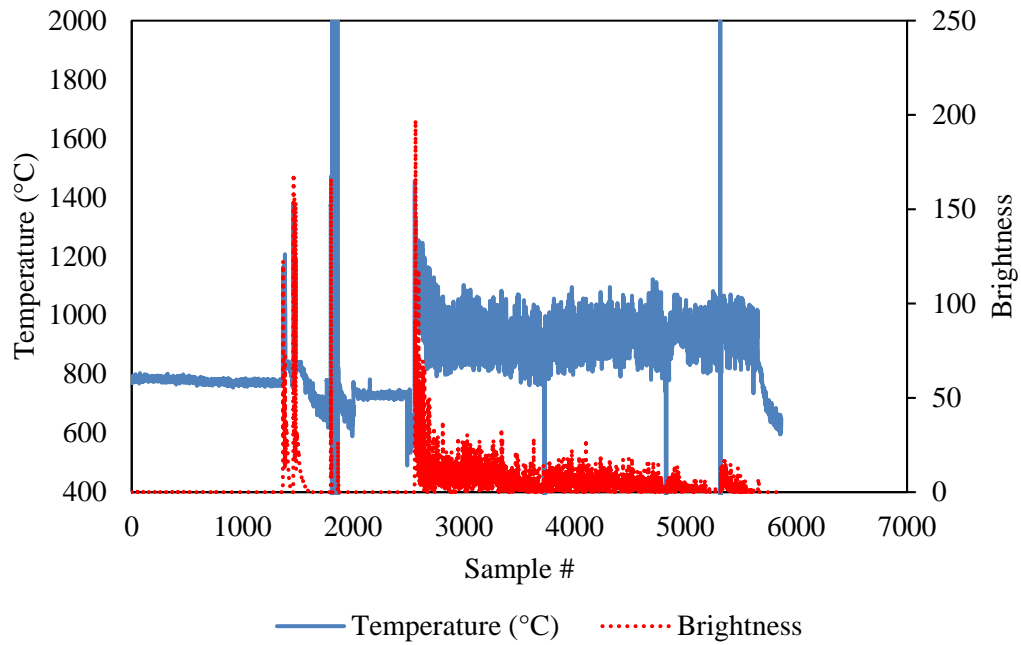


**Figure 54: Concentrate B,  $O_2/S = 1.9$ , %  $O_2 = 45$**

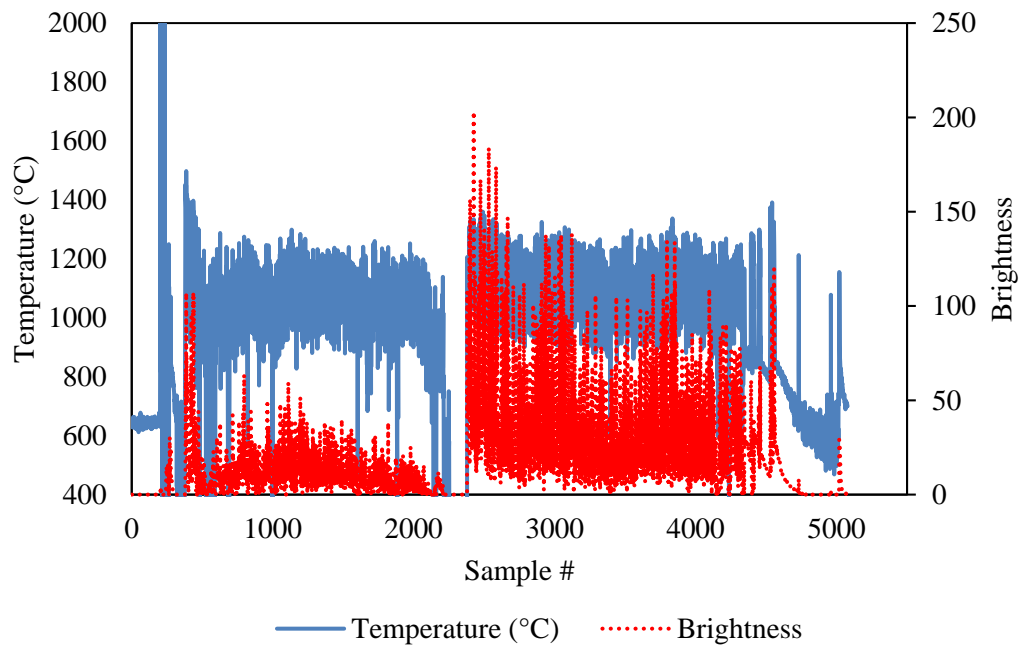


**Figure 55: Concentrate B,  $O_2/S = 2.5$ , %  $O_2 = 60$**

### Concentrate AB

The experimental temperature and brightness data from tests with Concentrate B is presented in Figure 56 to Figure 58.

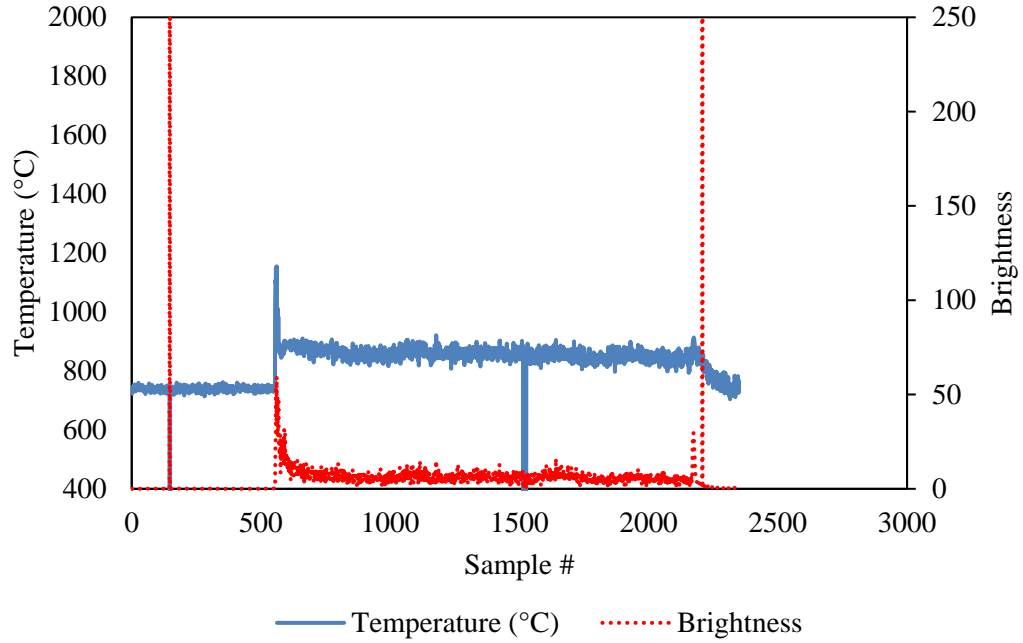


**Figure 56: Concentrate AB,  $O_2/S = 1.0$ , %  $O_2 = 25$**

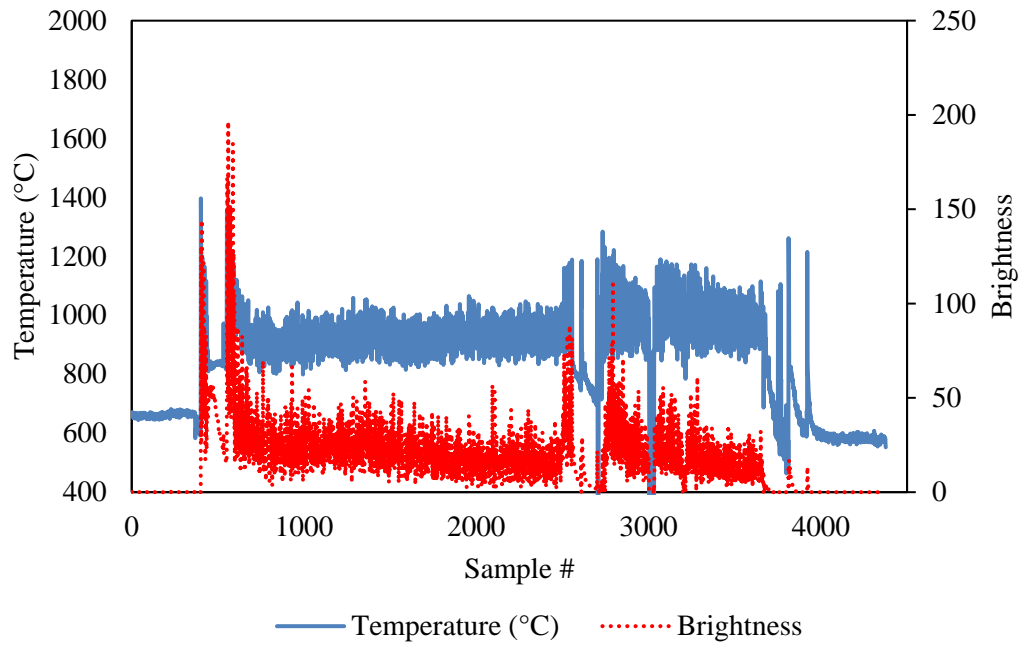


**Figure 57: Concentrate AB,  $O_2/S = 1.9$ , %  $O_2 = 45$**

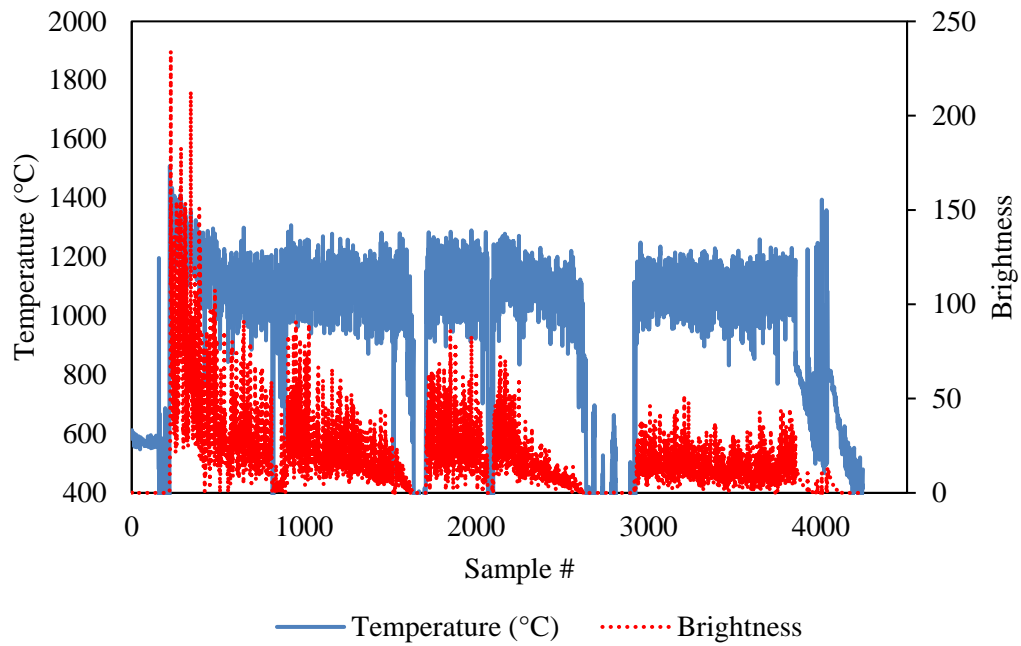


**Figure 58: Concentrate AB,  $O_2/S = 2.5$ , %  $O_2 = 60$**